

12-2012

# Analysis and Evaluation of Existing and Novel Turbulent Dynamic Pressure Based Methods for Measuring Bridge Pier and Abutment Scour

Murray Fisher  
*Clemson University*

Follow this and additional works at: [https://tigerprints.clemson.edu/all\\_dissertations](https://tigerprints.clemson.edu/all_dissertations)

 Part of the [Civil Engineering Commons](#)

---

## Recommended Citation

Fisher, Murray, "Analysis and Evaluation of Existing and Novel Turbulent Dynamic Pressure Based Methods for Measuring Bridge Pier and Abutment Scour" (2012). *All Dissertations*. 1608.

[https://tigerprints.clemson.edu/all\\_dissertations/1608](https://tigerprints.clemson.edu/all_dissertations/1608)

This Dissertation is brought to you for free and open access by the Dissertations at TigerPrints. It has been accepted for inclusion in All Dissertations by an authorized administrator of TigerPrints. For more information, please contact [kokeefe@clemson.edu](mailto:kokeefe@clemson.edu).

ANALYSIS AND EVALUATION OF EXISTING AND NOVEL TURBULENT  
DYNAMIC PRESSURE BASED METHODS FOR MEASURING  
BRIGE PIER AND ABUTMENT SCOUR.

---

A Dissertation  
Presented to  
the Graduate School of  
Clemson University

---

In Partial Fulfillment  
of the Requirements for the Degree  
Doctor of Philosophy  
Civil Engineering

---

by  
Murray Fisher  
December 2012

---

Accepted by:  
Dr. Abdul Khan, Committee Chair  
Dr. Sez Atamturktur  
Dr. Nigel Kaye  
Dr. Lawrence Murdoch

## ABSTRACT

Scour is one of the most significant threats to bridge infrastructure and is the leading cause of failure within the United States. Given this risk to the nation's transportation infrastructure, it is necessary to understand the development of scour holes around bridge piers and abutments. This can be achieved with scour monitoring, a Federal Highway Administration approved scour countermeasure. As the monitoring techniques available range from simple devices that rest on or in the channel bed to advanced scanning systems that provide a bed contour profile, a concise study of the state of the art in real time scour measurement capabilities is required. This is accomplished in this work, along with the development of a scour monitoring technique that is shown to provide reliable information during a wide variety of channel conditions. The current technologies available for monitoring scour are reviewed to highlight the governing physics, to evaluate the field performance, and to identify the effect of environmental factors on the performance. From this assessment, two devices are selected for further study; a sonar fathometer and a time domain reflectometry device. Several environmental factors are highlighted that influence these devices, including channel temperature, salinity, and suspended sediment concentration. A novel device is proposed which exploits the turbulence in open channels as a means of monitoring the bed level. The device uses a sensor that is sensitive to the dynamic pressure due to the natural turbulence in open channels. This sensor vibrates at a significantly higher magnitude when in the channel flow relative to an identical sensor located in the sediment. The vibration-based method, time domain reflectometry, and sonar devices are then evaluated against

simulated field conditions in order to determine their relative sensitivities to environmental conditions. These tests reveal that sonar and time domain reflectometry devices can be influenced by channel salinity and temperature. In addition, the sonar device is shown to be sensitive to the suspended sediment concentration in the channel. The vibration-based method is shown to be insensitive to the suspended sediment concentration as well as bed sediment type. The effect of flow angle is also evaluated for the vibration method, and reveals that the novel device operates in highly misaligned flows. Lastly, an analytical model is built for further optimization of the device. The model is then verified, calibrated and validated with experimental data. The validated model is used to develop a field prototype, which is tested experimentally and reveals satisfactory performance for deployment to bridge sites.

## DEDICATION

To Sara and Gabriella, your unconditional love and support sustains me.

## ACKNOWLEDGMENTS

To a great many I am indebted, so let me in a few words say thank you to those who have made a mark on me, and this project in particular. Without the support and encouragement of my family, and in particular my parents David and Ruth Fisher, this work would not have been possible. I would also like to formally acknowledge the support, guidance, and direction that I have received from my two co-chairs, Dr. Abdul Khan and Dr. Sez Atamturktur. Your insight has guided me through the challenges in this project, to which I am grateful. To Dr. Nigel Kaye and Dr. Lawrence Murdoch I would also like to express my words of thanks for your willingness to mentor me and provide key insights. Lastly, I would like to conclude by acknowledging the support of the South Carolina Department of Transportation and Clemson University for their financial support during this project.

## TABLE OF CONTENTS

	Page
TITLE PAGE .....	i
ABSTRACT .....	ii
DEDICATION .....	iii
ACKNOWLEDGMENTS .....	iv
LIST OF TABLES .....	viii
LIST OF FIGURES .....	ix
CHAPTER	
I.    CHAPTER ONE - INTRODUCTION.....	1
II.   CHAPTER TWO – THE STATE OF THE ART IN SCOUR MONITORING.....	4
Introduction.....	4
Point Scour Measurement Methods .....	7
Distributed Scour Measurement Methods .....	43
Summary of the State of the Art in Scour Monitoring.....	58
References.....	63
III.  CHAPTER THREE – A NOVEL VIBRATION-BASED MONITOURING TECHNIQUE FOR BRIDE PIER AND ABUTMENT SCOUR.....	69
Introduction.....	69
Numerical Proof of Concept .....	73
Experimental Setup.....	84
Results and Discussion .....	86
Conclusions.....	97
References.....	99
IV.  CHAPTER FOUR – THE EFFECT OF CHANNEL CONDITIONS ON SCOUR MEASUREMENTS.....	101
Introduction.....	101

Table of Contents (Continued)

	Page
Theory and Background.....	106
Measurement Setup.....	111
Results and Discussion .....	113
Conclusions.....	120
References.....	122
V.    CHAPTER FIVE – OPTIMIZATION OF VTP FOR FIELD DEPLOYMENT .....	127
Introduction.....	127
Modeling Approach .....	128
Model Verification, Calibration, and Validation .....	144
VTP Optimization for Field Deployment .....	159
Field Prototype Performance .....	161
Conclusions.....	165
References.....	166
VI.   CHAPTER SIX - CONCLUSIONS.....	169
Summary of Research.....	169
Advancements to the State of the Art .....	171
Limitations of the Work and Avenues for Further Study .....	174
APPENDICES .....	176



## LIST OF TABLES

Table		Page
2.1	Soil properties pertinent for radar EM techniques.....	47
2.2	Proposed severity ratings for FMEA analysis of scour monitoring system.....	59
2.3	Proposed occurrence ratings for FMEA analysis of scour monitoring system.....	60
2.4	Proposed detectability ratings for FMEA analysis of scour monitoring system.....	60
2.5	Example FMEA analysis for TDR system.....	60
2.6	Summary of scour monitoring devices .....	61
5.1	Model and measured natural frequencies for modes in neoprene.....	147
5.2	Flow parameters for CHL flume tests.....	148

## LIST OF FIGURES

Figure	Page
2.1 Example of flout-out device installation.....	11
2.2 Example of magnetic sliding collar installation.....	14
2.3 Typical sonar system installation.....	17
2.4 Typical TDR waveform .....	24
2.5 Piezoelectric film sensor .....	41
3.1 Model response for prototype VTP based upon SDOF model and turbulent spectra. ....	81
3.2 Circular and square VTP normalized mean square response as computed from the response spectrum from 10 to 400 Hz for circular and square VTPs, for various plate areas, and material types. ....	82
3.3 Prototype VTP configuration diagram .....	85
3.4 Prototype VTP array installed in flume bed .....	86
3.5 Energy content of prototype VTPs as a function of distance from the water/ sediment interface. ....	89
3.6 VTP energy content of prototype VTPs versus flume flow rates .....	90
3.7 Turbulent energy content of prototype VTPs in un-scoured and 0.056 m scoured channel bed. ....	92
3.8 Energy content of prototype VTPs in scour holes of various sizes .....	94
3.9 VTP measured scour depth versus actual scour values .....	96
4.1 VTP setup as installed in CHL flume for channel effects study. ....	112

List of Figures (Continued)

Figure	Page
4.2 VTP energy content for various turbidity levels and channel flow velocities.. .....	116
4.3 VTP energy content as a function of the flow misalignment.....	118
4.4 Variation of VTP energy content with channel velocity. ....	119
4.5 Variation in VTP energy content for various bed sediment types.....	120
5.1 Channel parameters relevant to Navier Stokes Equations. ....	129
5.2 Sample turbulent velocity time history. ....	130
5.3 Area integration of dynamic turbulent pressure distribution across VTP disk.....	138
5.4 Components of joint acceptance for the 1 <sup>st</sup> plate mode. ....	143
5.5 Variation in VTP turbulent pressure, as a function of the number of elements.....	145
5.6 Distribution of $U/U_*$ as a function of depth in the channel, for Run 1.....	149
5.7 Distribution of $u'v'$ as a function of depth in channel, for Run 1.....	150
5.8 Measured and model root mean square of $u'$ ratio with friction velocity, as a function of depth in channel.....	151
5.9 Comparison on model turbulent velocity fluctuation spectra with published results from Figure 7b of Kironto and Craff (1994).. .....	152
5.10 Comparison on model turbulent velocity fluctuation spectra with published results from Figure 4.15 of Nakagawa and Nezu (1993).. .....	152

List of Figures (Continued)

Figure	Page
5.11 Power spectral density of $u'$ at a $y/h = 0.1$ , from run 1. ....	153
5.12 Power spectral density of $u'$ at a $y/h = 0.2$ , from run 1. ....	154
5.13 Power spectral density of $u'$ at a $y/h = 0.3$ , from run 1. ....	154
5.14 Measured and model acceleration response spectra for run 3 conditions, $y/h = 0.35$ . ....	158
5.15 Measured and model acceleration response spectra for run 3 conditions, $y/h = 0.66$ . ....	158
5.16 Optimization of VTP size and thickness for field deployment. ....	160
5.17 Schematic of field VTP configuration. ....	162
5.18 Field prototype. ....	162
5.19 Performance of field prototype in CHL flume. ....	163
5.20 Measured and model response as a function of flow misalignment. ....	165

## CHAPTER ONE

### INTRODUCTION

One of the most significant financial investments in any transportation infrastructure system are the bridges that connect otherwise geographically isolated communities. Failure of these structures can have significant impacts, both in financial and human terms. The leading cause of failures in the United States is due to the removal of bed material surrounding the foundations of bridge piers and abutments, a process known as scour. Scour failures, accounting for 60% of all bridge failures (Legasse et al., 1997), have resulted in the direct loss of lives, and have accounted for hundreds of millions of dollars in repair damage. Additionally, bridge failures due to scour can have a dramatic impact on the local community, with the financial impact estimated to be five times the actual repair cost (Rhodes and Trent, 1993). Therefore, it is necessary to protect these critical infrastructure elements against scour damage.

Scour damage can be prevented by armoring the bed to reduce the amount of scour or by adjusting the river hydraulics to reduce the peak flow, requiring significant amounts of time and financial resources for implementation. Scour monitoring, however, can be implemented relatively quickly and at reduced cost relative to the other preventative measures. For this reason the Federal Highway Administration's Highway Engineering Circular #23 lists scour monitoring as a viable countermeasure for scour critical bridges (Legasse et al., 2009). Scour at bridges occurs over time, with peak flow events progressively adding to the scour around the pier or abutment. Thus, by

monitoring the history of scour at a bridge, it is possible to determine if the scour depth is approaching the critical value determined during the bridge design. As the scour depth approaches this threshold value, it is possible to begin planning the more extensive armoring or river training mechanisms required to protect the bridge. Given the importance of scour monitoring in determining the health of the bridge related to this threshold, it is necessary to understand and advance the state of the art in scour monitoring.

To that end, a study has been conducted with the following objectives:

Objective 1: Understand the state of the art in scour monitoring, highlighting the physical principles behind the operation of the devices, documented field performance, and sensitivities to environmental factors that can influence the scour measurements.

Objective 2: Evaluate the best in class scour monitoring instruments under simulated field conditions to explore their sensitivity to common environmental factors in natural channels, such as salinity, temperature, and suspended sediment.

Objective 3: Evaluate the feasibility of a novel scour monitoring method that exploits the natural turbulence in open channels as a means to determine the water/sediment interface.

Objective 4: Optimize the novel method for field deployment.

Objective 5: Confirm the performance of the novel method with laboratory experiments.

The following manuscript outlines the work conducted to accomplish these objectives. In Chapter 2, the state of the art in scour monitoring is explored by evaluating the currently available measurement techniques, of which the best in class devices were determined to be the sonar fathometer and the time domain reflectometry (TDR) method.

Chapter 3 focuses on the feasibility study of the novel method. Chapter 4 discusses the results of several experiments that were conducted for the sonar, TDR, and novel methods under common environmental conditions. Chapter 5 outlines the optimization of a prototype device for field deployment. Finally, Chapter 6 summarizes the key contributions to the state of art in scour monitoring.

Through the work discussed in this manuscript, deficiencies in the current capabilities of scour monitoring are identified and the development and validation of a novel method that advances the state of the art in scour monitoring are presented.

## **References**

- Lagasse, P.F., Richardson, E.V., Schall, J.D., Price, G.R., (1997). Instrumentation for measuring scour at bridge piers and abutments. NCHRP Report 396, TRB, National Research Council, Washington, D.C., 1997.
- Lagasse, P.F., Clopper, P.E., Pagán-Oriz, J.E., Zevenbergen, L.W., Arneson, L.A., Schall, J.D., Girard, L.G., (2009). Bridge scour and stream instability countermeasures: Experience, selection and design guidance. Hydraulic Engineering Circular No.23, 3rd Ed., Publication No. FHWA-NHI-09-111, U.S. Department of Transportation, Federal Highway Administration.
- N.T.S.B., (1987). Collapse of New York Thruway (I-90) Bridge, Schoharie Creek, near Amsterdam, New York, April 5, 1987. NTSB Number: HAR-88/02, NTIS Number: PB88-916202.
- N.T.S.B., (1989). "Collapse of the northbound U.S. Route 51 Bridge spans over the Hatchie River, near Covington, Tennessee, April 1, 1989", NTSB Number: HAR-90/01, NTIS Number: PB90-916201.
- Rhodes, J., Trent, R., (1993). Economics of floods, scour and bridge failures. In Hydraulic Engineering '93: Proceedings of 1993 Conference, Ed: Shen, H.W., Su, S.T., Wen. F., July 25-30, 1993, San Francisco, CA, ASCE.

## CHAPTER TWO

### THE STATE OF THE ART IN SCOUR MONITORING

#### **2.1 Introduction**

Scour around bridge piers and abutments occurs when high velocity flows impinge on the riverbed, leading to the removal of bed material, which undermines the structural stability of bridge elements located in the flow. Scour monitoring, in turn, is critically important because it allows the infrastructure owner to monitor the health of their bridge hardware. Additionally, scour monitoring is an approved countermeasure, as are traditional physical countermeasures such as rip-rap (Lagasse et al., 2009). Therefore, it is necessary, to understand the physical operating principles and past field performance of any device deployed to measure scour.

The degradation of the channel bed around bridge piers and abutments occurs in natural channels around the globe and has historically caused failure of bridges, is costly to repair, and can result in the loss of lives. Several bridge failures have been directly attributed to scour including the I-90 Bridge over the Schoharie Creek in New York in 1987, the U.S. 51 Bridge over the Hatchie River in Tennessee in 1989, and the I-5 Bridge over the Arroyo Pasajero River in California in 1995. The NTSB investigated both the Schoharie Creek and Hatchie River Bridge failures and concluded that scour was the cause of failure. The I-90 Bridge failure was attributed to inadequate protection of a pier footing leading to the formation of a scour hole that undermined the pier, while the U.S.



51 failure was attributed to the migration of the main channel, which undermined a bridge column, leading to the collapse of the bridge (NTSB, 1987; NTSB, 1989). The I-5 collapse was attributed to a 3 m scour hole, which developed over the long-term, and led to the collapse of the bridge columns (Arneson et al., 2012). Additionally, the United States Geological Survey (USGS) reported that the number of bridges damaged during flood events ranged from 17 in the U.S. Northeast in 1987 to more than 2,500 in the Midwest during the 1993 flood season (Mueller, 2000). Murillo (1987) reported that during 1961-1974, 46 of the 86 major failures of bridges in the U.S. were due to scour, more than any other cause. Lin et al. (2004) reported that 68 bridges in the U.S. were damaged due to scour from 1996 to 2001. Furthermore, Richardson and Price (1993) reported that in 1993, 109,464 bridges in the U.S. were scour critical or scour susceptible and required countermeasures. Hunt (2009) reported that of the 590,000 bridges in the U.S., 20,904 are scour critical. Overall, estimates place scour as the leading cause of bridge failure, accounting for approximately 60% of all events (Lagasse et al., 1997).

Not only is scour widespread, it can result in significant human and financial costs. The human impact is associated directly with the loss of life during a bridge collapse as well as the indirect costs associated with loss of infrastructure. During the Schoharie Bridge collapse, 10 individuals lost their lives (NTSB,1987). The U.S. 51 bridge collapse in Tennessee cost 8 lives, while the I-5 Bridge failure over the Arroyo Pasajero River cost the lives of 7 individuals (NTSB, 1989; Arneson et al., 2012). In addition to the direct cost of human lives, the indirect human impact is felt in the loss of critical infrastructure, which can impede both evacuation routes (e.g., during a hurricane)

or relief and recovery efforts after a flood. Butch (1996) reported that the cost of flood repairs during the 1980s was estimated to be \$300 million. More recently, the USGS reported that from 1993 to 1995, floods in the Midwest, Georgia and Virginia cost \$178 million, \$130 million and \$40 million, respectively (Mueller, 2000). These figures account for the total cost of damage from floods. Brice and Blodgett (1978) estimated the cost of repairing a bridge with scour damage to be \$100 million per event during 1964-1972. Lagasse et al. (1997) reported that \$30 million is spent annually on scour related bridge repairs. In addition to the cost of the failures and associated repairs, the economic impact of a bridge failure to the local community is estimated to be as much as five times the repair costs (Rhodes and Trent, 1993).

Thus, given the widespread nature of scour damage, the rapid time frame in which scour hole formation can occur, and the ancillary costs of repair, an adequate methodology for monitoring the formation of scour holes around bridge structural elements is essential. In an effort to accomplish this goal, 32 states have deployed scour monitoring systems and employed 164 sonar fathometers on 48 bridges (Lagasse et al., 1997). In addition, several state level Departments of Transportation and the Federal Highway Administration have funded various scour monitoring programs. In order to make use of the field information gained from these and other projects, it is necessary, therefore to review the performance of the various devices used in scour monitoring campaigns.

To that end, available scour monitoring methods are reviewed, including both single point techniques, covered in Section 2, and distributed techniques, discussed in

Section 3. The operating principle for each of the devices is discussed along with pertinent performance results from the various field deployments. A review of the environmental factors that affect the operation of the devices are also included, with the goal of highlighting the strengths and weaknesses of each device and to provide the engineering community with a solid understanding of the tools at their disposal for scour monitoring. Section 4 follows with a summary of the state-of-the-art including both deficiencies in the various methods and avenues for further study

By evaluating the various scour monitoring methods available, it will be possible to determine the operating principles, strengths and weaknesses of each device, and to highlight the channel conditions that may favor one device over another. Engineers designing future bridge monitoring campaigns can use the information provided herein to select the optimal measurement systems for their particular field conditions and install a more robust system with improved scour monitoring capabilities.

## **2.2 Point Scour Measurement Methods**

### 2.2.1 Sounding Rods

Sounding rods and sounding weights, adapted from depth finding methods on naval vessels, have been used since the early 19<sup>th</sup> century to monitor the depth to the riverbed from bridge platforms (Lagasse et al., 1997). The latest embodiment consists of a solid rod and baseplate that rests on the riverbed surface (Zabilansky, 1996). As the scour hole develops, the rod moves down with the bed surface from inside its support housing. This motion is tracked with a chain that connects the rod to the support housing,

but does not provide any resistance to motion. The downward movement of this chain is then tracked from the bridge deck or another fixed datum, permitting measurement of the maximum scour underneath the rod location. During a refill event, the baseplate and rod will be buried and will not provide information about the aggradation of material in the scour hole. The ability to record refill is important for scour monitoring as it provides information that is not obtained via regular bridge inspections. Refill typically occurs with material of different properties than the native bed. Thus, a refilled scour hole can appear as acceptable during a survey, but in reality the foundation is undermined.

Sounding rods were tested during both scaled laboratory and full-scale field testing as part of the National Cooperative Highway Research Program (NCHRP) 21-3. During the laboratory testing, two baseplate sizes (0.0762 and 0.127 m) were tested for multiple channel bed materials. Overall, the results showed that with either baseplate, the scour readings were within +/- 10% of the scour depth (Lagasse et al., 1997). During the field installation at the Orchard Bridge site in Colorado, the device provided readings of the location of the channel bed; however various challenges were encountered with the device.

The sounding rod tests indicated several factors that should be considered in scour measurements. In both the laboratory and the field environments, the experimental results indicated that the rod itself could penetrate the riverbed and gave a false depth reading. In the scaled testing, this was overcome via the addition of a larger baseplate, which in the scaled model was three times the diameter of the rod. Adding the larger baseplate, however, influenced the scour hole development. During the field campaign,

measurements showed that the device had significant self-burial problems with the standard baseplate. Additionally, a total failure of the device occurred during a major scour event in which the sounding rod travelled out of the bottom of the support pipe and in the process, damaged the encoder chain. Even during normal operation of the device the encoder that logged the depth of the rod was problematic; as such further tests with this device were abandoned (Lagasse et al., 1997).

Overall, sounding rods are limited in that they can only record the maximum scour, the device itself can penetrate the bed, depending upon the baseplate size it is possible that the scour hole formation may be influenced, and the device is not robust in that a large scour hole can result in total loss of the device.

### 2.2.2 Float-Out Devices

The range of devices that fall into this category vary greatly from basic buoyant floats to sophisticated radio transmitters that measure movement. Some of the commonly used float devices are shown in Figure 2.1. The simplest float-out devices are colored or numbered floats connected by a tether to a weight that acts as an anchor (DeFalco and Mele, 2002). Multiple floats and anchors are buried at various layers in the sediment, and as a scour event occurs, the float corresponding to the depth of degradation rise to the water surface. Field staff can then review those floats that have reached the surface to determine the depth of scour. In addition to the basic buoyant floats, several researchers have developed automated devices. Yao et al. (2011) reported on the use of switches that are tethered to a rod buried in the sediment, denoted as tethered-buried-switches. The device consists of switch housed inside a sealed aluminum tube that triggers when the

unit orientation changes to a horizontal position. As the scour develops and uncovers the device, drag forces pull the sensor along the sediment surface, triggering the device. Zabilansky (1996) developed a more sophisticated form of a float-out device based upon wildlife movement tracking units consisting of a wireless transmitter that emits a timing pulse, which varies if the device is in motion. These transmitters are instrumented along a support rod that is then buried in the sediment. If a transmitter is buried, it is not subject to any of the turbulent flow and therefore the timing pulse is stable. After a scour event, in which the transmitter is uncovered, the water flowing past the transmitter causes it to move and vibrate, resulting in a change in the timing pulse. Thus, by monitoring the signal from each transmitter, it is possible to determine the depth of the scour hole present in the channel bed. In the field setup, each transmitter is assigned an individual frequency and the timing pulse of each is monitored by a telemetry system and data logger located on the bridge. A minimum of 0.102 m/s of flow past the transmitter is required in order for the transmitter to register movement. An advantage of the transmitter based device over the other float-out devices discussed earlier is that during a refill event, where material is deposited in the scour hole, the transmitters will be re-buried. Thus, the wildlife tracker based transmitters can record maximum scour and refill, while the buoyant floats and tethered-buried-switches can only provide information on the maximum scour.

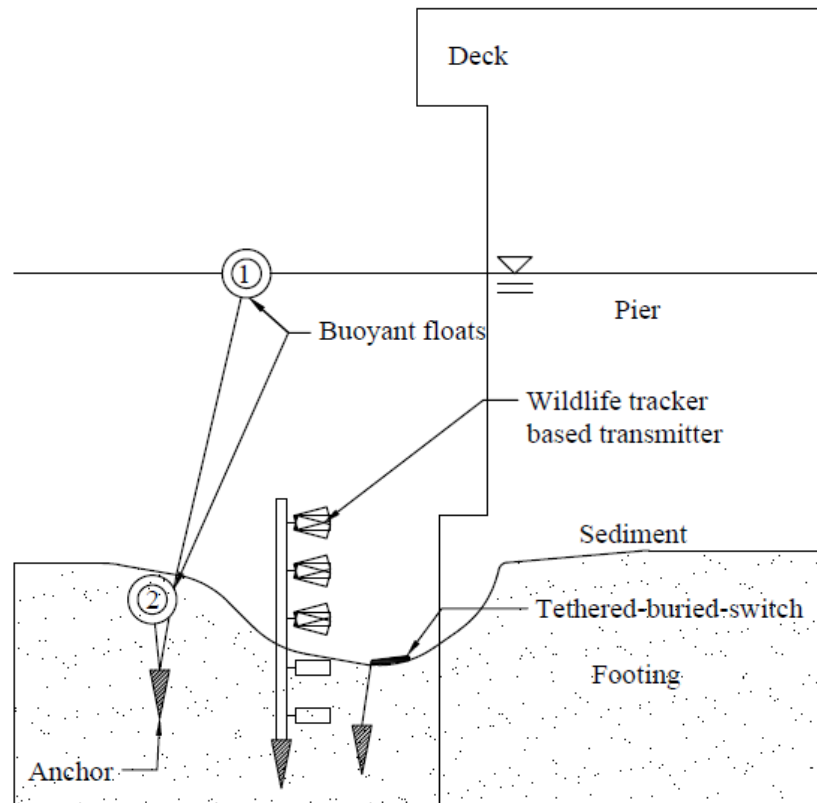


Figure 2.1 - Example of float-out device installation. Highlights buoyant floats, tethered-buried switches, and wildlife tracker based transmitters. Based upon Yao et al (2011) and Zabilansky (1996).

The tethered-buried-switches were deployed at two bridges in Texas, the US 59 Bridge over the Guadalupe River and the SH 80 Bridge over the San Antonio River. During the reported measurement period for both bridges, the device failed to trigger due to a lack of scour hole formation (Yoa et al., 2011). As a part of an ice and scour monitoring project (Zabilansky, 1996), fifteen of the wildlife based tracking transmitters were deployed around a bridge pier at the Bridge Street Bridge over the White River junction in Vermont. The transmitters were distributed over four rods and were placed at an interval of 0.152 m. Though two transmitters were lost due to potential damage during

the field campaign, one transmitter recorded a scour event for nine hours before it was reburied after the breakup of the surface ice.

While the field performance of the float-out devices is limited, several potential factors that could influence the performance of these devices are anticipated. Since the tethered-buried-switches lie on the riverbed once exposed by the scour, debris in the flow can damage the unit. Additionally, if the depth of scour exceeds the depth of the anchor for the tethered-buried-switch, the entire device can fail. The removal of the anchor by scour is also a potential problem with the buoyant floats and the wildlife tracker based transmitters. Furthermore, failure of individual devices due to debris is a concern as reported in the Vermont field tests, where two transmitters were lost.

Overall, for all float out devices in general, and for the buoyant floats and the tethered-buried-switches in particular, the main disadvantage is that they require reinstallation after a scour event and thus, can only record the maximum scour depth. This difficulty was resolved with the wildlife tracker based transmitters that remain tethered to the support rod, allowing for reburial of the transmitters during a refill event. With the exception of the transmitter units, scour the use of float out devices during a long-term campaign is difficult and requires extensive use of field staff. Finally, as with all devices mounted in the channel bed, float-out devices are susceptible to debris damage and they also only provide information about the scour depth at the point immediately surrounding the location where they are installed.



### 2.2.3 Magnetic Sliding Collars

The magnetic sliding collar, MSC, is one of the several rod-and-collar based scour monitoring devices. MSC consists of a rod buried in the riverbed with an attached collar. The collar rests on the riverbed, and during a scour event the collar moves down the rod, thus measuring the bed scour. The MSC device was preceded by a rod equipped with a collar housing a radioactive element (Lagasse et al., 1997). A detector capable of sensing the presence of the radioactive element is used to track the movement of the collar. This detector is lowered inside the rod from the bridge deck, through a guide tube. Due to environmental concerns regarding the use of a radioactive element on the collar, this device was abandoned in favor of a similar device that relies upon a magnetic element installed on the collar (Lagasse et al., 1997). To monitor the location of the collar, two variations of the MSC device were developed and patented (Richardson et al, 1996). In the first embodiment, the location of the magnet is detected by lowering a magnetic switch on a chain from the bridge deck inside a guide tube that is connected to the rod mounted in the riverbed, see Figure 2.2. When this switch nears the collar, the field from the collar's magnet trips the switch. The position of the chain at this point is then recorded, and thus, by knowing the chain length, the depth of scour can be determined. This approach however, is difficult to automate for remote monitoring applications. To overcome this weakness, a second version was developed that equipped the rod with magnetic switches located every 0.3 m along its length. As the collar moves down the rod, these switches are tripped; the time and location of each tripped switch during an event is recorded by a data acquisition system located on the bridge. Typically, a 0.15 m

magnet is fixed to the collar, resulting in scour depth measurements at intervals of +/- 0.15 m (Lagasse et al., 1997).

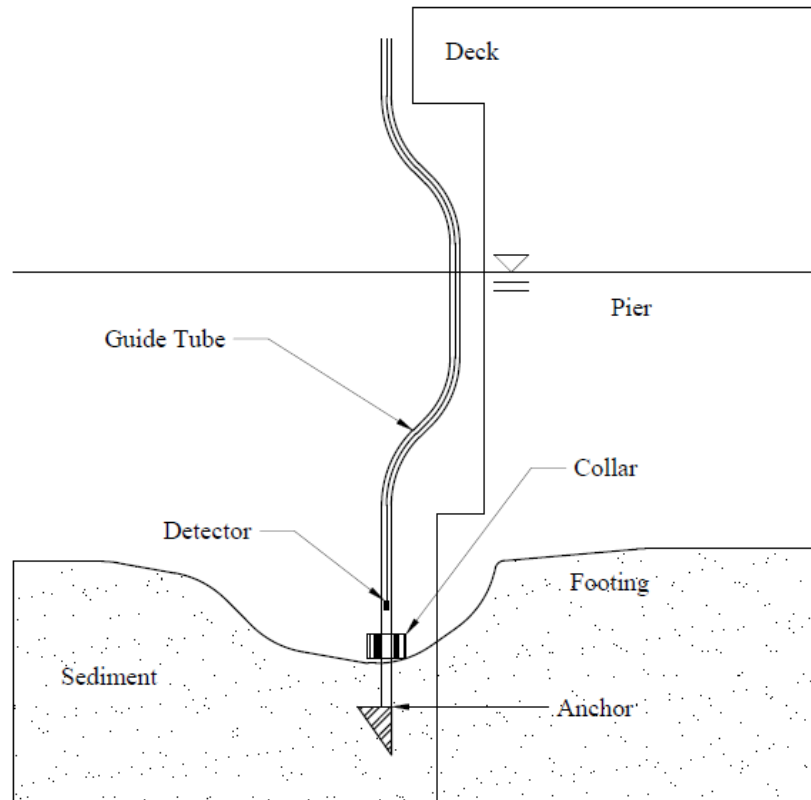


Figure 2.2 - Example of magnetic sliding collar installation. Figure shows the first embodiment of the MSC device, adapted from (Richardson et al, 1996; Nassif et al., 2002).

MSC rods were deployed as scour monitoring devices as part of the NCHRP 21-3 Research Program, as well as in separate projects by the New Jersey and Indiana State Departments of Transportation. The first embodiment of the MSC device was installed at two bridges, one located in Colorado and one in New Mexico. A 1.5 m scour event was measured with this device in Colorado while a 0.86 m event was recorded in New Mexico (Lagasse et al., 1997). Two automated MSC devices were installed on the Kersey

Bridge Abutment in Colorado and the Nassau Sound Bridge in Florida. A 0.6 to 0.9 m scour event was recorded with the automatic device in Colorado while no scour was observed during the Florida field tests (Lagasse et al., 1997). Additional tests were conducted in Michigan, Minnesota, and Texas by various state Departments of Transportations or the FHWA as part of the broader NCHRP project. Though various installation issues were encountered, scour events were measured in these additional field tests from 0.24 to 1.5 m in depth. Automatic MSC devices were also installed on two bridges in New Jersey, which recorded a 0.45 m deep scour event on the Passaic Bridge (Nassif et al., 2002). Cooper et al. (2000) discussed the performance of both MSC and sonar devices on two bridges in Indiana. During the program, several scour events were recorded with the MSC collars ranging from 0.15 to 0.45 m in depth, which were also typically well correlated with the sonar readings taken during the same period.

During the field operation of the first MSC embodiment in Colorado, debris impacted the guide pipe needed to route the detector from the bridge deck, through the water column, and to the rod. This damage, however, did not prevent the operation of the device (Lagasse et al., 1997). In the New Jersey study, subsequent analysis of the available data revealed that while the MSC collar was able to record scour events, the success of the entire measurement was highly dependent upon a reliable data logger (Nassif et al., 2002). In the Indiana study, the most significant issue encountered in the field was the survival of the sensors (Cooper et al., 2000). At the Wabash River site, the MSC rod was lost entirely, which was attributed to debris colliding with the sensor. At the Wildcat Creek site, though the rod survived debris damage, the cable to the data

acquisition system was damaged resulting in the loss of the data. Additionally, during the development of the MSC device, it was reported that the space between the collar and the rod could fill with sediment, causing the collar to stick and give a false reading (Lagasse et al., 1997).

Based upon these results, the main channel condition that can affect the survivability of MSC devices is the presence of debris. As indicated, several of the devices themselves or the cabling connecting the rods to the data acquisition units were damaged. An additional problem with a collar based system is that the collar/rod clearance must be controlled to prevent sediment from obstructing the collar. Finally, as the collar rests on the bed surface, if the scour hole were to refill with additional material after the high flow event, the collar would become submerged. Any subsequent scour events with a magnitude less than the event that submerged the collar would not be recorded.

#### 2.2.4 Sonar/Fathometer

A sonar based scour monitoring system consists of a sonar transducer (or an array of transducers), often-called fathometers or echo sounders, and the associated data collection and monitoring equipment. A typical installation is shown in Figure 2.3. Sonar transducers employ piezoelectric crystals that are either connected to a membrane or diaphragm. When an electric potential is applied across the crystal, an electric field is induced, which causes strain and thus, displacement of the crystal and the membrane. This field is then cycled, yielding an acoustic wave that is generated in the surrounding fluid (Jaffe and Berlincourt, 1965; Guo et al., 1992). As the sound wave propagates

through the channel, it will encounter various surfaces and objects that will cause a portion of the signal to reflect, called the echo signal. The time between when the original signal was emitted and when the echo is received,  $t_{ER}$ , can be measured. Typically, this measurement is made from the point at which the pulse was emitted, called the zero line, and the beginning of the upward pulse of the received echo (Hayes and Drummond, 1995). During this time, the signal traveled twice the distance to the object,  $D$ , as it traveled out to the object and back to the receiver. This wave travels at the speed of sound,  $c$ , in the water. From the measured travel time, the distance  $D$  can be calculated, as shown in Equation (2.1) (Burchynski, 1982).

$$D = \frac{c \cdot t_{ER}}{2} \quad (2.1)$$

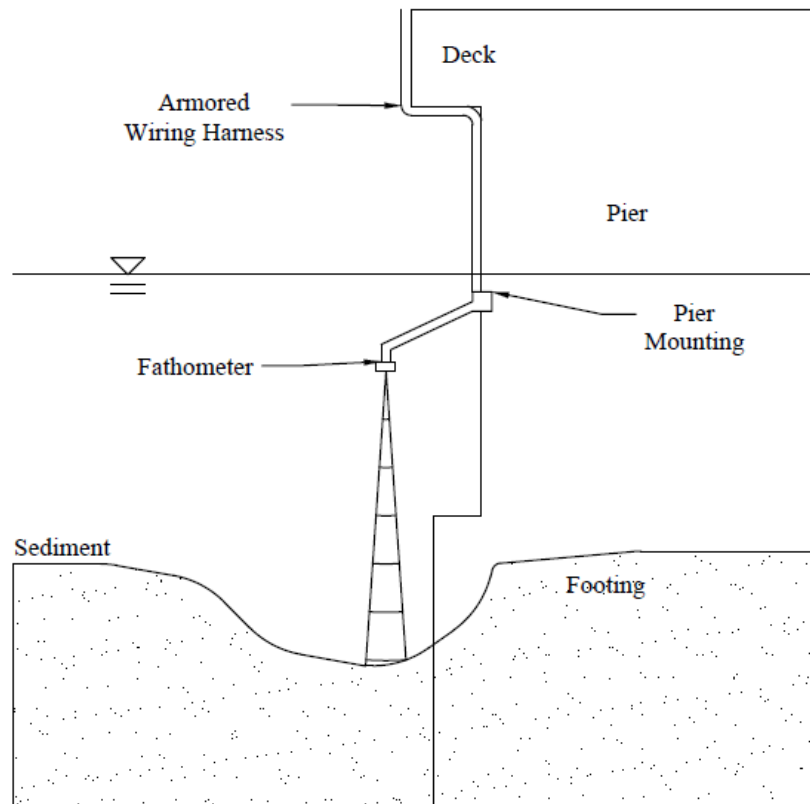


Figure 2.3 - Typical sonar system installation. Based upon Nassif et al (2002).

The resolution of the sonar system is a function of pulse duration,  $t_D$ , the time during which the transducer emits its pulse, and the pulse frequency,  $f$ . The effect of the pulse duration can be determined from Equation (2.1), by replacing the echo time with the pulse duration. For example, if the speed of sound in water is 1,500 m/s and the pulse duration is 0.1 milliseconds, the resolution of the device is limited to 7.5 cm. The ability to resolve the riverbed features is also a function of the frequency of the acoustic wave. For example, if the pulse consisted of only a single complete cycle of vibration of the transducer, then the resolution would become a function of the period of the wave. The period of the wave is inversely proportional to the frequency, thus as the frequency increases, the minimum size of an object that can be resolved by the device decreases. For example, a 50 kHz signal can resolve objects greater than 1.5 cm where as a 200 kHz signal can resolve an object down to the size of 3.75 mm.

While increasing the sonar frequency improves the ability to resolve small-scale structures in the riverbed, it also affects the attenuation of the sonic pulse. Attenuation occurs due to the scattering and absorption from the presence of particles in the flow (both suspended particles and the fluid particles) as well as due to friction (Burczynski, 1982; Urick, 1975). As the frequency increases, the attenuation increases, and the amount of signal returned to the transducer is reduced, limiting the maximum distance of the device.

Sonar systems were evaluated as part of several research projects. Lagasse et al. (1997) instrumented several bridges with fathometers, including the Orchard Bridge in

Colorado, the San Antonio Bridge test site in New Mexico, Johns Pass Bridge in Florida, and the Kersey Bridge Abutment in Colorado. During these field measurements, the sonar units recorded scour events of 0.23 m, 1.2 m, 0.91 m, and 0.5 m, respectively, as well as refill at some of the sites. The Florida site also showed that the sonar system could operate in a marine environment and during a peak flow event generated during Hurricane Opal. In a study for the New Jersey Department of Transportation, Nassif et al. (2002) reported on the performance of sonar systems on two bridges. During the 23 months of testing, two scour events were observed; the initial event resulted in the development of a 0.5 m deep scour hole, followed by aggradation of material that refilled the hole within 2 hours. A subsequent scour event of approximately 0.3 m in depth was observed. Hunt (2005) reported on the development and installation of several sonic fathometer systems in New York and in the District of Columbia. As the channel depths made an MSC approach unfeasible, fathometers were installed. Though some of these devices had been operational for seven years at the time of the report, the reliability of the data or any conclusions regarding the magnitude of scour events were not discussed. Mason and Sheppard (1994) collected data from a sonar monitoring system installed at the Herbert C. Bonner Bridge in North Carolina. The system consisted of 16 different sensors installed 1.5 m from the channel bed and 1.8 to 4 m below the water surface. During Hurricane Emily, the system recorded the development of a 0.6 m scour hole followed by refill, as well as 1 m of erosion and refill of the main channel. The performance of the system was also compared with several calibration measurements taken by divers at the measurement sites. The results from the sonar systems and the

divers were well correlated. In addition, De Falco and Mele (2002) reported on the performance of two sonar scour monitoring systems installed at two separate railway bridges in Italy. Their results indicated scour hole developments of 1.5 to 2.0 m at the Mezzana Corti Bridge and 0.9 m at the Borgoforte Bridge. These results were then compared to prediction models and showed agreement between the measured and computed scour depths, with a 7% difference for the Mezzana Corti bridge and 10% difference for the Borgoforte pier. Finally, Holnbeck and McCarthy (2011) reported on the performance of a USGS sonar monitoring system at the I-90 Bridge over the Blackfoot River in Montana. A downstream dam was removed from this reach in 2008 resulting in an increase in the flow velocity through the bridge contraction. To monitor the performance of several scour countermeasures and to record the overall bed/foundation health, four sonar fathometers were installed on the two piers in the channel. A scour event of 1.2m was observed, which was later confirmed by a follow-up survey.

Sonar fathometers have shown the ability to record both maximum scour and refill, it is necessary therefore to evaluate their performance under typical natural channel conditions. Since the operation of the sonar device relies upon measuring the time when the echo signal is received, any false echoes recorded by the device can lead to errors in the measurements. These false echoes can occur due to air entrainment or debris in the channel. In addition to the field test discussed previously, Lagasse et al (1997) also conducted laboratory tests and showed that sonar fathometers are susceptible to air entrainment, which prevented the sonar device from determining the depth to the bed.



Similarly, DeFalco and Mele (2002) reported that during their field campaign, the sonar results often showed peaks in the time history data of approximately 5 m in depth, which were not correlated to scour but instead to the presence of air bubbles, sediment load and turbidity in the channels. Holnbeck and McCarthy (2011) reported that air entrainment and channel turbulence was responsible for failure of three out of the four installed sensors. Debris in the channel can also provide false echo signals, leading to errors in the sonar signal. To overcome this problem, Nassif et al. (2002) reported on the development of a debris detection algorithm that helped to eliminate false readings. In addition to the false readings that can occur from debris, sonar devices are also susceptible to debris damage. Cooper et al. (2000) reported that the sonar instrument itself was susceptible to debris, as was the cable to the data acquisition system. Indeed, in one case, the sensor and cable were completely removed from the pier due to debris impacting the hardware. In addition to debris damage, the environmental conditions that affect the speed of sound within the channel, including water temperature and salinity, can also affect the performance of sonar systems. At the John's Pass Bridge site in Florida, Lagasse et al. (1997) reported that it was necessary to correct the measured signal, with an average correction of 0.46 m, for these two parameters. Additionally, since the sonar pulse expands with distance from the transducer, the beam width may exceed the scour hole dimensions. It is then possible to have multiple echoes from the edge of the hole, the sides of the hole and the bottom of the scour hole itself. As part of the NCHRP 21-3 project, testing was conducted on the ability of a sonar unit to observe the scour hole. This was accomplished with a Lowrance X-25 sensor subjected to unit steps in depth in a

series of tests in a swimming pool. During the analysis, it was determined that the sonar unit recorded the depth at the center of the beam and not an average over the entire beam width (Lagasse et al., 1997). Finally, low levels of reliability from some sonar fathometer installations have been attributed to electronic interference issues and cross talk between multiple sensors (Mason and Sheppard, 1994).

As indicated previously, the sonar systems can provide reliable measurements of the river bottom including the maximum scour and refill during peak flow periods. Sonar systems, however, are also susceptible to the environmental conditions in the channel (i.e., salinity, temperature of the water, the amount of channel turbulence and air entrainment, electronic noise, debris-damage, false echoes, as well as size of the scour hole relative to the sonar beam). Some of these parameters can be accounted for by either calibration methods or measuring additional channel parameters, e.g., salinity and temperature, while other factors, such as debris, can cause device failure directly. Despite these complications, sonar devices are one of the most commonly deployed units because of their ability to record both maximum scour and refill.

#### 2.2.5 Time Domain Reflectometry

A time domain reflectometry (TDR) scour monitoring system consists of a coaxial cable and scour probe connected to an electro-magnetic pulse generator and signal analyzer; the latter component is referred to as the TDR device itself, which emits a sharp rising voltage pulse into the cable. As the pulse travels along the cable it encounters various changes in material surrounding the cable that cause reflections, which then travel back to the pulse emitter. The scour probe typically consists of two or

three metal rods of various thicknesses separated by a non-conducting material. The device employed by Yankielun and Zabilansky (1994) consisted of two black iron pipes of 3 cm in diameter and 86 cm in length with the ends held together with Plexiglas clamps. Yu and Yu (2011) used commercially available soil moisture probes, such as the Campbell Scientific CS605, consisting of three probes of 9.5 mm in diameter and 204 mm in length, spaced 66 mm apart. The TDR pulse emitting devices used in the literature vary from the Tektronic 1502 B, 1503C TDRs to the Campbell Scientific (CS) TDR100. Of these instruments, the currently commercially available unit is the CS TDR100, which employs a rising voltage pulse of 250 mV in amplitude that lasts for 14 microseconds. The rise time of the signal is less than 300 picoseconds (Campbell Scientific, 2011).

The EM pulse travelling through the TDR cable and scour probe will reflect a portion of the emitted pulse at each change in interface. These reflections occur due to changes in the cable/scour sensor itself and changes in the external medium surrounding the cable/probes, with a critical reflection occurring at the cable/scour probe interface. If the impedance of this interface is poorly matched, a large portion of the signal can be reflected back to the emitter, preventing a sufficient portion of the signal from entering the probe (Yankeilun and Zabilansky, 1999). Additional reflections will occur at the air/water interface (should it occur), at the water/sediment interface, and the end of the probe, see Figure 2.4.

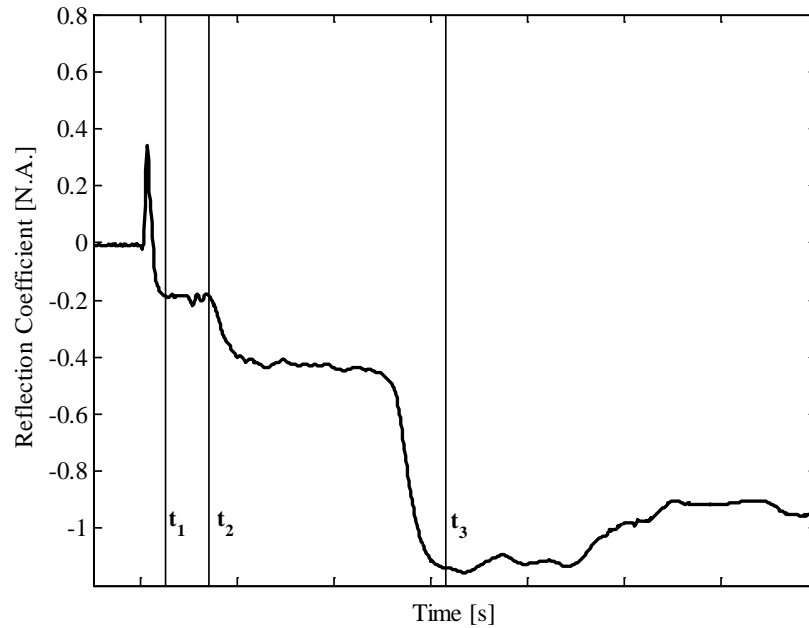


Figure 2.4 - Typical TDR waveform.

As with sonar device, the velocity of the EM pulse through the scour probe depends upon the material surrounding the probe. The EM pulse is affected by the apparent dielectric constant,  $K_A$ , of the media, through which it travels. In some media the pulse will travel faster than in others. The actual travel speed of the pulse,  $v$ , is the ratio of the speed of light in a vacuum,  $c_L$ , to the square root of the dielectric constant, as shown in Equation (2.2) (Yankeilun and Zabilansky, 1999).

$$v = \frac{c_L}{\sqrt{K_A}} \quad (2.2)$$

If the speed of the pulse is known, then the depth to the sediment can be determined by analyzing the TDR signal for the time when the reflection occurs from the start of the probe,  $t_1$ , the water/sediment interface,  $t_2$ , and the end of the probe,  $t_3$ , as shown in Figure 2.4. For each point in the waveform in Figure 2.4, the pulse travels from

the TDR emitter, to the point of the reflection, and then the reflected wave travels back to the TDR unit, covering twice the physical distance to this interface. Therefore, assuming that the wave travels at the speed of light, then the product of one half of the travel time from points 1 to 2 in Figure 2.4, and the speed of light represents the distance covered during this period, known as the apparent length of the probe in the water,  $L_{A1}$ . The length is called the apparent length since it assumes that the pulse traveled at the speed of light. A similar expression for the apparent length of the probe in the sediment,  $L_{A2}$ , is computed from the product of the speed of light with one half of the travel time  $t_3 - t_2$ . Both of these apparent lengths are related to the actual length by the apparent dielectric constant of the water and saturated sediment,  $K_{A,W}$  and  $K_{A,S}$  respectively, (Yankeilun and Zabilansky, 1999), as shown in Equations (2.3) and (2.4).

$$L_1 = \frac{L_{A1}}{\sqrt{K_{A,W}}} \quad (2.3)$$

$$L_2 = \frac{L_{A2}}{\sqrt{K_{A,S}}} \quad (2.4)$$

To determine the actual lengths, it is necessary to know the values of the apparent dielectric constants for each medium. While it has been argued that the value for water is relatively constant, the value for the sediment is dependent upon the nature of the riverbed and cannot be known *a priori*. Therefore, for the three unknowns,  $L_1$ ,  $L_2$ , and  $K_{A,S}$ , it is necessary to add an additional equation. Two equations are available, either based upon the total apparent length,  $L_A$ , or the physical lengths,  $L$ , of the probe, as

shown in Equations (2.5) and (2.6) provided by 0. The apparent length,  $L_A$ , is based upon the travel time  $t_3 - t_1$  and the speed of light.

$$L_A = L_1\sqrt{K_{A,W}} + L_2\sqrt{K_{A,S}} \quad (2.5)$$

$$L = L_1 + L_2 \quad (2.6)$$

In the method outlined above, an apparent dielectric constant for the water in the channel must be assumed. Yu and Yu (2011) developed another method that calibrates the response of the TDR signal/system for the conditions expected in the field. Their method is based on the volumetric mixing model for dielectric materials by Birchak et al. (1974), which defines the apparent dielectric constant of the mixture,  $K_M$ , as the sum of the product of the volume fractions of each layers,  $f_i$ , with the apparent dielectric constant for that layer,  $K_i$ , as shown in Equation (2.7).

$$\sqrt{K_M} = f_1\sqrt{K_1} + (1 - f_1)\sqrt{K_2} \quad (2.7)$$

Yu and Yu (2011) extended this model to the water and saturated sediment surrounding a TDR probe by replacing the volume fractions with the lengths of each layer, which is valid assuming that the EM pulse passes through the same interface area in each layer. To use the model, as shown in Equation (2.8), the mixture dielectric constant is necessary, which can be found from the TDR waveform as the ratio of the apparent length to the physical length of the total probe.

$$L\sqrt{K_M} = L_1\sqrt{K_{A,W}} + L_2\sqrt{K_{A,S}} \quad (2.8)$$

Using Equation (2.6), Yu and Yu (2011) manipulated Equation (2.8) into a linear form that can be calibrated to the specific sediment in place in the riverbed, the modified

form of which is shown in Equation (2.9), where  $X_R$  is the ratio of the sediment length to the total probe length.

$$\frac{\sqrt{K_M}}{\sqrt{K_{A,W}}} = X_R \left( \frac{\sqrt{K_{A,S}}}{\sqrt{K_{A,W}}} - 1 \right) + 1 = aX_R + b \quad (2.9)$$

Using this model, it is possible to measure the slope of Equation (2.9) experimentally by using sediments similar to those in the riverbed as a calibration test. Such measurements require measuring the apparent dielectric constant of the water and the saturated sediment for different layer lengths. Yu and Yu (2011) also developed a method to calculate the slope of the Equation (2.9), again using the Birchak et al. (1974) volumetric model, but here they applied it to the saturated sediment only, as shown in Equation (2.10). The additional parameters introduced include the porosity of the sediment,  $n$ , and the apparent dielectric constant of the dry sediment,  $K_{A,DS}$ . This model assumes that the porosity and apparent dielectric constant of the dry sediment are known for the riverbed material from sediment surveys of the riverbed.

$$\sqrt{K_{A,S}} = n\sqrt{K_{A,W}} + (1-n)\sqrt{K_{A,DS}} \quad (2.10)$$

In addition to providing the soil/water interface location, the measurements made with a TDR system can also reveal information about the soil properties. Topp et al. (1980) showed that the volumetric water content,  $\theta$ , of the soil/sediment could be calculated from the dielectric constant, as shown in Equation (2.11). Similarly, Drnevich et al. (2001) showed that the gravimetric water content,  $w$ , could also be determined from the measured dielectric constant of the sediment layer, provided that the dry soil density,  $\rho_D$ , is known, as shown in Equation (2.12). They also hypothesize that for most

soils, the values for the constants  $a$  and  $b$  in Equation (2.12) are approximately 1 and 8, respectively. These two water content relationships are related as shown in Equation (2.13), where  $\rho_w$  is the density of water.

$$\theta = 4.3 \cdot 10^{-6} K_A^3 - 5.5 \cdot 10^{-4} K_A^2 + 2.92 \cdot 10^{-2} K_A - 5.3 \cdot 10^{-2} \quad (2.11)$$

$$w = \frac{1}{b} \left( \frac{\rho_w}{\rho_D} \sqrt{K_A} - a \right) \quad (2.12)$$

$$w = \theta \frac{\rho_w}{\rho_D} \quad (2.13)$$

The laboratory and field performance of TDR probe under various environmental factors must also be evaluated. Yankielun and Zabilansky (1999) validated their method, Equations (2.5) and (2.6), in the laboratory for several sediment types, from sand to pea gravel to cobble stones. The results from the experiments conducted revealed that for depths up to 1 m, the linearity of the results were within 5-7% of the independently measured scour depth. Similarly, in the tests conducted by Yu and Zabilansky (2006), the TDR and independently measured lengths of the sediment were well correlated, with a linear fit through the data yielding an  $R^2$  value of 99 %. Using the second measurement method, Equation (2.9), Yu and Yu (2011) showed that for a saturated sediment constant of 6, the slope measured experimentally and the slope calculated using Equation (2.9) fell within a 5% range of error. In addition to the measured sediment depth, Yu and Yu (2006) also tested the performance of the methods for predicting the soil properties for volumetric and gravimetric moisture contents in the range of 0.023 to 0.145 and 0.014 to 0.092, respectively, and found reasonable agreement between the TDR and independently measured parameters. The listed mean squares of the errors were on the order of  $10^{-3}$  with



equally small standard deviations of the errors listed. An analysis of these results determined that the percentage error for the values listed varied greatly for different soil conditions from as little as less than one percent to as much as several tens of percent and beyond. While the available literature on TDR systems performance in laboratory and simulated cases is extensive, there is limited field performance data. The US Army Corps tested seven TDR probes to record the impact of ice formation on channel stability on the Highway 16 Bridge in Missouri, as reported in Zabilansky and Ettema (2002) and Ettema and Zabilansky (2004), and observed several instances of scour and refill on the order of 0.15 m (0.5 ft).

While the experimental results have shown primarily that the TDR device works well in the laboratory, it is necessary to consider conditions that can occur in the field that can impact the performance of the method. These include the variability of the sediment dielectric constants present in natural channels, and the impact of water salinity and temperature. To consider the impact of the riverbed conditions on the 2<sup>nd</sup> post processing method, Equation (2.9), it is possible to evaluate the impact of the dry sediment dielectric constant on the results. Yu and Yu (2011) used a value of 6 for the dry sediment, though the range can vary from 3 to 8 (Yankielun and Zabilansky, 1999). If the full range of the apparent dielectric constant of the dry sediment is used, the slope can vary by 6 to 11%, versus the data from Yu and Yu (2011). Such discrepancies indicate that in order to use the linear slope model, the system must either be calibrated onsite with the actual sediment in the riverbed or samples must be obtained so as to determine the actual value for the dry sediment, thus enabling an off-site calibration of the data. Also, given that

scour hole refill typically consists of a material of a different porosity (and sediment type), the ability to record significant refill with the linear fit method should be verified experimentally. In addition to the impact of sediment, TDR results can also be influenced by the water conditions. Yu and Yu (2011) tested the performance of the TDR probe in saline solutions up to 750 parts per million (PPM) sodium chloride. Based on the tests, the TDR results typically fell within 5% of the independently measured results, however, some conditions exceeded this 5% error range. It should be noted that the salinity range tested is limited, since in estuarine environments, the specific conductance, a measure of the salinity, can vary from a yearly average of approximately 100  $\mu\text{S}/\text{cm}$  to a maximum of 25,000  $\mu\text{S}/\text{cm}$  corresponding to approximately 50 to 17,500 parts per million concentration (USGS, 2006a; USGS, 2006b), well above the range tested in the laboratory. Thus the salinity conditions tested in the laboratory are below those expected in the field, which does not guarantee performance. The temperature effect can be evaluated theoretically by adjusting the dielectric constant for the temperature in the channel, using, for example, the dielectric constant model developed by Stogryn (1971). For arguments sake, if a 0.8 m scour probe is buried 0.7 m deep in sediment, the percent error in the results when the temperature change is not accounted for can amount to 7% for a temperature change of 20 °C.

Though TDR systems can provide detailed information about the riverbed condition including the water/sediment interface, the soil dielectric constant and the volumetric constant, water and sediment based parameter must either be known or

assumed. These assumptions, whether they are for the dielectric constant of the sediment or the water, can result in errors between 5 and 10%.

### 2.2.6 Fiber Optics

Fiber optic sensors have been used as method for undertaking scour measurement in recent years, consisting of either wavelength or intensity based measurement methods. Wavelength based devices are the most common type of fiber optic sensor employed for scour analysis and include the devices developed by Ansari (2010) and Lin et al. (2004; 2006), which are discussed after a brief overview of the physical operation of wavelength and intensity based fiber optic methods. The wavelength based sensors consist of Fiber Bragg Gratings (FBG) that consist of a length of the fiber, in which a series of periodic changes to the refractive index of the fiber core have been altered. When broadband light is incident to the FBG, based upon the pitch of the FBG, the reflected light is narrowband with a discrete, measureable wavelength. The reflected wavelength then shifts when the FBG is strained, and is correlated to the amount of strain in the fiber, as shown in Equation (2.14) (Guemes and Menendez, 2006; Manzoni et al., 2011a). The wavelength shift,  $\Delta\lambda_R$ , is related to the original reflected wavelength and the amount of mechanical and thermal strain in the fiber,  $\varepsilon_M$  and  $\varepsilon_T$ , respectively. A gauge specific constant,  $K_G$ , is used to calibrate the device. Additionally, it is necessary to consider the thermal strain in the fiber, given by the linear expansion coefficient of the refractive index,  $\alpha_F$ , and the temperature change,  $\Delta T$ .

$$\frac{\Delta\lambda_R}{\lambda_R} = K_G (\varepsilon_M + \varepsilon_T) + \alpha_F \Delta T \quad (2.14)$$

In contrast to measuring the reflected wavelength, intensity based measurements compare the amount of light emitted into the fiber relative to the amount reflected back from the fiber termination. Based upon Fresnel's Law, it is possible to predict the reflection index,  $R$ , based upon the refractive index of the core and the external environment at the fiber termination,  $n_{CORE}$  and  $n_{ENV}$  respectively, as shown in (2.15) (Guemes and Menendez, 2006).

$$R = \left( \frac{n_{CORE}/n_{ENV} - 1}{n_{CORE}/n_{ENV} + 1} \right)^2 \quad (2.15)$$

In order to apply these two techniques to monitor scour, several researchers have developed methods that utilize fiber sensors in instruments buried in the riverbed. FBG based devices will be reviewed first, followed by intensity based methods. Ansari (2010) developed an instrument consisting of a buried rod instrumented with FBG sensors acting as dynamic strain gauges. The rod vibrates at a certain natural frequency depending upon the depth of burial, which can be predicted based upon material and geometric properties of the rod and surrounding soil. As the scour hole develops, the length of rod that is buried will decrease and the natural frequency of the rod will change. In order to relate the change in natural frequency to the amount of exposed rod, the method proposed by Ansari (2010) relies upon the use of a finite element model for calibration. Lin et al. (2004; 2006) proposed several additional measurement techniques that employ FBG sensors. In the first configuration, sensors are attached at discrete points along a flexible

rod buried in the riverbed. As the rod is uncovered due to scour, it deflects with the flow, inducing a strain in the FBG sensors located further down the rod. The depth can then be recorded by the distribution of strain along the rod. In the second configuration, a series of thin, cantilevered plates are distributed on a rod covering the length of the pier. The deflection of the plates is greater in the flow than in the sediment, thus the scouring process can be recorded by monitoring the time history of the strain distribution along the rod. A modified version of the second device was developed by Lin et al. (2006) and deployed on bridges in Taiwan. This modified approach consists of encasing the FBG sensors in a button housing that deflects due to the water pressure, causing strain on the FBG. The arrays of FBG units are housed within two concrete-steel tubes (CSTs) for protection of the fiber. By measuring the strain of each FBG along the length of the CSTs, it is possible to determine which positions are surrounded by water, and therefore it is possible to locate the riverbed surface.

In addition to the wavelength based devices, a scour monitoring device that exploits the intensity based method was proposed by Isley et al. (2006) and consists of a rod with multiple fibers embedded within. These fibers terminate into the surrounding media at discrete points along the length of the rod. By monitoring the intensity of the light reflected back in each fiber, it is possible to distinguish whether the material surrounding each fiber termination is water or sediment.

Considering the experimental performance of the FBG units, Ansari (2010) reported on both laboratory and field results of the dynamic FBG based method that monitored the natural frequency of a buried rod. The laboratory tests were conducted in a

tank with a sediment layer submerged in flowing water, circulated by a pump. Bed material was removed and deposited from the region surrounding the rod to simulate scour and refill, which was measured by the rod and independently by a fixed, graduated ruler. Based upon the measured results, the correlation coefficients ( $R^2$ ) of the rod based to actual scour hole depths were 0.89 and 0.96 for the degradation and aggradation process, respectively. Two short term field tests were also conducted, the results of which indicated that the device was able to resolve the riverbed surface location to within 0.0254 m (Ansari, 2010). Laboratory and field experiments were conducted on the various systems developed by Lin et al. (2004; 2006). The results for the cantilevered rod approach revealed that the amount of strain recorded by an FBG, as it was exposed, resulted in a step change in the strain signal, however this change was small compared to the apparent noise in the signal. For the cantilevered plate method, the laboratory results indicated that the presence of water flowing around the plate resulted in a step change of 0.02 nm in the reflected wavelength, while the increase in strain due to scour only added an additional 0.005 nm, again resulting in a small signal-to-noise ratio. Lin et al. (2004) reported on the performance of the cantilevered plate based FBG system during the I-Li Typhoon in August of 2004, however, only wavelength shifts were reported, and not actual scour depths, nor was any attempt made to correlate the FBG results with an independent scour measurement. Lastly, Lin et al. (2006) also reported the performance of the CST based method during Typhon Aere in 2004. One CST was installed upstream of pier 12 and an additional unit was located downstream of the same pier on the Dadu Bridge over the Wu River in Taiwan. During Typhoon Aere, the upstream CST recorded

the development and refill of a 3 m scour hole while the downstream unit recorded a 0.5 m scour hole. As with the other field installation, no independent scour monitoring device was deployed to verify these results. Lastly, for the intensity based scour monitoring technique, Isley et al. (2006) reported the results of various laboratory experiments. The results showed that while the device could distinguish if the surrounding material was water or sediment, it was not able to distinguish the sediment/water interface when the water was a turbid mix.

Performance data for the various fiber optic based scour monitoring devices is limited, thus evaluating the reliability of the device in changing environmental conditions from field data is not possible. It can be postulated, however, what the potential impacts that various conditions could have on the performance of the various fiber optic based scour monitoring methods. Beginning with the natural frequency based method proposed by Ansari (2010), the main weakness of the approach lies in the reliance upon a finite element model to correlate the natural frequency to the depth of burial. Since the riverbed material will change from site to site (and even within a site) the accuracy of the finite element model for each particular installation location must be assured before the results can be deemed reliable. Additionally, the natural frequency of the rod can change for reasons unrelated to the development of a scour hole, such as temperature changes of the rod or water; thus the monitoring of the natural frequency as a means of determining the scour depth is complicated. Similarly, the responses of the FBG based methods proposed by Lin et al. (2004; 2006) were shown in the laboratory experiments to be sensitive to the flow temperature. Additionally, the cantilevered beam method will have limited

performance during a refill event, since it will remain in its deflected shape. Finally, as with most rod based devices, any instrument located in the channel has the potential to suffer from debris impact damage. Given the protection provided by the CST housing, it is likely that this device could withstand field deployment for long term monitoring campaigns.

Overall, both the laboratory and field performance data suggest that it is possible to undertake scour measurements with fiber optic techniques. While the FBG sensors cannot record scour alone, it is possible to develop devices that transfer the change in the bed conditions to strain on the sensor. These devices are subject to debris impact damage, as are other rod based devices, however it is possible to provide additional protection, as with the CSTs. The natural frequency based method proposed by Ansari (2010) is also dependent upon the accuracy of the field calibration and potentially the temperature. Lastly, the intensity based methods fail to perform in turbid water, a common characteristic of natural channels.

### 2.2.7 Temperature Measurements

Temperature variations across a riverbed have also been used to measure the water/sediment interface and thus, scour. Camp et al. (1998) developed a thermocouple based scour monitoring system consisting of a series of thermocouples located every five cm along a partially buried rod. The device operates on the premise that the water temperature in the saturated sediment is at a consistently lower value than the water in a river channel. Thus, by measuring the temperature gradient along the length of the rod, it is possible to determine the location of the riverbed, and the amount of scour. In addition



to the thermocouple based measurement methods, a novel method developed by Manzoni et al. (2011a; 2011b) utilized FBG sensors as thermocouples instrumented along the length of a rod buried in the sediment. A heating element located next to each FBG on the rod is activated periodically, leading to a temperature change within the fiber. The fibers in the sediment are surrounded by stagnant, saturated sediment and the only source of heat loss is via conduction into the surrounding media. For the FBGs in the flow, the dominant heat loss mechanism is accomplished via convection. As such, the rate of heat loss in the flow exceeds the heat loss occurring in the sediment. Therefore, for a uniform heat load, the steady state temperature change between unheated and heated states in the sediment will exceed the temperature change in the portion of the rod in the flow.

The thermocouple based method, developed by Camp et al. (1998), was tested in laboratory conditions and in a short term field operation. During the laboratory tests, the rod was partially buried in a tank of sediment while heated water flowed past the partially exposed upper portion of the device. The thermal gradient along the length of the pipe was measured and revealed that thermal diffusion of the water temperature into the bed only occurred in the upper 0.051 m of the sediment. Thus, by observing the location of the largest thermal gradient, it was possible to determine the location of the water/sediment interface. Additionally, as sediment was removed, the thermocouples recorded a temperature change from that of the sediment to that of the water. A field unit was also deployed and revealed a fluctuating time history for the thermocouples that corresponded with the atmospheric temperature fluctuations. The daily variation in the thermocouples located in the riverbed was of the order of 1.5 °C, while the

thermocouples in the flow varied from 5 to 7.5 °C (Camp et al., 1998). Despite this variation, it was still possible to determine the presence of the water/sediment interface and thus monitor scour. Manzoni et al. (2011a; 2011b) also reported the experimental verification in the laboratory of the heat load based method. They observed that for heat loads greater than 10-15 W/m, the resulting temperature change was large enough to be detected, with a 95% confidence, and that the uncertainty in the temperature difference measurements was  $\pm 1.72$  °C. The FBG sensors were also capable of recording the time constant associated with the transient temperature change that occurred at the start of the heating cycle. The laboratory results showed that for flow rates of 0.4 m/s, the time constant for the FBGs in the sediment was between 9 to 14 s while the time constant for the FBG sensors in the flow was 4-6 s, for 5-50 W/m. Thus, it was shown that heat load based method also provides a means of recording the water/sediment interface and could therefore monitor the development of a scour hole.

The research on temperature based scour measurements to date has focused on evaluating the feasibility of the methods, with only limited field performance data available. Despite this deficiency, it is possible to estimate the potential impact that changes in channel conditions will have on the two methods discussed previously. The environmental conditions that often affect the performance of scour monitoring methods are debris, turbidity, and the presence of a live bed. As with all scour monitoring methods anchored in the channel bed, any debris that impacts the device can damage the measurement rod or its attached power and data cables. The two temperature based methods are sensitive to this factor. Similarly, for water turbidity, it is expected that the

impact to either the temperature gradient or the step change in response to a fixed heat load will be minor, thus both measurements are expected to be relatively insensitive to the sediment load in the channel waters. If the channel conditions, however, are such that there is a live bed, it is possible that the presence of this mobile sediment layer will affect the thermal gradient between the channel and the riverbed. Since the live bed temperature is likely to be between the riverbed and channel flow temperatures, the sharpness of the thermal gradient may be lessened, and thus the determination of the point of maximum gradient, may become less distinct as this region increases in size. Without the experimental data from either the laboratory or the field, it is difficult to determine how significant this impact could be on the results. In a similar manner, the presence of a live bed around the heat load based scour measurement rod may also affect the step change and the time constant for any measurement points in the region of moving sediment. It is expected that these values will be between the channel flow and the riverbed, again making the exact point of the transition between the water and the sediment less distinct. Finally, for the heat load based method, the research to date has not considered at what minimum flow rates the temperature change between the sediment and the channel flow is still valid. Additionally, no attempt is made to correlate the flow speed with the time constant for the heated condition.

In summary, temperature based methods that exploit either the amount of heat lost or the natural temperature variation between the channel flow and riverbed are available to monitor scour. These devices have been tested in laboratory conditions to evaluate the feasibility of the methods. However, field data available to assess the performance of

temperature based methods in natural channels is scarce. However, it can be anticipated that debris impact to the hardware itself or the presence of a live bed are conditions that may affect both temperature based measurement devices.

#### 2.2.8 Piezoelectric Film Sensors

A novel sensor consisting of a flexible fin like structure attached to a rod has also been used to measure scour (Lagasse et al., 1997). A flexible piezoelectric film is attached to each fin that generates a voltage when subject to the turbulent fluctuations of the flow past the rod, which can be measured by a standard voltmeter or data logger. An instrumented rod with multiple films attached on the downstream side is then buried in the sediment around a pier. The sensors in the flow will vibrate, generating a measureable voltage, which in turn indicates the water/sediment interface location, see Figure 2.5.

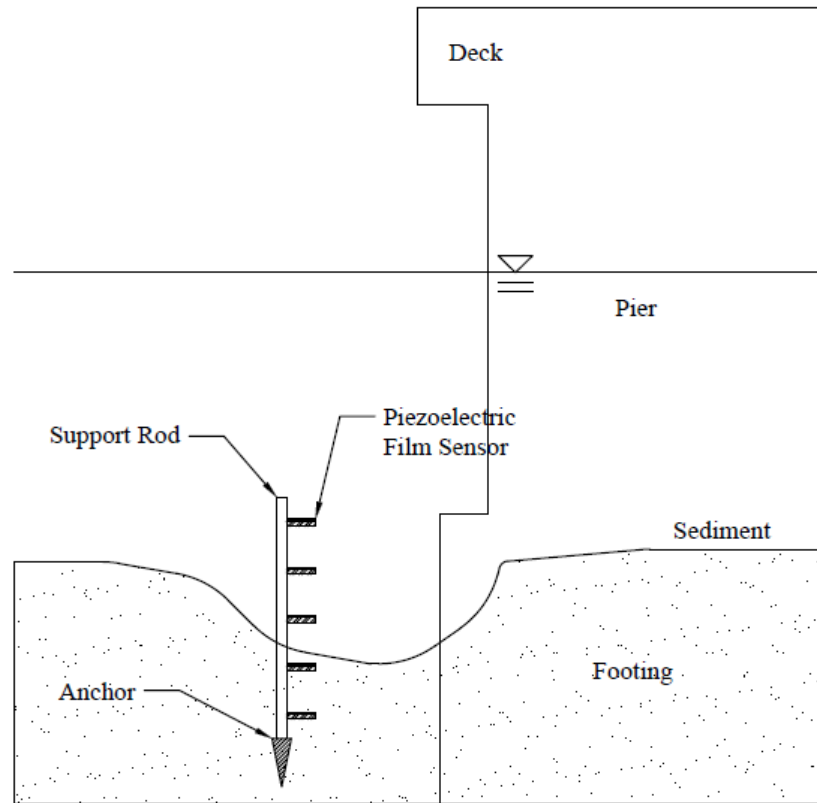


Figure 2.5 - Piezoelectric film sensor. Based upon Lagasse et al. (1997).

During laboratory testing, several additional measures were undertaken to improve the long-term survival rate of the devices with the optimal configuration being to bond the film sensor to a section of flexible silicone tubing (Lagasse et al., 1997). The devices were also field tested at the Orchard Bridge and Sandy River sites in Colorado as part of NCHRP project 21-3. At the Orchard Bridge site, a rod was instrumented with six sensors spaced 0.15 m apart for the bottom four sensors and 0.3 m apart for the top two sensors. During the testing, voltage readings were observed from all of the sensors. It was determined that the bridge structural vibrations lead to movements of all of the piezoelectric films, which caused erroneous results. The Sandy River site revealed the

ability to measure scour even after being hit by debris, however the USGS did not indicate the scour depth during this event.

In terms of environmental factors that can affect the device, it has already been shown that structural vibrations of the bridge can influence the reliability of the results. In addition, the piezoelectric film can de-bond from the fin or the device itself can degrade over time, leading to a failure of the sensor. In addition, as with any rod-based device, they also suffer from susceptibility to debris damage. The overall conclusion of the NCHRP project 21-3 was not to use these devices for future field tests.

#### 2.2.9 Mercury Tip Switches

A mercury tip switch system consists of commercially available mercury switches, with each switch composed of small chambers housing two terminals. The chamber contains a small amount of liquid mercury and is attached to a buried rod. As the switch is rotated, gravity pulls the mercury around the chamber and either closes or opens the circuit between the two terminals. In the scour application, the initial position of the sensors was such that it was folded up against the rod. As the scour hole develops, these switches are exposed and fold down, opening the circuit. By monitoring the condition of each circuit on the rod, it is possible to determine the depth of maximum scour in the riverbed. Due to the deployment of the switch during a scouring event, it is only possible to record the maximum scour with this device since the switch is not returned to its neutral position by the refill of material into the hole.

The laboratory test results of this device indicated that the switch often tripped as the scour depth approached the sensor position, but before the actual depth had reached

the sensor (Lagasse et al., 1997). This is likely due to the buoyant force of the chamber pushing out on the layer of soil holding it in place. An additional disadvantage of this device is that it contains mercury, which is a hazardous substance and should not be released into the environment. Due to the limitations of this device and due to the fear of environmental contamination, mercury tip switches were eliminated from further testing as part of the NCHRP project (Lagasse et al., 1997).

## **2.3 Distributed Scour Measurement Methods**

### 2.3.1 Radar

In addition to TDR, other techniques are available that employ electromagnetic (EM) waves. Specifically, a Ground Penetrating Radar (GPR) system uses the EM waves in a manner to which a sonar system uses sonic pulses. As with the sonar method, the waves reflect off of objects in the path of the wave. The radar system has emitting and receiving transducers, called antenna, to send and receive reflected EM waves, typically designated Tx and Rx, respectively. This technique has been adopted from traditional non-destructive testing (NDT) and geotechnical surveys methods and applied to scour monitoring. Typical NDT testing on concrete or masonry send EM pulses with frequencies in the range of 500 MHz to 1 GHz, while geotechnical surveys employ frequencies in the range of 50 to 300 MHz, the main difference being the desired resolution of the reflected signals (Millard et al., 1998). For NDT, a higher frequency signal is used in order to increase the resolution of the Radar image at the cost of depth of penetration. Geotechnical surveys, however, are focused on determining the nature of

various layers of soil/rock in the subsurface and are less critical of the resolution but more interested in maximizing the depth of propagation; hence, lower frequencies are employed. Both ranges have been employed in scour monitoring applications (Millard et al., 1998; Webb et al., 2000; Paczek and Haeni, 1995). As with the TDR system, the speed of propagation is governed by the dielectric constant of the medium through which the EM pulse is transmitted, see Equation (2.2). Thus, by knowing the time between emitting and receiving a reflection as well as the speed of light, the distance to the object that causes the reflection can be determined. GPR can provide an image of the riverbed, recording depth as the unit is traversed across the channel. Typically this can be accomplished at rates of 1 m/s for handheld units and up to 50 km/h for vehicle based systems (Manzoni et al., 2011b). The reflections are processed by the GPR unit into depths values by first assuming the EM wave propagated with the speed of light. These initial images are then reprocessed into actual depth values by accounting for the dielectric constant of the channel flow. Unlike the TDR method, it is necessary to use an assumed dielectric constant of water and river bed material, since the actual dielectric constant is not determined as part of the post processing. Given the unknown dielectric constant below the river bed, any depth values below the water/sediment interface are only relative values and cannot be regarded as true depths. For an open, unfilled scour hole this is not a hindrance to the method since the depth can be determined directly as the EM wave only travels in the water column. This is not the case, when the scour hole has been refilled with additional sediment, therefore it is only possible to qualitatively



observe the presence of a refilled scour hole, the magnitude of which cannot be quantified.

As mentioned previously, GPR systems have been deployed in NDT and geophysical site surveys. In order to evaluate the performance of GPS systems for scour monitoring, several laboratory and field measurements have been conducted to assess their performance. Millard et al. (1998) conducted laboratory tests using GPR to measure scour holes around concrete piers and to profile the sub bottom of a refilled scour hole. Though the GPR recorded the profile, no quantitative measure of the precision was provided. Also, the presence of the concrete pier resulted in additional reflections, complicating the results during the laboratory testing. In addition, they determined that the nature of the refill material can complicate the profile of a refilled scour. If the infill and riverbed materials have similar dielectric constants, it is difficult to discern the presence of a refilled scour hole. In field surveys conducted in the Dee, Ribble, Severn and Coln Rivers in the U.K, Millard et al. (1998) investigated the performance of various GPR frequencies of the GSSI SIR-2 system, which varied from 300 to 500, 900 MHz and 1 GHz. The reported results indicated that 300 and 500 MHz are optimal due to increased attenuation at higher frequencies, reducing the strength of the reflected wave. A scour hole was observed around a local bridge pier on the River Ribble and was confirmed with a sonar fathometer survey. However, a quantitative comparison of the two depths was not provided. In a report on the performance of a GPR unit at measuring scour holes and riverbed profiles at ten bridges in Missouri, Webb et al. (2000) used equipment consisting of a GSSI SIR-10B GPR unit with 200 MHz and 400 MHz antennas, which were

traversed across the channel either from the bridge deck or from a boat. Survey scans conducted at a rate of 50 scans per second with traces of 125 to 350 ns in length found that this method was adequate for measuring scour holes (holes up to 0.73 m deep were recorded), the presence of refilled scour holes, and in some cases multiple layers of scoured and refilled material in one hole. Similarly, in their study of the field performance of GPR and sonar systems on six bridges in Connecticut, Placzek and Haeni (1995) found that their GPR units were effective in measuring the refilled scour holes or subsurface gravel layers in the channel profiles. For the 80, 100 and 300 MHz units tested, the resolution achieved in the field were 0.76, 0.61 and 0.30 m, respectively, the corresponding penetration depths were reported to be 15, 12 and 3.0 m. into the sub bottom. The performance of the system was equivalent to the Continuous Seismic-Reflection Profilers (CSP) also employed in this field-testing program, which are discussed in a subsequent section.

One of the challenges in using a radar system for scour monitoring is that the speed is altered by changes in the temperature and salinity of the water column as discussed earlier for TDR. In addition to these effects, the attenuation coefficient of the medium,  $\alpha$ , is correlated to the conductivity. As the conductivity of the medium increases, so does the attenuation coefficient (see Table 2.1). The attenuation of the signal can be modeled as shown in Equation (2.16), where  $E_o$  is the initial signal amplitude, and  $E_x$  is the attenuated amplitude of the EM pulse at a depth  $d$ . Thus, in salt water the maximum depth is of the order of several centimeters, while Millard et al. (1998)

reported achieving measurements at depths of up to 8 m in freshwater river scour monitoring applications.

$$E_x = E_o e^{-\alpha d} \quad (2.16)$$

Table 2.1 - Soil Properties Pertinent for Radar EM Techniques, adapted from Millard et al. (1998)

Material	Dielectric Constant	Conductivity [S/m]	Attenuation Coefficient [m <sup>-1</sup> ]
Air	~1	0	0.0
Freshwater	77-87	10 <sup>-3</sup>	0.04
Saltwater	65-75	4	~74
Saturated Sand	15-25	10 <sup>-4</sup> - 10 <sup>-2</sup>	0.53
Saturated Clay	15-60	10 <sup>-1</sup> - 1	4.6
Gravel	22	0.02-0.025	2.1

In addition to the problems of attenuation in saline environments, none of the field measurements conducted to date have consisted of fixed GPR installations. Instead, all of the measurements have consisted of traversed systems, which are reliant on operators to reposition and monitor the equipment. Despite these challenges, the benefits of a GPR scour monitoring system lies in its capability to provide sub bottom information, including the presence of a scour hole even after refill has occurred. Temperature and salinity affects also pose problems, as with the TDR method. However, these effects can be accounted for by measuring the temperature and salinity in the river. Finally, in order to generate a 2D profile or a 3D contour, a means of tracking the unit across the channel is necessary, which adds complications for a long-term deployment of the scour monitoring system.

### 2.3.2 Bridge Vibration Measurements

The objective of all scour monitoring systems is to measure indicators of the bridge health in order to determine conditions, under which a bridge may become unstable. With traditional measurements, determining the margin to the stability limits is accomplished by comparing the current scour depth to a previously determined maximum allowable scour depth, which is based upon model or experimental data that indicates at what point the foundation becomes unreliable. Another approach, which focuses on determining the 'health' of the bridge pier directly, measures the ambient vibration of the bridge to assess changes in the vibration response resulting from a change in the foundation stability.

Samizo et al. (2007; 2011) developed a method for measuring the response of the bridge piers to microtremors, excitation forces derived from either man-made or natural sources that leads to a general background vibration of the bridge and surrounding sediment. The system consists of two vibration sensors located on the upstream and downstream sides of the bridge pier. The units measured the vibration of the bridge in three axes at 100 Hz for 5 minutes, occurring once every hour (Samizon et al., 2011). The measured vibrations were then transformed from the time domain into the frequency domain using a moving window with 2/3 overlap of 30 seconds each. The average spectral shape during the five minutes was monitored to observe changes in the natural frequencies of the pier, which were assumed to correspond to changes in its stability (Samizo et al., 2007). In a similar approach, Ko et al. (2011) proposed to monitor both the natural frequency of the bridge as well as changes in the mode shape, which they

argued could be attributed to changes in the amount of material surrounding the foundation, thus scour. Yao et al. (2011) proposed an additional vibration parameter that could be monitored to indicate changes in the pier foundation. Their approach consisted of computing the ratio of the root mean square (RMS) of each accelerometer axis with its orthogonal axes ( $\sqrt{\ddot{x}^2}/\sqrt{\ddot{y}^2}$ ,  $\sqrt{\ddot{x}^2}/\sqrt{\ddot{z}^2}$ , and  $\sqrt{\ddot{y}^2}/\sqrt{\ddot{z}^2}$ , for example).

Several field and laboratory experiments were conducted to evaluate the utility of the vibration based method to determine changes in the pier due to scour. Integral to the method proposed by Samizo et al. (2007; 2011) is the ability to use microtremors as the source of excitation for the pier, which then allows for the determination of the first natural frequency of the pier from the accelerometer measurements. This hypothesis was tested on bridge A (unidentified Japanese railway bridge), where the first natural frequency of the bridge was measured with both traditional impact and microtremor based measurements before and after a 4 m excavation, a simulated scour event. The impact testing results indicated that the natural frequency of the bridge shifted from 14.6 Hz in the unscoured condition to 5.9 Hz in the scoured condition. For the microtremor based measurements, the broad spectral response of the bridge in the unscoured condition was characterized by a lack of discernable peaks, while the scoured case exhibited a clearly distinct peak at 6 Hz. On a separate bridge, Bridge B, impact and microtremor testing on the bridge also revealed that the natural frequency were consistent with each other, 11.3 and 11.5 Hz, respectively (Samizo et al., 2007). They concluded that microtremors were capable of providing adequate input to the pier to excite the structure as well as indicating that the 1<sup>st</sup> natural frequency of the pier declined as the scour depth

increased. To verify these results, experiments were conducted on a model pier consisting of steel beams (3.85 m long) and a single concrete bridge pier (1.5 x 0.25 x 0.75 m) supported on a bed of crushed stone less than 20 mm in diameter (Samizo et al., 2011). Initially buried 0.5 m below the sediment surface, the stone surrounding the foundation was progressively removed in order to simulate various scour states. For both impact testing and microtremors, the results of the vibration testing for this model indicated that the first natural frequency of the bridge decreased with increasing amounts of pier foundation exposure. For the fully exposed foundation the natural frequencies declined by as much as 60 to 80%, depending upon the bearing capacity of the sediment, which was also varied (Samizo et al., 2011). In addition to this fundamental work on the use of pier natural frequencies to detect for scour, Ko et al. (2011) conducted field measurements on the Wensui and Hsichou Bridges in Taiwan. The measured results, the natural frequency and mode shape, were compared with a finite element model of the simply supported, single span bridge units for this site. The foundation was modeled with springs around the piers and the depth of support was varied to correspond to different scour events. During the model evaluation, it was determined that the horizontal-longitudinal (HL) and horizontal-transverse (HT) mode shapes were useful for determining scour. Measurements were then conducted on the two bridges in the field during various reconstruction efforts when the pier foundations were exposed by varying amounts. The measurements were conducted for 10 to 20 minutes on each bridge during non-peak traffic periods. The measurements were taken at a sampling rate of 200 Hz and the average spectra were computed using overlapped windows. For the Wensui Bridge,

two piers were partially exposed with Pier Three (P3) being exposed 6-7 m while Pier Two (P2) was only partially exposed. The spectral response, in the HT direction, showed a peak at 1.7 Hz for both piers. The response on P3 had a larger amplitude compared to P2, indicating more scour at this location than on P2. For the Hsichou Bridge, Pier 36 (P36) was exposed 4.5 m and 7.5 m before and during renovations on the bridge. The HT spectral response indicated a frequency of 2 and 1.5 Hz for the 4.5 and 7.5 m exposed cases, a shift of 20%. Yao et al. (2011) also reported on the use of vibration sensors to monitor bridge pier health during laboratory and field experiments in Texas. During the laboratory testing, a simulated pier was instrumented with three axis accelerometers, sampling at 124 Hz. The first natural frequency of the pier in each direction was monitored during a transient scour event along with the ratio of the RMS time histories of each axis. The results indicated a shift in the first vertical natural frequency after the initial formation of the scour hole. In addition, the RMS ratios for the main flow direction versus the lateral direction and for the main flow direction versus the vertical direction showed a shift when the scour hole reached the base of the foundation, at which point an ancillary tilt meter detected settling of the pier.

From the various laboratory and field tests conducted it is possible to conclude that the proposed methods show promise in determining the changes in the health of the bridge pier associated with scour. Various factors, can affect the measured vibration characteristics including changes in the flow rate, the ambient temperature, and potentially the background vibration level. Samizo et al. (2007; 2011) addressed the first of these conditions by conducting long-term experiments on Bridge B and D

(unidentified Japanese railway bridges) to determine the relationship between the flow rate and the natural frequency of the pier. On Bridge B, the spectral shape at low and high flow rates consisted of similar natural frequency peaks, with the only difference being the amplitude of various peaks. This result indicated that as the flow rate increases, the amplitudes of the main peaks become increasingly apparent improving the ability to detect changes during high flow periods typically associated with rapid scour hole formation (Samizo et al., 2007). Bridge D spectra results indicated that the peak frequency from the microtremor measurements occurred between 2.5 and 3 Hz for low and high flow rates, respectively. Additional modes occurring at 3.1 and 2.8 Hz, determined during impact testing on bridge D, made it impossible to assign a particular frequency to the pier (Samizo et al., 2007). Despite this complication, the overall trend observed on Bridge D indicated a convergence of microtremor results with a corresponding increase in water depth. These results suggest that as the flooding progresses, the pier natural frequency increases in amplitude and become more apparent. Thus, a shift occurring in this frequency during a flood is a likely indicator that scour has occurred. Additional field measurements were conducted by Yao et al. (2011) on the US 59 Bridge over the Guadalupe River and the SH 80 Bridge over the San Antonio River in Texas. The reported results indicated that the RMS ratio was the only vibration based measurement that yielded usable results on the US 59 Bridge. The ability to detect the natural frequencies was complicated due to background noise from traffic. For the SH 80 Bridge, the data was reportedly unusable and the vibration-based systems were removed in favor of tilt sensors. In addition to problems with the background noise, variations in



the ambient temperature, traffic loading or possible migration of the main channel in the river can lead to changes in the natural frequency of a pier that are unrelated to scour. While it is possible, to decouple these shifts from those due to scour, this is a complicated endeavor that requires sophisticated pattern recognition techniques. Therefore, monitoring just the natural frequency and mode shape alone as the sole indication of the formation of a scour hole is complicated at best.

Overall, the results of the various vibration-based measurements indicate the potential for using microtremors to monitor the health of the pier directly. The main challenge is to determine which of the frequencies can be associated with the pier itself. It is necessary to have a distinct peak for the pier that can be monitored over time. The RMS ratio of the various axes also proved useful in the lab, with only limited success in the field. Additionally, monitoring the natural frequency and making a correlation to scour depth is complicated at best since changes in measured frequencies can occur from temperature variations, changes in traffic or loading patterns, wind loading patterns, etc., that make a direct cause and effect relationship difficult to quantify.

### 2.3.3 Advanced Sonar Techniques

In addition to the standard fixed fathometers discussed previously, there are other sonar based systems that can be deployed that provide detailed information about the riverbed. These vary from fixed frequency fathometers that are tracked during a traverse to provide a profile, Side Scan Sonar units, Sector Scanning Sonar, Lens Based Multi-Beam Sonar, and Continuous Seismic-Reflection Profilers (CSP). Each of these units will

be discussed briefly below, along with a summary of their performance in various field tests.

Fixed fathometer units only provide information about the bed depth at one position. To overcome this, it is possible to traverse the sonar unit across the channel, either in a boat or from the bridge deck. In either case, an additional tracking unit is required, and is typically accomplished with robotic/automatic total-stations. However, this additional equipment is not well suited for long-term monitoring of scour hole formation. Side-Scan Sonar can achieve a 2-D profile and consist of a linear array of sonar units, resulting in a sonar pulse that is narrow in the azimuthal direction (direction of travel of the sonar unit) while it is very wide in the elevation direction (Spindel, 1998). Typically these units also employ a 2<sup>nd</sup> array of units to act as a receiving array to allow for differential time measurements, and thus depths. The frequencies employed typically range from 80 to 800 KHz (Browne, 2011). The wide angle of the sonar beam allows for a quick survey of a large profile and if used in a fixed orientation does not require a traverse to provide a 2D profile. Typically, the units are deployed from a boat in the channel and allow for the determination of a 3D contour of the riverbed. While the additional information is beneficial it is also complicated by the need to account for the position of the unit with time and for roll and pitch of the boat or float housing the unit. A modification to the Side-Scan Sonar technique is the Sector-Scanning Sonar method, which employs a fan shaped acoustic pulse from a rotating head. The unit emits a pulse, waits for a set period to receive the reflected signals, and then rotates to a new position and repeats the measurement. Post-processing of the reflections permits the determination

of 2D channel bottom images. These units typically operate in the 330 KHz to 2.25 MHz range with the most commonly deployed units operating at 675 KHz (Browne, 2011). Hayden and Puleo (2011) have proposed a two unit scanning sonar arrangement that can be installed on bridge piers and utilize 250 KH transducers with a beam width of 3°, housed inside an oil filled lenses. The units are mounted to motors that can rotate 180° in both azimuth and tilt, leading to a full hemispherical view of the river bottom. The device records 40,000 data points during the measurement sequence which are then interpolated onto a 2 x 2 m grid to provide a full 3D contour map of the scour hole development over the entire channel bed. The final advanced sonar technique that has been deployed in the field to measure scour holes around bridge elements is the Continuous Seismic-Reflection Profilers (CSP) unit, which has been adopted from geotechnical surveys. The main difference between these sonar units and standard fixed fathometers is the operating frequency of the acoustic pulse. CSP units typically operate in the 2-20 KHz range as opposed to the 50 to 300 KHz range registered by fathometers (Placzek and Haeni, 1995). This lower frequency means that less of the signal is attenuated and stronger reflections are obtained from subsurface features in the riverbed. In addition, CSP units employ either fixed or variable frequencies, called chirp frequencies. The fixed units typically come in 3.5, 7 and 14 KHz units while chirp CSP units typically use an increasing frequency pulse from 2 to 16 KHz (Placzek and Haeni, 1995). The variable frequency units combine the benefits of a low frequency CSP, i.e., greater depth penetration, with the improved accuracy of a higher frequency CSP. The downsides of the variable

frequency are multiple side lobes and a subsequent increase in noise due to scatter from piers, etc. (Browne, 2011).

While the physical principles behind the operation of the advanced sonar techniques are not significantly different from that of a fixed fathometer, it is still useful to review the field performance of these devices. Beginning with the side-scan sonar systems, Eilertsen and Hansen (2008) reported the use of one such device for measuring general river scour in the Øyeren Delta in Norway. The system used a 250 KHz Geoswath interferometric side-scan sonar to record both depth and the amount of reflected signal, which can be correlated to the sediment type. Fourteen scour events were recorded throughout the delta with the largest being a 24 m deep scour hole adjacent to a sandbar that constricted the main channel flow. Hayden and Puleo (2011) reported on the deployment of two lens based sonar systems on the Indian River Inlet in Delaware, which is a scour prone site. Throughout their field campaign, the performance of this system was compared with both Army Corp of Engineers (USACE) and University of Delaware surveys conducted with a 500 KHz, single unit fathometer linked with a GPS unit and motion tracker. While the USACE data was conducted three years prior to the installation of the two sensors, the interpolated dataset indicated that 82% of the results were within 3 m of the each other. Using the University of Delaware data conducted on the same date as a dataset from the two scanning units resulted in a linear correlation with a slope of 0.98 and an  $R^2$  value of 0.84, indicating a well correlated data set. Lastly, Placzek and Haeni (1995) conducted several field tests of multiple sonar and GPR technologies at six bridges in Connecticut. At the Old Baldwin Bridge over the Connecticut River, a 200

kHz fathometer survey was conducted that revealed several scour holes around the bridge piers. A 3.0 m hole was recorded upstream of a pier, which was then surveyed with a 3.5 kHz CSP system and measured a 0.61 m gravel refill layer. Similar measurements were conducted on the replacement for the old Baldwin Bridge and indicated 6.4 and 4.6 m scour holes on the bridge piers (200 KHz Fathometer), which was confirmed by a 3.5 KHz fixed frequency CSP survey that also indicated 1.5 m of refill in a scour hole upstream of one of the bridge piers that was not detected by the fathometer. A swept frequency CSP unit was also used to survey the same bridge as the fixed frequency unit and indicated the same results, with an improved accuracy. The I-84 Buckley Bridge over the Connecticut River was also surveyed as part of this USGS project. The 200 KHz fathometer survey revealed the presence of a 15 m by 46 m scour hole upstream of pier four. The survey data was used to generate a 3D contour of the riverbed and scour hole. CSP units and a 100 MHz GPR was also deployed on this site and confirmed the fathometer results, adding details on the amount of refill through the bridge section. Two additional bridges were surveyed with fathometers and CSP units and indicated the presence of scour holes without any refill material or significant sub bottom characteristics. The overall performance results of the Placzek and Haeni (1995) testing revealed that the 20 and 200 KHz fathometers had a resolution of 0.30 and 0.15 m, respectively, while the CSP performance indicated a resolution of 0.30, 0.60, 0.76 and 0.3 m for the 14, 7, 3.5 and 2 KHz units, respectively. The depth of penetration into the bed varied from 6.1, 7.62, 15 and 15 m for the same CSP units, respectively (Placzek and Haeni, 1995).

In regards to environmental conditions that can influence the results, only one research team reported on the performance of the advanced sonar techniques under non-ideal conditions. Hayden and Puleo (2011) attributed some of the variability in the measured datasets for the Indian River Inlet to the nature of the active bed and the turbidity of the inlet. In addition to the impact of a live bed on the measured results, the amount of time required for post-processing of the signal was not indicated, and only daily recordings were indicated. Since a long term monitoring campaign necessitates obtaining multiple measurements within an hour, the frequency of the measurements must be increased before the system can be used for long term monitoring. In addition to these factors, since the operation of the devices considered is very similar to that of standard fathometers, factors that affect the performance of the latter, such as temperature, salinity, and debris, may also impact the results obtained with the advanced sonar techniques.

Overall, the advanced sonar techniques provide additional information about the riverbed, such as 2D and 3D profiles, as well as sub bottom information and refill. Typically, these systems either require a tracking unit and traverse or complicated data interpolation routines. With the exception of the installation of the two lens-based sonar units on the Indian River Inlet, none of the instruments discussed have been deployed for long term monitoring.

## **2.4 Summary**

The Failure Modes and Effects Analysis (FMEA), often used in evaluating product designs, can be used by engineers in the design of a scour monitoring system

considering the potential factors that can influence the field performance. The FMEA consists of evaluating a system or device against a known failure mode. For each failure mode, the effects of the failure are reviewed and given a severity rating (SEV) between 1 – 10, with one being a failure mode that has little effect, and ten being a failure that prevents the ability to monitor scour entirely. After evaluating the severity of the failure mode, the likelihood of occurrence is evaluated next (OCC) and also given a rating on a 1 – 10 scale. Next, the ability of the system or operator to detect the failure mode (DET) is assessed. Scores are given to the detectability also on a scale of 1 – 10. The three ratings, SEV, OCC and DET are then multiplied together to come up with a Risk Priority Number (RPN). This RPN can then be used to evaluate the potential failure modes for the scour monitoring installation and highlights the areas that should be considered before any field installation begins. The identification of these risk remediation efforts is a critical aspect of the FMEA. Ranking scales for each of the FMEA components are identified in Table 2.2, Table 2.3, and Table 2.4, followed by an example analysis on a hypothetical TDR based scour monitoring system in Table 2.5. Through FMEA, it is possible to utilize the information discussed previously for each measurement system to determine their ability to monitor scour under intended field conditions.

Table 2.2 - Proposed Severity Ratings for FMEA Analysis of Scour Monitoring System.

Ranking	Severity Rating
1	Impact to scour monitoring system is minor
2-4	Increasing inaccuracies in measured scour results
5	Scour results are available. Magnitude may be incorrect
6-9	As failure mode increases, results become harder to obtain
10	Scour results not available

Table 2.3 - Proposed Occurrence Ratings for FMEA Analysis of Scour Monitoring System.

Ranking	Occurrence Rating
1	Event with a 50 yr. return period (P=0.02)
2-4	Increasing probability of event (P>0.02, P<0.10)
5	Event with a 10 yr. return period (P=0.10)
6-9	Increasing probability of event (P>0.10, P<0.50)
10	Event with a 2 yr. return period (P=0.50)

Table 2.4 - Proposed Detectability Ratings for FMEA Analysis of Scour Monitoring System.

Ranking	Detectability Rating
1	Scour monitoring device can detect failure mode itself
2-4	Increasing inaccuracy of device to detect failure mode
5	Failure mode can be detected via additional instrumentation
6-9	Decreasing ability of additional instrumentation to detect physical failure, i.e. interpreting based on associated parameters
10	Failure mode cannot be detected, except by user onsite

Table 2.5 - Example FMEA Analysis for TDR System.

Comp.	Failure Mode	Effect of Failure	SEV	OCC	DET	RPN
TDR System	Water Turbidity Changes	Dielectric constant changes a small amount	1	7	10	70
	Water Temperature Changes	Dielectric constant changes a significant amount	5	9	10	450
	Loss of Power	Loss of data	10	3	2	60



To facilitate the FMEA analysis for a potential bridge scenario, the apparent sensitivities of each of the scour measurement device is reviewed in Table 2.6. Each device is rated against a scale of high, medium and low, to represent their relative sensitivity to the environmental parameters discussed.

Table 2.6 - Summary of Scour Monitoring Devices.

Device	Max Scour	Refill	Debris		Temp.	Salinity	Other
			Impact	Obst.			
2.1 Sounding Rods	Y	N	M	L	L	L	Bed penetration
2.2 Float-Out Devices	Y	Y-N	L-M	L	L	L	N.A.
2.3 MSC	Y	N	H	L	L	L	Fouling of collar clearance
2.4 Sonar Fathometer	Y	Y	H	H	M	M	Air entrainment, pulse versus scour hole size, electronic noise
2.5 TDR	Y	Y	M	L	M	H	Sediment dielectric
2.6 Fiber Optics	Y	Y	M	L	L	L	Sediment calibration
2.7 Temperature	Y	Y	M	L	N.A.	L	Live bed
2.8 Piezoelectric Film	Y	Y	M	L	L	L	Structural vibrations
2.9 Mercury Tip Switch	Y	N	M	L	L	L	Mercury
3.1 Radar	Y	Y	L	L	M	H	Attenuation in brackish waters
3.2 Pier Vibrations	Y	Y	L	L	M	L	Changes in loading patterns
3.3 Advanced Sonar	Y	Y	M	L	M	M	Live Bed

Thus, all of the scour monitoring systems can be analyzed with the FMEA process, leading to a more robust field system. A summary for each of the various techniques for monitoring scour is reviewed below.

Regarding rod based devices, they typically suffer from two main weaknesses:

The rods themselves and any attached cabling are subject to damage by debris impacting the hardware;

Measurements are made at only one point in the channel bottom.

In its simplest form, the fixed sonar fathometer units provide both maximum scour and refill information for one position in the channel bed. Additional information can be obtained by including tracking units or scanning the unit across the channel bed. However, this increases the system complexity and post processing requirements. In all of its forms, sonar devices are subject to various environmental conditions that can hamper the performance of the unit in the field. These variations include:

Temperature variations;

Salinity in near coastal waters;

Sediment loads and turbidity;

Air entrainment;

Debris, either impacting the device or causing false echoes;

The relative size of the scour hole and the sonar beam width.

Further study should be conducted into the effects of these environmental parameters on the sonar system results in order to develop means of accounting for these effects.

EM based techniques, both TDR and GPR, can be used to determine the depth of scour holes present in a river profile. The technique is sensitive to environmental parameters, particularly temperature and salinity and data on the field performance of these units is limited. Further study should focus on the performance of these units in the field as well as in the laboratory to identify the impact of the various environmental parameters on the TDR results.

The vibration based measurement methods discussed provide information about the overall health of the bridge directly and do not directly measure the scour hole size. The use of this method requires the determination of trends in the vibrational characteristic of the pier, which are complicated in practice due to environmental changes, such as temperature variations and traffic pattern shifts, as well as channel conditions.

There also exists a series of novel and unique scour monitoring systems that exploit various facets of the channel flow from the temperature gradient within the sub bottom to movement of devices, which can be linked to the presence of the channel flow. These devices have typically been employed in the laboratory and in limited field campaigns. Further work on these devices should focus on translating these ideas into robust methods with proven track records in the field.

## **2.5 References**

- Ansari, F., (2010). Simple cost-effective scour sensor. Research Report ICT-10-070, Illinois Center for Transportation.
- Arneson, L.A., Zevenbergen, L.W., Lagasse, P.F., Clopper, P.E., (2012). Evaluating scour at bridges. Hydraulic Engineering Circular No.18, 5th Ed., Publication No.

FHWA-HIF-12-003, US Department of Transportation, Federal Highway Administration, Washington, D.C.

Birchak, J.R., Cardner, C.G., Hipp, J.E., Victor, J.M., (1974). High dielectric constant microwave probes for sensing soil moisture. *Proceedings of the IEEE*, 62(1), 93-98.

Brice, J.C., Blodgett, J.C. (1978). Countermeasures for hydraulic problems at bridges. Vol. 1 & 2, FHWA/RD-78-162 & 163, Federal Highway Administration, U.S., Department of Transportation, Washington, DC.

Browne, T.M., (2011). Underwater acoustic imaging devices for portable scour monitoring. In *Scour and Erosion: Proceedings of 5th International Conference on Scour and Erosion*. Ed: Burns, S.E., Bhatia, S.K., Avila, C. M. C., Hunt, B. E., November 7-10, 2010, San Francisco, CA., ASCE.

Burczynski, J., (1982). Introduction to the use of sonar systems for estimating fish biomass. FAO Fisheries Technical Paper, No. 191, Revision 1. FIRU/T191, Rev 1.

Butch, G.K., (1996). Evaluation of selected instruments for monitoring scour at bridges in New York. North American Water and Environment Congress & Destructive Water, ASCE, 4164-4171.

Camp, C.V., Pezeshk, S., Leatherwood, T.D., (1998). Detecting bridge scour by measuring the thermal variation across the stream bed. International Water Resources Engineering Conference, Memphis, TN, August 3-6.

Campbell Scientific, (2010). TDR 100 instruction manual. Revision: 2/10.

Cooper, T., Chen, H.L., Lyn, D., Rao, A.R., Altschaeffel, A.G., (2000). A field study of scour-monitoring devices for Indiana streams: Final report. FHWA/IN/JTRP-2000/13.

DeFalco, F., Mele, R., (2002). The monitoring of bridges for scour and sediment. *NDT&E International*, 35, 117-123.

Drnevich, V.P., Siddiqui, S.I., Lovell, J., Yi, Q. (2001). Water content and density of soil insitu by the Purdue TDR method. TDR 2001: Innovative Applications of TDR Technology, Infrastructure Technology Institute, Northwestern University, Evanston, IL.

Eilertsen, R.S., Hansen, L., (2008). Morphology of river bed scour on a delta plain revealed by interferometric sonar. *Geomorphology*, 94, 58-68.

- Ettema, R., Zabilansk, L., (2004). Ice influences on channel stability: Insights from Missouri's Fort Peck Reach. *Journal of Hydraulic Engineering*, ASCE, 130(4), 279-292.
- Guemes, A., Menendez, J.M., (2006). Chapter 3: Fiber-optic sensors. In *Structural Health Monitoring*, Ed: Balageas, D. Fritzen, C.P., Guemes, A. ISTE Ltd, 225-285.
- Guo, N., Cawley, P., Hitchins, D., (1992). The finite element analysis of the vibrational characteristics of a piezoelectric disks. *Journal of Sound and Vibration*, 159(1), 115-138.
- Hayden, J.T., Puleo, J.A., (2011). Near real-time scour monitoring system: Application to Indian River Inlet, Delaware. *Journal of Hydraulic Engineering*, ASCE, 137(9), 1037-1046.
- Hayes, D.C., Drummond, F.E., (1995). Use of fathometers and electrical-conductivity probes to monitor riverbed scour at bridge piers. USGS, Water Resource Investigations Report 94-4165, Richmond, VA.
- Hunt, B.E., (2005). Scour monitoring programs for bridge health. *Transportation Research Record*, Journal of the Transportation Research Board, Washington D.C., 531-536.
- Hunt, D., (2009). "Monitoring scour critical bridges. NCHRP Synthesis 396, Transportation Research Board, Washington, DC.
- Holnbeck, S.R., McCarthy, P.M., (2011). Monitoring hydraulic conditions and scour at I-90 bridges on Blackfoot River following removal of Milltown Dam near Bonner, Montana, 2009. In *Scour and Erosion: Proceedings of 5th International Conference on Scour and Erosion*, Ed: Burns, S.E., Bhatia, S.K., Avila, C. M. C., Hunt, B. E., November 7-10, 2010, San Francisco, CA., ASCE.
- Isley II, J., Saafi, M., Julius, J. (2006) MEMS-based sensor networks for bridge stability safety monitoring during flood induced scour. In *Bridge Maintenance, Safety, Management, Life-cycle Performance and Cost: Proceedings of the Third International Conference on Bridge Maintenance, Safety and Management*, Ed: Cruz, P. J. S., Frangopol, D. M., Porto, Portugal, 16 - 19 July 2006.
- Jaffe, H., Berlincourt, D.A., (1965). Piezoelectric transducer materials. *Proceedings of the IEEE*, 53(10), 1372-1386.
- Ko, Y.Y., Lee, W.F., Chang, W.K., Mei, H.T., Chen, C.H., (2011). Scour evaluation of bridge foundations using vibration measurement. In *Scour and Erosion: Proceedings*

of 5th International Conference on Scour and Erosion, Ed: Burns, S.E., Bhatia, S.K., Avila, C. M. C., Hunt, B. E., November 7-10, 2010, San Francisco, CA., ASCE.

Lagasse, P.F., Richardson, E.V., Schall, J.D., Price, G.R., (1997). Instrumentation for measuring scour at bridge piers and abutments. NCHRP Report 396, TRB, National Research Council, Washington, D.C., 1997.

Lagasse, P.F., Clopper, P.E., Pagán-Oriz, J.E., Zevenbergen, L.W., Arneson, L.A., Schall, J.D., Girard, L.G., (2009). Bridge scour and stream instability countermeasures: Experience, selection and design guidance. Hydraulic Engineering Circular No.23, 3rd Ed., Publication No. FHWA-NHI-09-111, U.S. Department of Transportation, Federal Highway Administration.

Lin, Y.B., Chang, K.C., Lai, J-S., Wu, I-W., (2004). Applications of optical fiber sensors on local scour monitoring. *Proceedings of the IEEE: Sensors*, 2, 832-835.

Lin, Y.B., Lai, J.S., Chang, K.C., Li, L.S., (2006). Flood scour monitoring system using fiber bragg grating sensors” *Smart Materials and Structures*, 15, 1950-1959.

Manzoni, S., Crotti, G., Cigada, A., Inzoli, F., Ballio, F., (2011a). Monitoring bridge scour by bragg grating array. In Scour and Erosion: Proceedings of 5th International Conference on Scour and Erosion, Ed: Burns, S.E., Bhatia, S.K., Avila, C. M. C., Hunt, B. E., November 7-10, 2010, San Francisco, CA., ASCE.

Manzoni, S., Crotti, G., Ballio, F., Cigada, A., Colombo, E., (2011b). BLESS: A fiber optic sedimenter. *Flow Measurement and Instrumentation*, 22(5), 447-455.

Mason, R.R., Sheppard, D.M., (1994). Field performance of an acoustical scour-depth monitoring system. In Fundamentals and Advancements in Hydraulic Measurements and Experiments, Ed: Pugh, C.A., Proceedings of the Symposium, Buffalo, N.Y., August 1-5, 1994. ASCE.

Millard, S.G., Bunget, J.H., Thomas, C., Soucos, M.N., Shaw, M.R., Patterson, A., (1998). Assessing bridge pier scour by radar. *NDT&E International*, 31(4), 251-258.

Mueller, D.S., (2000). National bridge scour program-measuring scour of the streambed at highway bridges. U.S. Geological Survey, Reston, Va.

Murillo, J.A., (1987). The scour of scour. *Civil Engineering*, July 1987, ASCE, pp: 66-69.

Nassif, H., Ertekin, A.O., Davis, J., (2002). Evaluation of bridge scour monitoring methods: Final report. Federal Highway Administration, Report FHWA-NJ-2003-09.

- N.T.S.B., (1987). Collapse of New York Thruway (I-90) Bridge, Schoharie Creek, near Amsterdam, New York, April 5, 1987. NTSB Number: HAR-88/02, NTIS Number: PB88-916202.
- N.T.S.B., (1989). "Collapse of the northbound U.S. Route 51 Bridge spans over the Hatchie River, near Covington, Tennessee, April 1, 1989", NTSB Number: HAR-90/01, NTIS Number: PB90-916201.
- Placzek, G., Haeni, F.P., (1995). Surface geophysical technique used to detect existing and infilled scour holes near bridge piers. USGS Water-Resources Investigations Report 95-4009.
- Richardson J.R., Price, G.R., Richardson, E.V., Lagasse, P.F., (1996). Modular magnetic scour monitoring device and method for using the same. U.S. Patent # 5532687, Issued July 2, 1996.
- Richardson, J.R., Price, J., (1993). Emergent techniques in scour monitoring devices. In Hydraulic Engineering, Ed: Wen Shen, H., Su, S.T., Wen, F., Proceedings of the 1993 Conference, San Francisco, CA, July 25-30, 1993, ASCE.
- Rhodes, J., Trent, R., (1993). Economics of floods, scour and bridge failures. In Hydraulic Engineering '93: Proceedings of 1993 Conference, Ed: Shen, H.W., Su, S.T., Wen, F., July 25-30, 1993, San Francisco, CA, ASCE.
- Samizo, M., Watanabe, S., Fuchiwaki, A, Sugiyama, T., (2007). Evaluation of structural integrity of bridge pier foundations using microtremors in flood conditions. *Quarterly Report of RTRI*, 48(3), 153-157.
- Samizo, M., Watanabe, S., Sugiyama, T, Okada, K., (2011). " Evaluation of the structural integrity of bridge pier foundations using microtremors in flood conditions. In Scour and Erosion: Proceedings of 5th International Conference on Scour and Erosion, Ed: Burns, S.E., Bhatia, S.K., Avila, C. M. C., Hunt, B. E., November 7-10, 2010, San Francisco, CA., ASCE.
- Spindel, R.C., (1998). Chapter 38: Oceanographic and navigational instruments. In Handbook of Acoustics, Ed: Crocker, M. J., John Wiley and Sons, Inc.
- Stogryn, A., (1971). Equations for calculating the dielectric constant of saline water. *IEEE Transactions on Microwave Theory and Techniques*, 19(8), 733-736.
- Topp, G.C., Davis, J.L., and Annan, A.P., (1980). Electromagnetic determination of soil water content: Measurements in coaxial transmission lines. *Water Resources Research*, 16(3), 574-582.

- Urlick, R.J., (1975). Principles of underwater sound. McGraw-Hill Inc.
- USGS, (2006), Water data report 2006: 02172053 Cooper River at Mobay near North Charleston, SC. U.S. Department of Interior, U.S. Geological Survey.
- USGS, (2006), Water Data Report 2006: 02156500 Broad River Near Carlisle, SC. U.S. Department of Interior, U.S. Geological Survey.
- Webb, D.J., Anderson, N.L., Newton, T., Cardimona, S., (2000). Bridge scour: Application of ground penetrating radar. FHWA and Missouri DOT Special Publication.
- Yankielun, N.E., Zabilansky, L. (1999). Laboratory investigation of time domain reflectometry system for monitoring bridge scour. *Journal of Hydraulic Engineering*, ASCE, 125(12), 1279-1284.
- Yao, C., Darby, C., Hurlebaus, S., Price, G.R., Sharma, H., Hunt, B.E., Yu, O.-Y., Chang, K.-A., Briaud, J.-L., (2011). Scour monitoring development for two bridges in Texas. In *Scour and Erosion: Proceedings of 5th International Conference on Scour and Erosion*, Ed: Burns, S.E., Bhatia, S.K., Avila, C. M. C., Hunt, B. E., November 7-10, 2010, San Francisco, CA., ASCE.
- Yu, X., Yu, X., (2006). Time domain reflectometry tests of multilayered soils. Proceedings of the TDR 2006, Purdue University, West Lafayette, USA.
- Yu, X., Yu, X., (2011). Development and evaluation of an automatic algorithm for a time-domain reflectometry bridge scour monitoring system. *Canadian Geotechnical Journal*, 48(1), 26-35.
- Yu, X., Zabilansky, L.J., (2006). "Time domain reflectometry for automatic bridge scour monitoring. In *GeoShanghai 2006: Site and Geomaterial Characterization*, GSP 149, Ed. Puppala, A. J., Fratta, D., Alshibli, K., and Pamukcu S., ASCE.
- Zabilansky, L., Ettema, R., Weubeen, J., Yankielun, N., (2002). Survey of river ice influences on channel bathymetry along the Fort Peck Reach of the Missouri River, Winter 1998–1999. Technical Report ERDC/CRREL TR-02-14., U.S. Army Corps of Engineers, Engineer Research and Development Center.
- Zabilansky, L.J. (1996). Ice force and scour instrumentation for the While River, Vermont. Special Report 96-6, U.S. Army Corps of Engineers, Cold Regions Research And Engineering Laboratory.



## CHAPTER THREE

### A NOVEL VIBRATION-BASED MONITORING TECHNIQUE FOR BRIDGE PIER AND ABUTMENT SCOUR

#### **3.1 Introduction**

Scouring occurs when high velocity flows erode the riverbed, removing the material surrounding the bridge piers and abutments, which ultimately affects the stability of the bridge foundation. Scour damage to these structural components can potentially result in the failure of the entire bridge. Bridge repair and restoration, from all types of damage, accounts for 19% of the federal emergency funds allocated for highway repairs (Rhodes and Trent, 1993). Between the 1960s and 1990s, of the 1000 bridge failures in the U.S., 60% were attributed to scour (Shirole and Holt, 1991). The financial cost associated with repairing scour damage to bridge structural elements was estimated to be \$100 million per scour event from 1964-1972 (Brice and Blodgett, 1978). Rapid riverbed scouring typically develops during high flow periods such as floods. Since bridges are often key infrastructure elements for the evacuation of the public or transportation of relief supplies, any structural failure of a bridge due to scour has an impact beyond the losses associated with the collapse of the bridge itself. Therefore, safeguarding bridges from failure due to scour, which can be achieved through real-time monitoring of scour development in riverbeds, is of critical importance.

During the last decade, various projects have been undertaken to evaluate existing scour monitoring techniques, the majority of which have involved the investigation of sonar fathometers and other riverbed mounted sensors. Sonar fathometers, mounted on the bridge piers or abutments, use acoustic signals to record the distance to the riverbed (Nassif et al, 2002). In previous experiments, fathometers have been used in the field to monitor both the maximum scour and subsequent refill during an event [(Nassif et al., 2002), (Cooper et al., 2000)]. These field studies, however, were typically hampered by various environmental and operational conditions, specifically channel debris, which for bridges in Indiana (Cooper et al., 2000) and in New Mexico (Lagasse et al., 1997), interrupted the signal reflected from the river bottom. Debris can also directly impact the sonar unit or cabling, resulting in a loss of the unit and/or signal altogether (Cooper et al., 2000). Aside from debris, turbulent water can further hinder the operational environment of sonar devices. Holnbeck and McCarthy (2011) reported that of the four sonar units installed on each pier of the I-90 bridge over the Blackfoot River in Montana, only one provided operational data due to highly turbulent water and air entrainment through the bridge section. Temperature and salinity in the channel also significantly affect sonar results. Lagasse et al. (1997) reported that for the John's Pass Bridge in Florida, it was necessary to adjust the measured signal by approximately 0.5 m on average to account for the temperature and salinity effects. Another commonly used instrument in scour observation is the magnetic sliding collar (MSC), a device consisting of a rod driven into the riverbed with a collar that rests on the bed surface and slides down the rod during a scour event (Lagasse et al., 1997). As the scour hole refills, however, the magnetic collar

is buried under the refill material and becomes incapable of recording any refill of the scour hole (Lagasse et al., 1997). As with sonar systems, MSC devices are also vulnerable to debris impacting the device that in turn damages the monitoring unit [5, 6]. It is also possible for sediment in the riverbed to foul the space between the collar and rod and prevent the collar from moving during a scour event (Lagasse et al., 1997).

The time domain reflectometry (TDR) method, which uses EM pulses transmitted through pipes buried in the riverbed, is another rod-based method used for scour observation (Yankeilun and Zabilansky, 1999). Here, the elimination of debris and jamming problems associated with sonar and MSC techniques permits the gathering of information regarding the refill of the scour hole. TDR however, is susceptible to temperature and salinity changes. Even though Yu and Yu (2009, 2010) reported that varying salinity levels from 0 to 750 ppm did not adversely affect the performance of the TDR method, these ranges are unsuitable for use in near coastal waters. In estuarine environments, for instance, the temperature can vary by 20 °C or more and the specific conductance, a measure of the salinity, can vary from a yearly average of approximately 100  $\mu\text{S}/\text{cm}$  to a maximum of 25,000  $\mu\text{S}/\text{cm}$  (approximately 50 to 17,500 parts per million) [(USGS, 2006a), (USGS, 2006b)], well above the range tested in the laboratory.

As shown in the relevant literature, available scour monitoring techniques (e.g. sonar fathometers, TDR, MSC) are susceptible to environmental and flow conditions, including temperature, salinity, turbidity, air entrainment and debris. Furthermore, MSC devices can only record the maximum scour depth and cannot record refill. In this

manuscript, the authors propose a novel technique that is more resilient to environmental and flow conditions and is capable of measuring both scour development and refill.

In the proposed method, several dynamic sensors mounted on thin, flexible plates, referred to as vibration-based turbulent pressure sensors (VTPs), are distributed along the length of a sealed pipe that is driven into the riverbed near the pier or abutment. The VTPs in the river are subjected to the natural turbulence of the river flow and are excited by the associated time varying dynamic pressure. The VTPs in the flow vibrate at amplitude levels detectable by modern vibration transducers. Conversely, a VTP in the sediment, which is not exposed to the turbulence, vibrates at lower amplitudes than those experienced by the VTPs in the flow. The time history of the vibrations of each sensor can be recorded by an accelerometer mounted on the inside surface of the plate. The captured signals can then be processed to quantify the mean squared acceleration response in the time domain, which is related to the signal energy content. By monitoring the energy content associated with several VTPs distributed throughout the depth of the pier or abutment, it is possible to correlate the changes in vibration response to the changes in the bed level. Determining the changes in the bed level allows the assessment of not only scour development but also the refill process.

The VTP mechanism is robust against many of the environmental conditions that plague existing scour monitoring devices. Debris in the channel causes false echoes in a sonar system, however the VTP method is unaffected by debris since debris accumulation does not affect its ability to determine the water/sediment interface. Turbidity, which hinders the performance of sonar fathometers, has a favorable effect on the performance

of the VTP due to the additional momentum contributed by the particles impacting the VTP surface. By the same argument, as salinity has a minimal influence on turbulent dynamic pressure, the VTP mechanism is theoretically immune to the changes in the salinity in the channel water, which has adverse affects on the TDR method. Finally, given the anticipated temperature range in natural rivers, which can affect both the TDR and sonar based methods, the response of the VTP method is likely to remain unchanged as any variation in the vibration characteristics of the thin flexible plates associated with temperature variations will be minor since it is possible to select materials with a low coefficient of thermal expansion.

Starting in Section 2, the underlying principle behind the VTP device is discussed along with the practical aspects regarding the development of a prototype VTP system. The laboratory experimental campaign is discussed in Section 3 with the results reviewed in Section 4. Pertinent conclusions drawn from the laboratory experiments in preparation for field implementation of the VTP method are discussed in Section 5 along with an overview of future work.

### **3.2 Numerical Proof of Concept**

A simplified numerical proof-of-concept model is built based upon the principles of dynamics for a plate subjected to an applied pressure distribution. It will be established that a single degree of freedom system (SDOF) provides an adequate means for estimating the dynamic response of the proposed VTP to the varying pressure caused by turbulence in the channel flow. It is useful to define the response of the VTP in the frequency domain since models for the response of a SDOF system are readily available.

In addition, the turbulent dynamic pressure in the channel is also described well in the frequency domain. By combining these models, it will be possible to predict the response of the VTP to the pressure associated with the turbulent fluctuation in the channel.

### 3.2.1 Modeling of Open Channel Turbulent Flow

Several features of the nature of turbulence within open channels lend themselves to being exploited by the VTP method. In particular, the distribution of the turbulent fluctuations in the mean flow direction,  $\sqrt{u'^2}$ , peaks near the riverbed in the wall region, at  $y^+$  of 15 (Nakagawa et al., 1975). The parameter  $y^+$  is equal to the product of the vertical position in the channel,  $y$ , and the friction velocity,  $U_*$ , divided by the kinematic viscosity of the fluid,  $\nu$ . Additionally, for open channel flows, once the flow is fully developed, the power spectral density of the turbulent velocity fluctuations,  $\Phi_{UU}(f)$ , is stationary. The power spectral density is related to the correlation function,  $R_x(r)$ , as shown in Equation (3.1), for two turbulent velocity measurements,  $u'(x)$  and  $u'(x+r)$ , spaced a distance  $r$  apart (Nezu and Nakagawa, 1993). The Taylor's hypothesis of frozen turbulence makes it possible to convert the spectra,  $\Phi_{UU}(k)$  from wave number space,  $k$ , to frequency space,  $f$ , as shown in Nezu and Nakagawa (1993). In addition, since  $R_x(r)$  can be determined from measurements of the velocities in open channel flows, it is possible to develop experimental representations of the power spectrum, through the use of the Fourier Transform. The resulting power spectrum can be non-dimensionalized for the range of flow conditions

typically found in open channels, thus various attempts have been made to develop models that matched the experimentally measured spectra.

$$\left. \begin{aligned} R_x(r) &= \frac{u'_x(x) \cdot u'_x(x+r)}{\overline{u'^2}} = \int_0^\infty \Phi_{UU}(k) \cos(k \cdot r) dk \\ \Phi_{UU}(k) &= \frac{2}{\pi} \int_0^\infty R_x(r) \cos(k \cdot r) dr \end{aligned} \right\} \quad (3.1)$$

One such model was developed by Von Karman (1948) for isotropic turbulence at high Reynolds number and is valid from the production to the inertial sub-range of the turbulent energy spectrum, Equation (3.2). Another model was developed by Heisenberg (Nakagawa and Nezu, 1975) and is shown in Equation (3.3), which is valid from the inertial sub-range to the point of viscous dissipation. These two models are used to predict the magnitude of the turbulent pressure impinging on the VTP. The reader is directed to Nakagawa et al. (1975), Nezu and Nakagawa (1993), and Von Karman (1948) for further details on the development of these models.

$$\overline{u'^2} \Phi_{UU}(f) = \overline{u'^2} \frac{4L_x}{U} \left( 1 + \left( \frac{f}{f_o} \right)^2 \right)^{-5/6} \quad (3.2)$$

$$\overline{u'^2} \Phi_{UU}(f) = \left( \frac{2\pi}{U} \right)^{-2/3} C \varepsilon^{2/3} \left( 1 + \gamma' \left( \frac{2\pi f}{U} \right)^4 \right)^{-4/3} \quad (3.3)$$

These models depend upon the mean eddy macroscale,  $L_x$ , the characteristic frequency,  $k_o$ , the dissipation rate of turbulent energy,  $\varepsilon$ , the mean flow velocity,  $U$ ,

the mean of the squared turbulence level,  $\sqrt{u'^2}$ , the constants  $\gamma'$  and  $C$ , and finally the Kolmogoroff length scale,  $\eta$ . The mean eddy macroscale, shown in Equation (3.4), is a function of vertical position in the channel, the channel depth,  $h$ , and an empirically determined constant,  $B_1$ , which varies from 1 to 1.1 [14].

$$\left. \begin{aligned} \frac{L_x}{h} &= B_1 \left( \frac{y}{h} \right)^{1/2} \quad \text{for } y/h < 0.6 \\ \frac{L_x}{h} &= 0.77 B_1 \quad \text{for } y/h > 0.6 \end{aligned} \right\} \quad (3.4)$$

The additional parameters in Equation (3.2) can be determined from the universal function for the turbulence intensity in open channels, which for the mean flow direction is shown in Equation (3.5) (Nezu and Nakagawa, 1993). Equation 5, in turn, is dependent upon the friction velocity, the friction Reynolds number,  $Re = hU_*/\nu$ ,  $y^+$  defined previously, and various empirical constants,  $D_U = 2.3$ ,  $B = 10$ ,  $C_1 = 0.3$ .

$$\left. \begin{aligned} \frac{\sqrt{u'^2}}{U_*} &= D_U \exp\left(\frac{-y^+}{Re_*}\right) \Gamma + C_1 y^+ (1 - \Gamma) \\ \Gamma &= 1 - \exp\left(\frac{-y^+}{B}\right) \end{aligned} \right\} \quad (3.5)$$

The dissipation rate for isotropic turbulence can be modeled as shown in Equation (3.6) (Nakagawa et al, 1975). Finally, the microlength scales ( $\eta$  and  $\varepsilon$ ) can be correlated to the macrolength scales via the relations in Equations (3.7) and (3.8) (Nezu and



Nakagawa, 1993), with  $\text{Re}_L = \sqrt{u'^2} L_x / \nu$  and  $K$  as given in Equation (3.9) (Nezu and Nakagawa, 1993).

$$\varepsilon = \frac{15\nu\sqrt{u'^2}}{\lambda^2} \quad (3.6)$$

$$\frac{L_x}{\lambda} = \left(\frac{K}{15}\right)^{1/2} \text{Re}_L^{1/2} \quad (3.7)$$

$$\frac{L_x}{\eta} = K^{1/4} \text{Re}_L^{3/4} \quad (3.8)$$

$$K = 0.691 + \frac{3.98}{\sqrt{\text{Re}_L}} \quad (3.9)$$

Given the spectra for the turbulent velocity fluctuations, the corresponding spectra for the associated pressure on the flexible plates is constructed as the product of the velocity spectra and the flow density,  $\rho$ , as shown in Equation (3.10).

$$\Phi_{PP}(f) = \frac{1}{2} \rho \overline{u'^2} \Phi_{UU}(f) \quad (3.10)$$

### 3.2.2 Modeling of VTP Dynamic Response:

Given the nature of the turbulent dynamic pressure in the channel, it is necessary to describe the response of a plate to this dynamic forcing function. Following the method developed by Blevins (1990), it can be shown that the response of a plate,  $w_i$ , for

each mode  $i$ , to the dynamic turbulent pressure,  $P_i$ , is governed by Equation (3.11), where  $\zeta_i$  is the modal damping factor and  $J_i$  is the joint acceptance between the mode shape and the pressure distribution.

$$\frac{1}{\omega_i^2} \ddot{w}_i + \frac{2\zeta_i}{\omega_i} \dot{w}_i + w_i = J_i P_i \quad (3.11)$$

The joint acceptance governs the manner in which the modal displacement response of the plate corresponds to the spatially varied pressure distribution for a given mode. Under the condition that the mode shape and the pressure distribution are aligned, the joint acceptance is 1 (Blevins, 1990), and the solution to Equation 10 for a sinusoidal pressure distribution becomes the classical harmonic excitation response of a SDOF system. Given that the turbulence in open channels is stationary and random, the autospectral density of the displacement response of the VTP,  $\Phi_{xx}(\omega)$ , can then be computed from the mean square of the classical harmonic excitation response to the autospectral density of the pressure distribution, as shown in Equation (3.12). What remains, is then to describe the means square response of the VTP, and couple that response function with the previously discussed turbulent pressure spectrum (Equation (3.10)).

$$\Phi_{xx}(\omega) = |H(\omega)|^2 \Phi_{pp}(\omega) \quad (3.12)$$

The steady state response function  $|H(\omega)|^2$  can be described from the modal damping, and the natural frequency,  $\omega_N$ , of the SDOF system, as shown in Equation (3.13) (Blevins, 1990, Craig, 1981).

$$|H(\omega)|^2 = \frac{1}{\left(1 + \left(\frac{\omega}{\omega_N}\right)^2\right)^2 + \left(2\zeta \frac{\omega}{\omega_N}\right)^2} \quad (3.13)$$

A closed form solution for the first natural frequency of a circular plate fixed at its circumference is given below in Equation (3.14) (Blevins, 1979), where  $r$  is the radius of the disk,  $E$  is the Young's modulus,  $\nu$  is the Poisson's ratio,  $\rho$  is the density and  $t$  is the plate thickness.

$$\omega_N = \frac{10.22}{r^2} \frac{Et^3}{\sqrt{12\rho t(1-\nu^2)}} \quad (3.14)$$

### 3.2.3 Numerical Model Results

The SDOF model and the input forcing function, discussed previously, are used to model the response of the VTP to the dynamic excitation from turbulent flow. The flow case considered has a mean flow speed of 0.3 m/s and a depth of 3 m with a VTP located at  $y/h$  of 0.1; a representative case for natural channels.

The displacement response spectra from the VTP model are shown in Figure 3.1, along with the velocity and acceleration spectra, computed from derivatives of Equation (3.11). The turbulent spectrum of the forcing function (due to turbulent pressure) is also

shown in Figure 3.1, including both the production and inertial sub-ranges. The spectrum exhibits a broad peak at low frequencies, less than 0.1 Hz, associated with the large eddy structures in the flow. The inertial sub-range encompasses approximately 0.1 to 40 Hz, at which point the declination in the amplitude of the input spectrum is observed. This reduction is associated with the transition to the viscous sub-range. Accordingly, an ideal VTP would be sensitive to the turbulent pressure within the 0.1 - 40 Hz frequency range.

The first natural frequency for a representative circular plate made from neoprene rubber, calculated using Equation 14, can be seen in all three response spectra for the VTP at approximately 250 Hz. The relative magnitudes between the acceleration, velocity and displacement spectra reveal in which frequency range various sensors would be useful in recording the response of the VTP. In the low, near DC, frequency range, less than 10 Hz, the results indicate that a position sensor would be optimal. However, in the range of 10 to 400 Hz, the figure indicates that an accelerometer would be better suited to measure the response. Accelerometers with sensitivities over the 10 to 400 Hz frequency range are commonly available. Therefore, for the initial prototype these accelerometers are selected for the development of the scaled prototype model.

During operation of the VTP, the variation in the energy content of the flexible plates throughout the depth of the pier or abutment must be monitored: a low energy content corresponds to sediment, while a high energy content corresponds to channel flow. Using the spectra shown in Figure 3.1, it is also possible to compute the mean value of the acceleration autospectrum of the vibration response over the frequency range of interest (Blevins, 1990). The response spectra computed for various geometric and

material configurations can then be used to evaluate the hypothesis behind the operation of the VTP device and to determine the optimal configuration for the prototype.

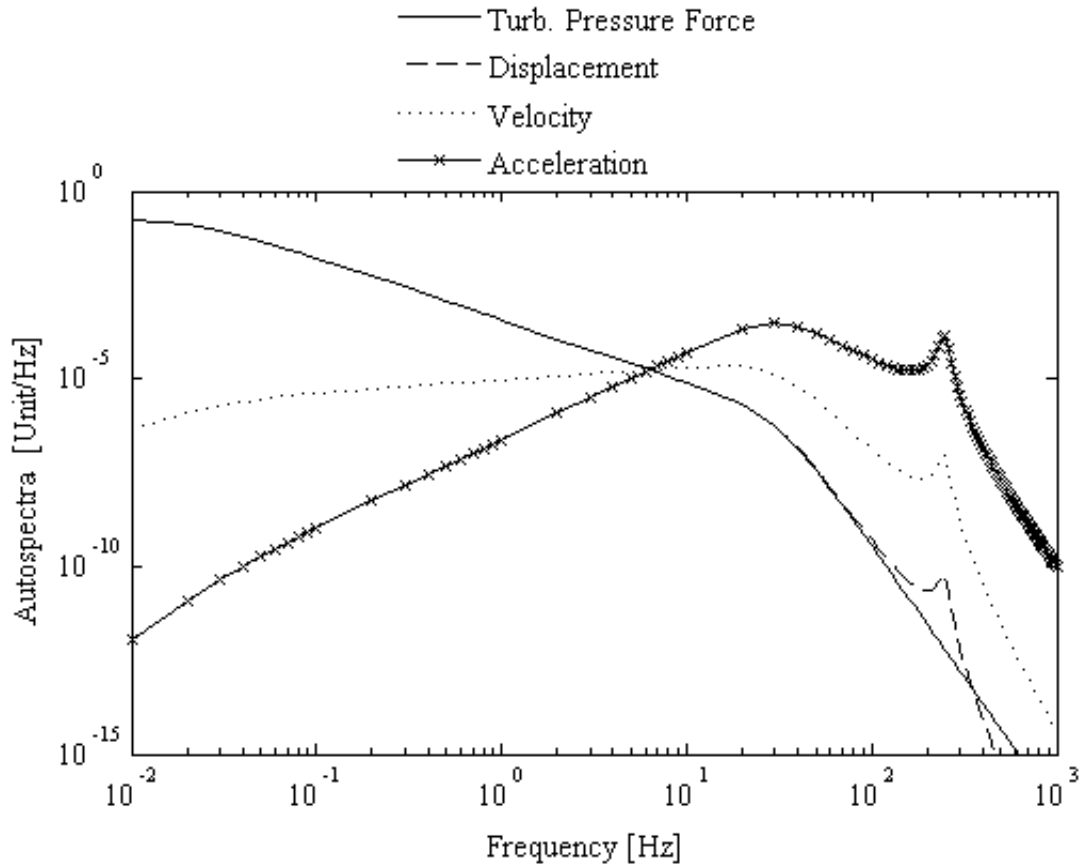


Figure 3.1 – Model response for prototype VTP based upon SDOF model and turbulent spectra. The units for displacement, velocity and acceleration autospectra are  $\text{m Hz}^{-1}$ ,  $\text{m s}^{-1}\text{Hz}^{-1}$ ,  $\text{m s}^{-2}\text{Hz}^{-1}$  respectively.

Based upon the numerical model results, an optimal VTP would respond to low frequency turbulent pressure fluctuations at a level detectable by commercially available accelerometers. The VTP prototype must be designed considering the competing constraints of maximizing the energy content response while keeping the dimensions of the plate small such that the spacing between VTP sensors is kept to a minimum.

For the VTP prototype, both metallic and non-metallic materials are considered, including stainless steel (304 Grade), aluminum, (6061-T6), brass, and three plastics, PVC, LDPE, and a neoprene rubber (durometer of 30A). Plates 3.2 mm in thickness with both circular and square geometric forms are considered. The simplified numerical model is used to analyze the response, with an appropriate change in Equation 14 for the square geometry (Blevins, 1979). The energy content response computed for various VTP plate areas are plotted in Figure 3.2.

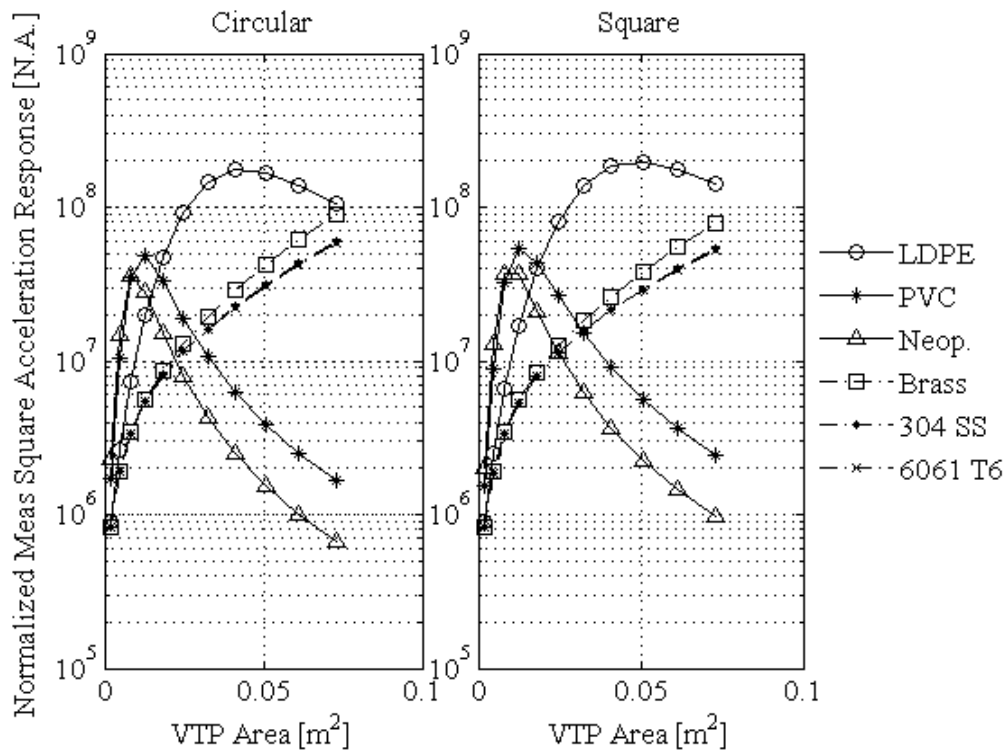


Figure 3.2 – Circular and square VTP normalized mean square response as computed from the response spectrum from 10 to 400 Hz for circular and square VTPs, for various plate areas, and material types. Each result is normalized by the deflected mode shape (Equation 3.13).

For the metallic materials, the circular VTP consistently has the higher energy content over the square VTP for a given area and material. For the largest VTP, with an

area of  $0.073 \text{ m}^2$ , the circular aluminum, brass and stainless steel VTPs have a mean response level 9, 13 and 10% greater than the square VTP. For each geometric shape, the brass VTP responds, on average, at a level 14% above that of the aluminum VTP and 18% above that of the stainless steel VTP. Therefore, for the metallic VTPs, the circular VTP is the preferred configuration, with the optimum metallic material being brass.

For the non-metallic materials, the optimal geometric configuration depends upon the VTP area. For instance, for the LDPE, the circular VTP at lower areas responds as much as 14% more than the square VTP, for the same area. However, as the area of the VTP increases, this trend shifts. For the LDPE VTP, this transition occurs at areas above  $0.03 \text{ m}^2$ , while for the PVC and neoprene VTPs this occurs at  $0.008$  and  $0.005 \text{ m}^2$ , respectively. Within a particular case, the optimal material also is a function of area. At lower VTP sizes ( $0.002$  to  $0.008 \text{ m}^2$ ), the neoprene VTP responds on average 19% more than the PVC VTP. For the  $0.01 \text{ m}^2$  case, however, the PVC response peaks 68% higher than the neoprene area of the same case and size. Then, from  $0.02$  to  $0.07 \text{ m}^2$ , the LDPE response peaks and is several orders of magnitude larger than that of the PVC or neoprene VTPs. Thus, for the non-metallic VTPs, the optimal geometry and material choice are a function of area. For smaller VTPs, a circular, neoprene VTP is optimal. For larger VTPs, an LDPE, square VTP is optimal.

When considering an optimal VTP configuration for evaluating the hypothesis behind the operation of the VTP devices, it is important to balance the desire to maximize the response level in the turbulent flow with the size of the plate. Therefore, a size limit of  $0.01 \text{ m}^2$  is imposed to keep the spacing in line with the resolution of an MSC device.

Based on this limit, it can be concluded that a circular VTP made from neoprene is optimal.

### 3.3 Experimental Setup

According to the materials and geometric form selected in the previous section, a prototype is constructed with eight neoprene VTPs of 0.0254 m radius. The VTPs are spaced approximately 0.10 m apart, on center, in a 0.10 m diameter PVC support pipe. A schematic of the prototype assembly is shown in Figure 3.3. The assembly consists of a compression pipe coupling mounted in the support pipe with a toroid disk sandwiched between the compression coupling components. The flexible plate is fixed to the toroid disk, as shown in Figure 3.3. Overall, the size of the VTP and the support pipe are small in comparison with the physical dimensions for a pier, which are typically 0.5 to 1 m or more in width. For such a device in a typical field case, the equilibrium scour depth predicted with the Neill equation (1964) is approximately 1.4 m, while the pipe would only result in a 0.3 m hole, well within the original scour depth. As such, the presence of the VTP is anticipated to have a limited affect on the flow around the pier, and any subsequent scouring of the riverbed.

The support pipe is buried below the sediment, with several sensors exposed to the flow and several sensors below the water/sediment interface. The experiments are conducted in the Clemson Hydraulic Laboratory in a 1.2 x 1.2 m square cross section, 18 m long flume. The flume is equipped with a recess for scour measurements, in which the support pipe and VTPs are located. The support pipe is fixed to the flume frame, as shown in Figure 3.4. The riverbed is simulated with quartz sand of a  $d_{50}$  of 1.5 mm. A



sand bed represents a worst case evaluation of the VTP method since the pressure waves impinging on the bed from the turbulent flow will have a greater depth of penetration in the quartz sand bed. Since the dissipation of a wave will be greatest in a clay or silt bed (Gutowski and Dym, 1976), the turbulent pressures incident on the sand bed will propagate furthest into the sand bed, leading to the highest possible response from a VTP in the sediment. The flow rates are varied from 0.028 to 0.14 cubic meters per second, which is measured with an FMG3101 magnetic flow meter.

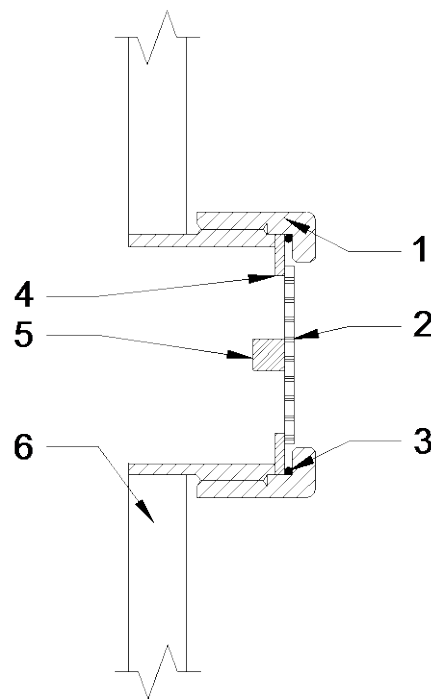


Figure 3.3 – Prototype VTP configuration diagram. Components include: (1) the compression fitting, (2) the plate material, (3) a washer (4) toroid disk (5) accelerometer and (6) the support pipe.

To measure the acceleration of the VTP plate, a B&K 4507 B 006 uni-axial transducer, with a sensitivity of approximately  $51 \text{ mV/m s}^{-2}$ , is mounted in the center of the flexible plate inside each VTP. These accelerometers are connected to a B&K LAN-

XI 3050A-060 data acquisition system. A sampling frequency of 25.6 kHz yields a converged RMS value of the acceleration response for a given flow condition, and is thus selected as the measurement frequency for the experiments. The measurements are recorded for 10 seconds each with 10 repeat measurements for each flow condition. The mean squared value is computed for each VTP from the measured signals, which is proportional to the energy of the time domain acceleration. The mean squared value will be referred to as the VTP energy content for the remainder of this manuscript. The experimental setup is shown in Figure 3.4.



Figure 3.4 – Prototype VTP array installed in flume bed. VTPs 1-4 are shown (right/left) above the sand bed, housed in support pipe (middle) connected to the flume frame.

### 3.4 Results and Discussion

The experiments are conducted with three objectives; (i) to supply a proof-of-concept, (ii) to evaluate the performance of the VTP system in a scour hole and (iii) to determine the precision of the VTPs.

### 3.4.1 Verification of the Hypothesis behind VTP

During this phase of testing, four VTPs are submerged in the flume: two in the sediment (VTPs #7 and #8) and two positioned in the flow (VTPs #5 and #6). VTPs #1-4 in this test are above the water free surface. VTP #8 is situated at the lowest position (0.16 m below the sediment bed) while VTP #5 is situated at the highest position (0.14 m above the sediment bed). The results of the tests are shown in Figures 5 and 6.

In Figure 3.5, the energy content response is calculated for four different flow rates ranging from 0.060 to 0.14 m<sup>3</sup> s<sup>-1</sup> (cms) and plotted against the distance from the sediment interface. The mean and standard deviation of the ten 10-second measurements are plotted to present the central tendency and the variability of the measurements. In Figure 3.5, the VTP within the flow and adjacent to the bed measures the peak energy content. The energy content decreases with increasing distance from the sediment surface, which is in agreement with the expected profile of the flow turbulence across the depth of the channel [13]. On the other hand, the VTP response in the sediment is one to two orders of magnitude lower than the measured energy content in the flow. This difference between the energy content levels of VTPs in the channel and in the sediment are well above the uncertainty bounds of the sensors in the flow; therefore, suggesting that the low-frequency vibration response of the VTP can be used to distinguish between channel flow and sediment.

In Figure 3.6, the mean square of the time domain response of VTP #5, located in the channel flow, is compared against that of VTP #8, located in the sediment, for varying flow rates. For each flow rate, the average for each of the ten 10-second

measurements are plotted. For all flow rates, the average difference between the VTPs in the flow and the sediment is  $0.028 \text{ m}^2 \text{ s}^{-4}$ . Depending upon the flow rate, the minimum difference between the two signals is one order of magnitude, while the largest difference increases to two orders of magnitude. Figure 3.6 shows a general trend where the measured energy content increases with flow rate, an observation consistent with expectations since the amplitude of the pressure fluctuations due to turbulence increases with the mean flow speed, and therefore with flow rate. Even at low flow rates, however, the difference between the mean square response in the flow and sediment is detectable. Thus, as the flow rate, and therefore the flow velocity increases, the difference in energy content levels for VTPs located in the flow versus the sediment increases, aiding in the observation of the water/sediment interface, as shown in Figure 3.6. It should be noted, however, that for the highest flow rate, the energy content level drops slightly from the value at a flow rate of 0.135 cms. This is attributed to the 10 second averaging time, which may not fully capture all of the large eddies in the flow. Future field tests should investigate longer averaging times to avoid this complication.

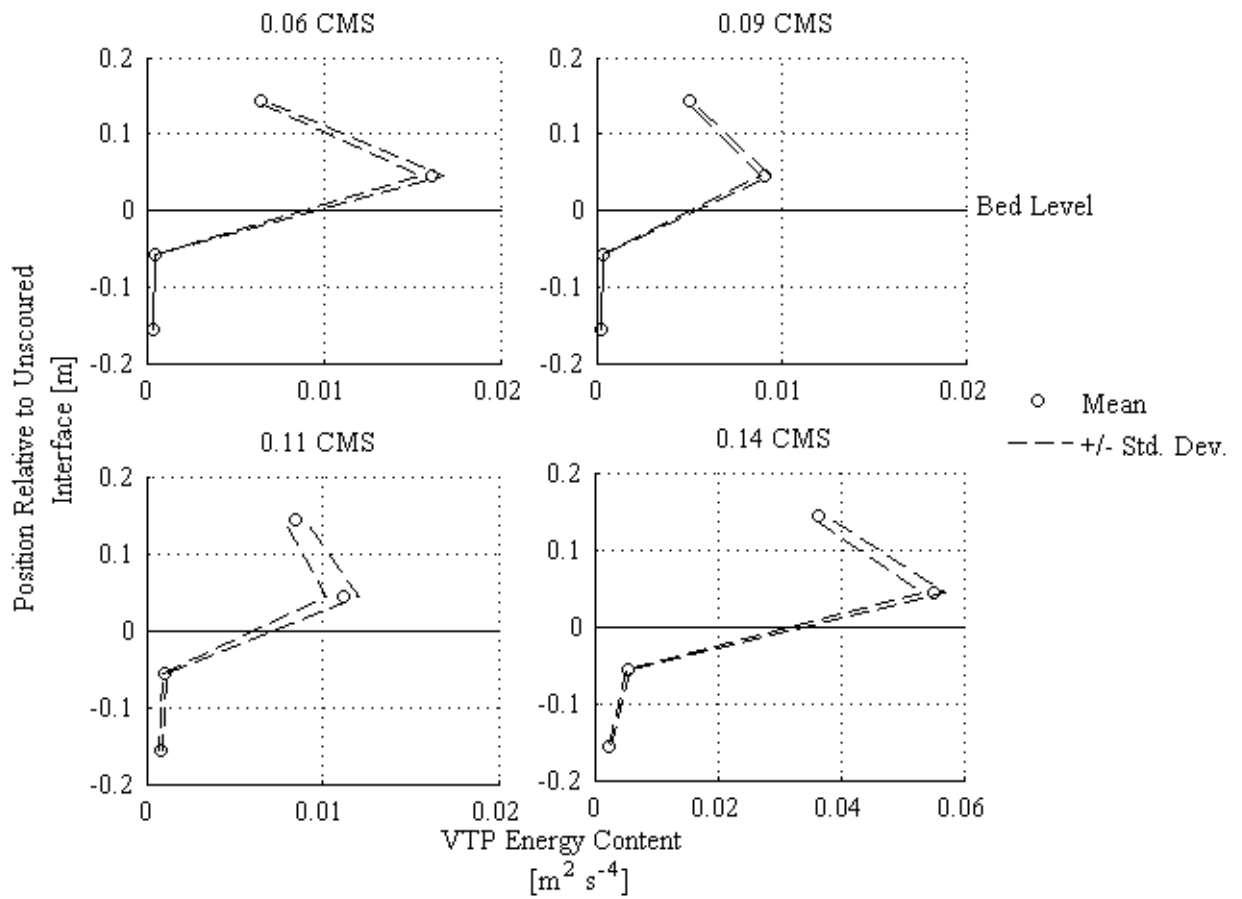


Figure 3.5 – Energy content of prototype VTPs as a function of distance from the water/sediment interface. Flow rates varied from 0.060 to 0.14 cms. Mean values plotted including  $\pm 1$  standard deviation, as well as the unscoured bed level.

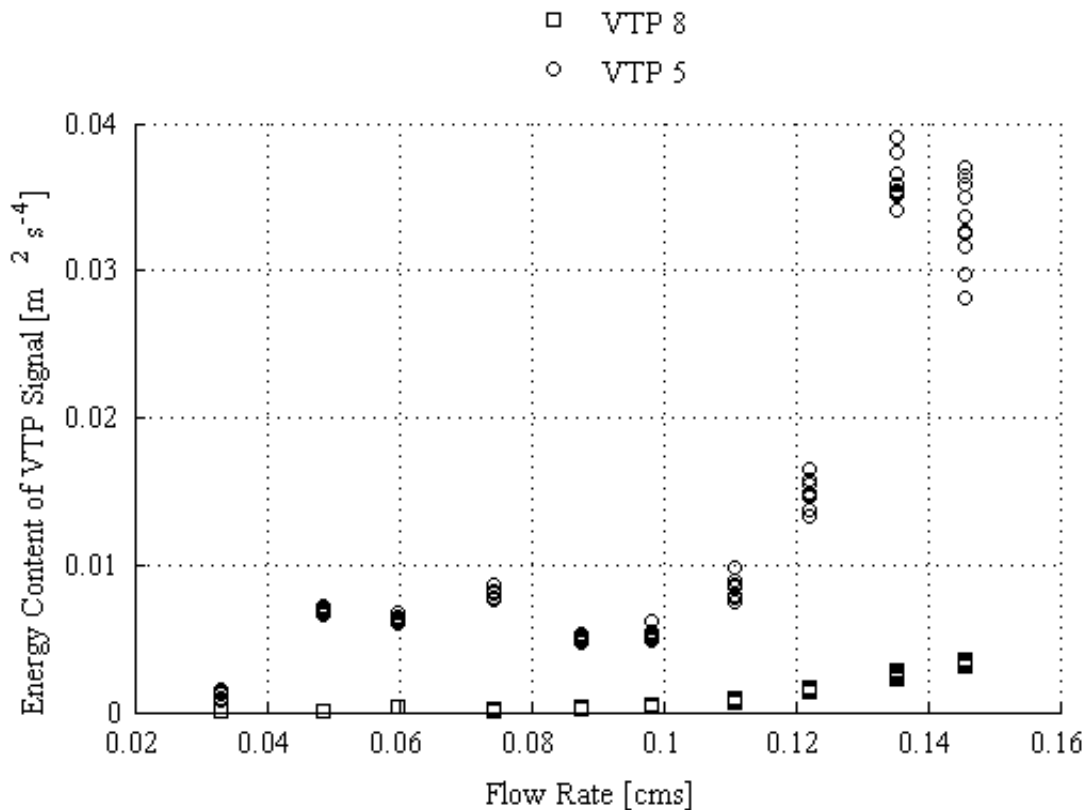


Figure 3.6 – VTP energy content of prototype VTPs versus flume flow rates<sup>1</sup>.

Additionally, Figure 3.6 highlights the potential impact that additional vibration sources can have on this method. The energy content of the VTPs in the sediment, which are dominated by noise vibration sources<sup>1</sup>, are an order of magnitude below the responses from the VTPs located in the flow, which are also subject to the same noise sources but are dominated by the vibrations due to the turbulent flow.

---

<sup>1</sup> Note that the energy content of the VTP buried in the sediment also increases in Figure 3.6. Additional experiments reveal that the flume used in the VTP evaluation is excited by the flow and pump used in the laboratory. Thus, the increase in the energy content of the VTP in the sediment is attributed to the vibration of the flume itself. Corrections to the signals to account for this additional structurally borne noise reveal the same trend as shown above. Such structural borne noise will, of course, not contribute to the field performance of this technique.

### 3.4.2 Assessing Scour Hole Performance

The nature of the turbulence in a scour hole varies in magnitude and spatial distribution from that in the channel flow, making it necessary to verify the performance of the VTPs in a scour hole. For this purpose, the response of the VTP located in a manually-developed 0.056 m deep scour hole is measured (Figure 3.7). The experiments are conducted where VTP #1 is partially submerged in the channel flow, VTPs #2-#4 fully submerged, VTP #5 partially visible in the unscoured bed and VTPs #6-#8 fully in the sediment, as shown in Figure 3.4. The energy content, computed as the mean square of the time domain acceleration response, is computed for each VTP and the mean and standard deviation are plotted against position relative to the bed in Figure 3.7.

Figure 3.7 indicates that VTP #5, which is fully uncovered by the scour hole development, is subject to an excitation level that is greater than the excitation in the main flow. This is expected however, since the turbulence intensity should be higher in the scour hole due to the separated flow (Dey and Barbhuiya, 2006). Thus, the presence of the scour hole itself improves the VTP approach's ability to detect the water/sediment interface.

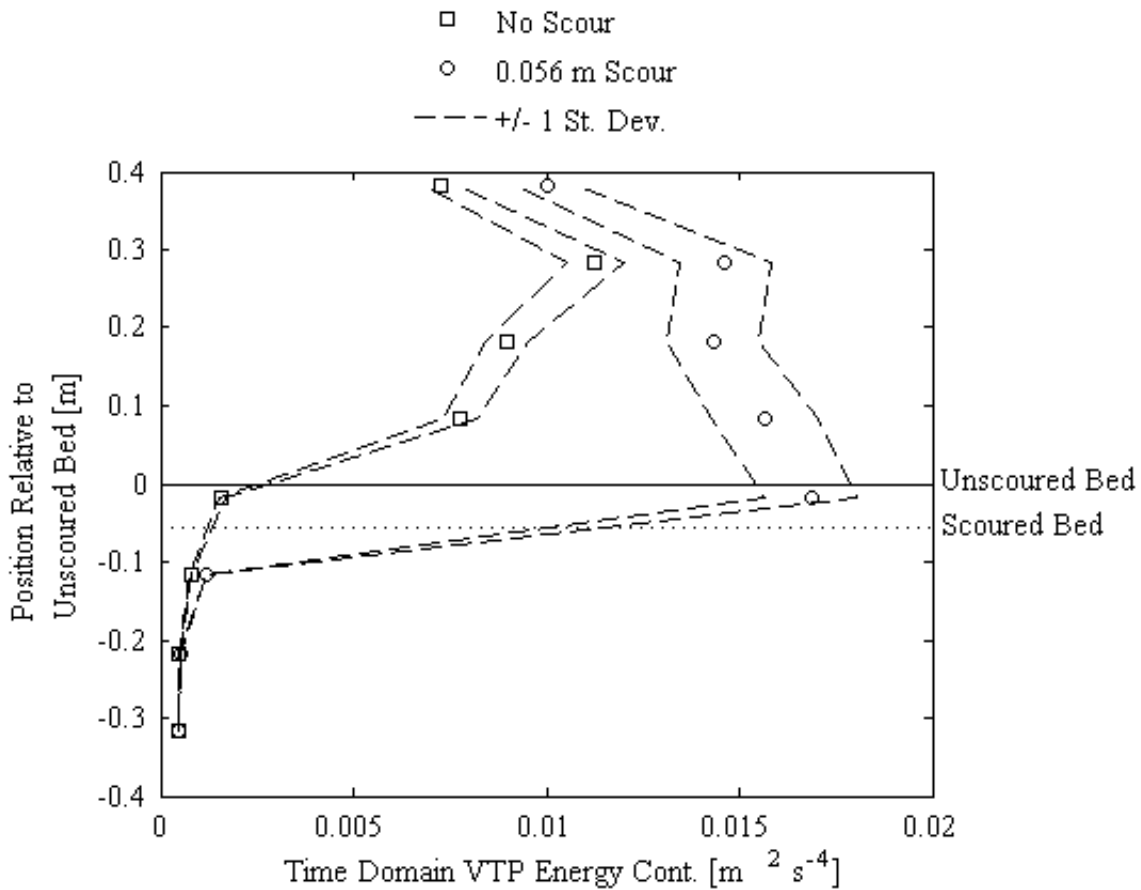


Figure 3.7 – Turbulent energy content of prototype VTPs in un-scoured and 0.056 m scoured channel bed. The mean values are denoted by the points while the dotted lines represent the standard deviation of the measured results around the mean value.

### 3.4.3 Precision Assessment

The precision of the VTP scour detection is investigated with several experimentally controlled scour holes ranging in depth from approximately 0.04 to 0.14 m. During these experiments, VTP #1 is partially submerged, VTP #2 to #4 are fully submerged, VTP #5-#8 is buried in the sediment and VTPs #5 and #6 are visible due to the various scour holes. The slope of the VTP energy content is computed along the depth, with the maximum gradient used as the determining point for the sediment interface. The depth of the scour hole is determined as the average height between the



two VTPs surrounding the point of maximum gradient. Figure 3.8 presents six profiles for the cases varying from no scour to the 0.14 m deep scour hole, along with the slope of the profiles. Figure 3.8 reveals that, for the 0.056 to 0.14 m deep scour holes, the point of maximum slope corresponds to the interface location.

Also shown in Figure 3.8 are the results for the 0 and 0.038 m deep scour holes, where the point of maximum slope is above the channel bed. Since it is only possible to locate the interface as the mid-height of the two VTP positions around the point of maximum slope, the VTP indicated water/sediment interface is 0.03 m above the original bed level. Additionally, in the 0.038 m deep scour hole case, VTP #5 responds at a level between its adjacent VTPs. In this case, VTP #5 is not fully exposed by the scour hole, indicating that a critical depth of scour around the VTP is required to observe enough of the turbulent flow to obtain an accurate measure of the water/sediment interface. As the scour hole deepens and uncovers more surface area of the VTP, the response increases, yielding a more accurate water/sediment interface location.

During the development of the scour hole shown in Figure 3.8, the 0.14 m scour event occurred prior to the 0.12 m event, thus the 0.12 m results represent a refilling scour hole scenario. For the 0.012 m case, VTP # 6 is partially exposed for approximately 50% of its diameter. Correspondingly, the energy content of VTP # 6 ( $0.0016 \text{ m}^2 \text{ s}^{-4}$ ) is between the values for the adjacent VTPs,  $0.011 \text{ m}^2 \text{ s}^{-4}$  for VTP # 5 in the flow and  $0.0005 \text{ m}^2 \text{ s}^{-4}$  for VTP # 7 in the sediment. As the refill process proceeds, however, the response of VTP #6 continues to drop, resulting in a determination of the interface location during refill.

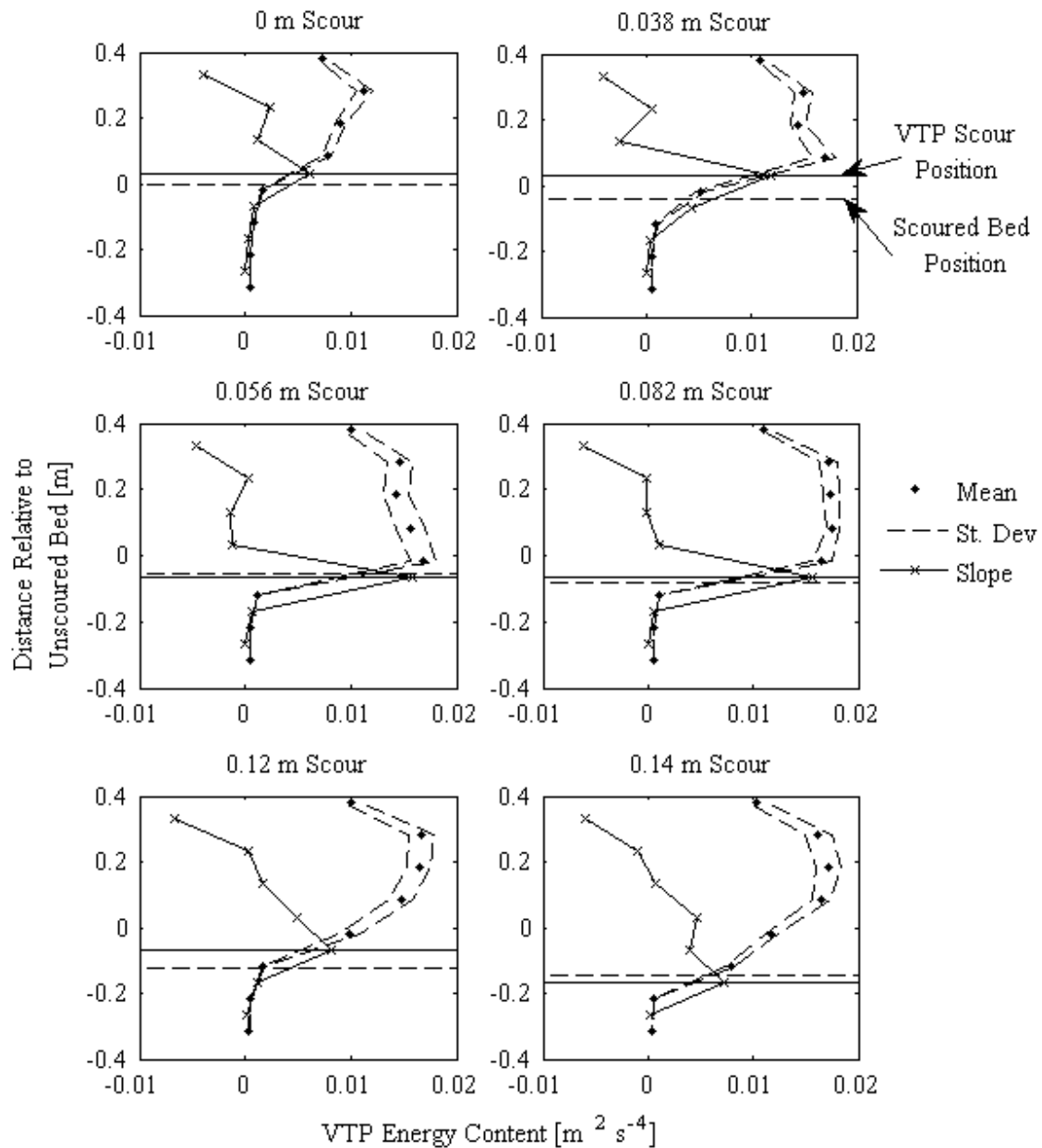


Figure 3.8 – Energy content of prototype VTPs in scour holes of various sizes. The mean profile is plotted alongside the slope of the mean profile, scaled by a factor of 1/10. The VTP and the independently measured scour hole depths are indicated for each experiment. (a) No Scour (b) 0.0385 m Scour (c) 0.056 m Scour (d) 0.0825 m Scour (e) 0.1235 m Scour (f) 0.142 m Scour.

The scour depth detected by the VTPs is then compared against the independently measured scour depth to assess the precision with which the VTP can determine the water/sediment interface (Figure 3.9). Ideally, this comparison would yield a straight line with a slope of 1:1. The results shown in Figure 3.9, however, highlight the coarse nature of the VTP spacing. Error bars plotted for each of the VTP interface locations represent  $\pm \frac{1}{2}$  of the spacing. Since the point of scour is determined by the average of the two VTPs above/below the point of maximum slope, having a larger number of closely spaced VTPs would decrease the spacing between detection points. This would lead to an improved precision in determining the scour hole location.

Figure 3.9 also illustrates that for the 0.12 m scour hole, where VTP #6 is uncovered for approximately 50% of its depth, the VTP determined scour depth, even considering the uncertainty bars, predicts a value below that of the independently measured depth. This result, in conjunction with the result from the 0.038 m scour case, where VTP #5 was uncovered for approximately 88% of its surface yet still indicated a scour position between VTPs #4-5 instead of #5-6, indicates that there is a minimum amount of VTP surface that must be uncovered by scour to register the presence of the turbulent flow. This result is attributed to the nature of the dynamic force due to turbulence impinging on the VTP surface. Since the magnitude of this force is a function of the exposed area, for a partially exposed VTP, the energy content is lower than for a fully exposed VTP. As the scour location is determined by the point of maximum slope, an energy content level between a partially exposed VTP and one in the sediment does not result in a significant change in the slope, leading to an inaccurate reading.

Conservatively, this minimum exposure can be taken as the entire surface of the VTP area. Further testing, however, is necessary for the final field version of the VTP device to verify this result.

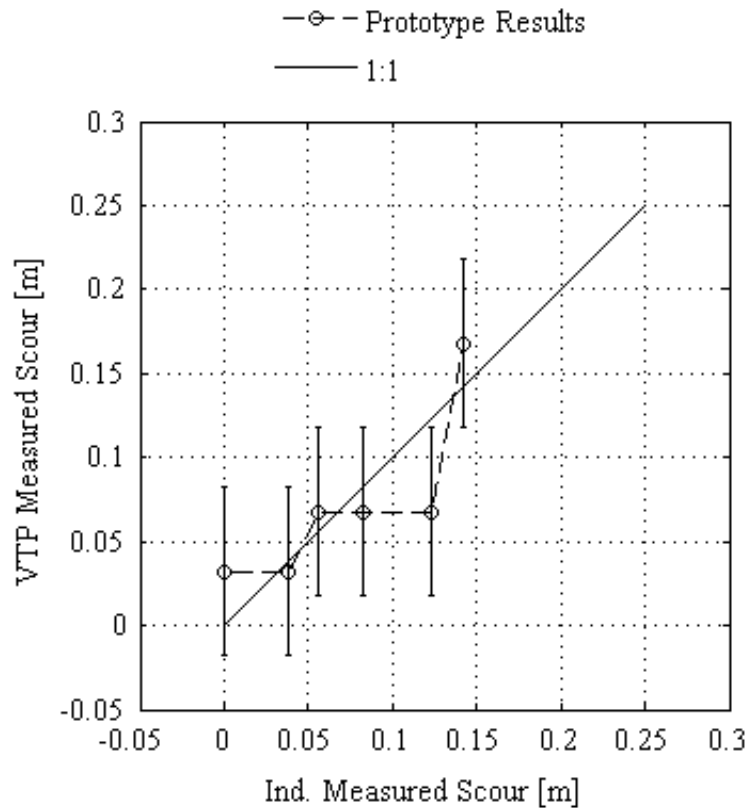


Figure 3.9 – VTP estimated scour depth versus actual scour values. The scour values determined from the VTP setup using the point of maximum slope are plotted against the actual physical scour depths. An ideal sensor would fall on the 1:1 line.

The results presented show that the VTPs are capable of distinguishing if the surrounding material is sediment or flowing water in a channel. The results also show that the method is feasible in the presence of a scour hole, in which the turbulence levels results in a dynamic pressure that is higher in magnitude than in the main, unscoured

channel. Also, the precision of the method is shown to be within the VTP spacing, which can be improved by reducing the spacing of the VTP units through further refinement of the device.

### **3.5 Conclusions**

Since scour damage to bridge piers and abutments accounts for the majority of bridge failures within the U.S., and given that the cost of these repairs can extend into the hundreds of millions of dollars, it is of critical importance to develop a robust real-time monitoring system that can detect the development and presence of scour. A survey of related literature has shown that many of the traditional measurement methods are sensitive to the environmental conditions within rivers such as water temperature, salinity, and debris in the channel.

Since measuring scour is of critical importance, and given that traditional devices are susceptible to many of the conditions in natural channels, a novel method is proposed that can determine scour depth in real time and is also insensitive to many of the conditions that cause other monitoring methods to fail. The proposed methodology consists of a series of vibration-based turbulent pressure sensors, referred to as VTPs, mounted along the length of a support pipe that is buried in the channel bed. The VTPs consist of an accelerometer attached to a thin plate, which is exposed to the channel. The mean squared acceleration response of the plate is computed in the time domain and used to determine if the material surrounding the VTP is water or sediment. Since the device is sensitive to the dynamic pressure in the flow associated with turbulent fluctuations, a VTP with high energy content indicates the presence of flowing water in the channel. A

VTP in the sediment however, is not subject to the same dynamic pressure as a device in the flow. Therefore, by measuring the profile of the energy content for multiple VTPs mounted along a bridge pier or abutment, it is possible to determine the location of the water/sediment interface.

Based upon the experimental results presented, the evidence demonstrates that the energy content of the VTPs located in the sediment is one to two orders of magnitude lower than that of the VTPs located in the channel flow. Therefore, the original hypothesis that it is possible to exploit the difference between the mean excitation level in the sediment and those in the flow to measure the water/sediment interface is demonstrated to be an effective means of monitoring the riverbed for scour. Additionally, the measurement results show that the slope of the energy content profile relative to depth is a reliable means of determining the location of the water/sediment interface, located by the point of maximum slope.

The presence of a scour hole is also shown to have little impact on the ability of the VTP method to determine the location of the water/sediment interface. The experimental results, however, reveal that the percentage of the VTP surface that is exposed to the flow affects the VTP response and thus the determination of the water/sediment interface. Even considering this result however, the precision of the VTPs are shown to be better than 0.10 m, which is more accurate than the MSC device (which has a precision of 0.15 m) but is below that of a sonar/fathometer (which is accurate to within 0.03 m).

The precision of the device is dependent upon the resolution of the sensors, and thus the VTP size. With further refinement of the sensors, the precision of the system can be improved. Additionally, further testing is needed to identify the critical amount of VTP surface exposure to the turbulent flow required to improve the identification of the presence of turbulent flow surrounding the VTP.

### 3.5 REFERENCES

- Blevins, R.D., (1990). *Flow Induced Vibration*. Van Nostrand Reinhold Co., New York.
- Blevins, R.D., (1979). *Formulas for Natural Frequency and Mode Shape*. Van Nostrand Reinhold Co., New York.
- Brice, J. C., and Blodgett, J. C. (1978). "Countermeasures for Hydraulic Problems at Bridges," Vol. 1 & 2, FHWA/RD-78-162 & 163, Federal Highway Administration, U.S. Department of Transportation, Washington, D.C.
- Cooper, T., Chen, H. L., Lyn, D., Rao, A. R., Altschaeffel, A.G., (2000). "A Field Study of Scour-Monitoring Devices for Indiana Streams: Final Report" FHWA/IN/JTRP-2000/13, October 2000.
- Craig, R. R., (1981). *Structural Dynamics: An Introduction to Computer Methods*, John Wiley and Sons, Inc.
- Dey, S., Barbhuiya, A.K., (2006). "Velocity and Turbulence in a Scour Hole a Vertical-Wall Abutment", *Flow Measurement and Instrumentation*, 17, pp.: 13-21.
- Gutowski, T.G., Dym, C.L., (1976). "Propagation of ground vibration: A review." *Journal of Sound and Vibration*, 49(2), pp. 179-193.
- Holnbeck, S. R., McCarthy, P. M., (2011). "Monitoring Hydraulic Conditions and Scour at I-90 Bridges on Blackfoot River Following Removal of Milltown Dam Near Bonner, Montana, 2009" in *Scour and Erosion: Proceedings of 5<sup>th</sup> International Conference on Scour and Erosion*. Ed: Burns, S.E., Bhatia, S.K., Avila, C. M. C., Hunt, B. E., November 7-10, 2010, San Francisco, CA., A.S.C.E.
- Lagasse, P. F., E. V. Richardson, J. D. Schall, and G. R. Price, (1997). *NCHRP Report 396: Instrumentation for Measuring Scour at Bridge Piers and Abutments*. TRB, National Research Council, Washington, D.C., 1997.

- Nakagawa, H., Nezu, I., Ueda, H., (1975). "Turbulence of Open Channel Flow Over Smooth and Rough Beds", Proceedings of the Journal of Society of Civil Engineers, No. 241, September.
- Nassif, H., Ertekin, A. O., Davis, J., (2002). "Evaluation of Bridge Scour Monitoring Methods: Final Report" Federal Highway Administration, Report FHWA-NJ-2003-09, March, 2002.
- Neill, C.R. (1964). "River Bed Scour, a Review for Bridge Engineers," Contract No. 281, Research Council of Alberta, Calgary, Alberta, Canada.
- Nezu, I., Nakagawa, H., (1993). *Turbulence in Open-Channel Flows*. IAHR, AIRH Monograph, A.A. Balkema Publishers, Rotterdam, Netherlands.
- Rhodes, J., Trent, R., (1993). "Economics of Floods, Scour and Bridge Failures" in *Hydraulic Engineering '93: Proceedings of 1993 Conference*. Ed: Shen, H.W., Su, S. T., Wen. F., July 25-30, 1993, San Francisco, CA, A.S.C.E.
- Shirole, A. M., Holt, R. C., (1991) "Planning for a Comprehensive Bridge Safety Assurance Program", Transportation Research Record, No. 1290, Vol. 1, Transportation Research Board, National Research Council, Washington, D.C.
- USGS, (2006), "Water Data Report 2006: 02172053 Cooper River at Mobay Near North Charleston, S.C.", U.S. Dept. of Interior, U.S. Geological Survey.
- USGS, (2006), "Water Data Report 2006: 02156500 Broad River Near Carlisle, S.C.", U.S. Dept. of Interior, U.S. Geological Survey.
- Von Karman, T. (1948). "Progress in the Statistical Theory of Turbulence." Proceedings of the National Academies in Science, Vol. 34, pp. 530-539.
- Yankielun, N.E., Zabilansky, L. (1999). "Laboratory Investigation of Time Domain Reflectometry System for Monitoring Bridge Scour", *ASCE Journal of Hydraulic Engineering*, Vol. 125, No. 12 pp. 1279-1284.
- Yu, X., Yu, X., (2009), "Time Domain Reflectometry Automatic Bridge Scour Measurement System: Principles and Potentials", *Structural Health Monitoring*, Vol. 8, No. 6., pp: 463-476.
- Yu, X., Yu, X., (2011). "Development and Evaluation of an Automatic Algorithm for a Time-Domain Reflectometry Bridge Scour Monitoring System" *Canadian Geotechnical Journal*, Vol. 48 pp. 26-35.



## CHAPTER FOUR

### THE EFFECT OF CHANNEL CONDITIONS ON SCOUR MEASUREMENTS

#### **4.1 Introduction**

Scour damage to bridges is widespread and costly, both in human and financial terms, and as pointed out in the US Federal Highway Administration HEC-23, can be countered with appropriate monitoring of the riverbed (Legasse et al., 2009). These monitoring methods are sensitive to many of the environmental conditions in natural channels, such as temperature, turbidity, etc. It is essential, therefore, to understand the impact these, and other, parameters may have on a scour monitoring method before deploying any monitoring system in the field.

Scour on bridge piers and abutments typically occurs during peak flood periods, such as floods or hurricanes, and has been directly linked to the failure of several bridges. Flooding in the Northeastern United States in 1987 resulted in damage to 17 bridges, while in 1993, 2,500 bridges in the Midwest were damaged (Mueller, 2000). During 1961-1974, of the 86 bridge failures that occurred, 46 were attributed to scour damage (Murillo, 1987). More recently, from 1996-2001, 68 bridge failures in the US were attributed to scour (Lin et al., 2006). The potential risk from scour to bridge infrastructure can be realized by considering the number of scour critical or scour susceptible bridges; 109,464 bridges in the US fall into one of these two categories (Richardson and Price, 1993). Hunt (2009) reported that of the 590,000 bridges in the US, 20,994 are scour

critical, the most serious of the two conditions. Overall, 60% of the failures of bridge structures are due to scour damage (Lagasse et al, 1997).

Floods, often the main source of the increased flows, lead to the development of scour holes and can cost millions of dollars in damage. In Virginia and the Midwest during 1993 to 1995, flooding caused \$40 to \$178 million in damages, respectively (Mueller, 2000). Butch (1996) reported that the repairs from flood damages in the 1980s amounted to \$300 million. The cost to repair bridges from scour damage have also been calculated. For example, Brice and Blodgett (1978) reported that the cost to repair the infrastructure is roughly \$100 million per scour event. On an aggregate basis, the total annual budget devoted to scour repairs by the US federal government (between Federal Emergency Management Agency and Federal Highway Administration projects) is \$20 million annually (Rhodes and Trent, 1993). These costs, however, only account for the impact to the infrastructure itself and neglect the additional costs to the afflicted population, who depend upon the bridge as a vital part of their transportation system. These additional costs have been estimated to be as much as five times the cost of the actual repairs (Rhodes and Trent, 1993).

While the financial costs can be significant, the loss of a bridge from scour that result directly in the loss of human life are even more costly. Three such failures have occurred, including the Schoharie Creek, Hatchie River, and Arroyo Pasajero River bridge failures. In 1987, the I-90 bridge failed due to a scour hole that formed around a pier footing with inadequate protection, resulting in the loss of 10 lives (NTSB, 1987). The U.S. 51 bridge failure over the Hatchie River in Tennessee in 1989 was caused by

the scour hole that formed due to migration of the main channel, which went undiagnosed (NTSB 1989), and resulted in the loss of eight lives. Seven lives were lost in 1995 in California when a 3 m deep scour hole formed on the I-5 bridge over the Arroyo Pasajero River (Arneson et al, 2012).

To counter these threats and to monitor the health of bridge infrastructure, 32 states have deployed scour monitoring systems. Sonic fathometers represent one of the most prominent methods for monitoring scour with 104 fathometers installed on 48 bridges (Lagasse et al., 1997). The performance of sonar based scour monitoring systems has been reported by Legasse et al. (1997), Nassif et al. (2002), Hunt (2005), Mason and Sheppard (1994), DeFalco and Mele (2002), Holnbeck and McCarthy (2011), and Cooper (2000). These reports have documented accurate measurements of scour holes from 0.23 to 1.2 m in depth as well as successful operation during hurricanes. While sonar systems have been used extensively, the environmental parameters in rivers can impact the performance of the device. These include air bubbles entrained in the flow, suspended sediment and turbidity, debris, salinity, and temperature. DeFalco and Mele (2002) attributed the cause of 5 m spikes in the measured time histories of two bridges in Italy to the presence of air bubbles and suspended sediment/turbidity in the channel flows. Legasse et al. (1997) reported on the performance of sonar devices in conditions with significant air entrainment, which lead to the inability of the system to determine the bed depth. Additionally, factors that affect the speed of sound, such as temperature and salinity, accounted for a 0.5 m offset in testing on a bridge over an inlet in Florida (Legasse et al., 1997). Another factor that can have a significant impact on the

performance of a sonar system is the presence of debris in the channel. Debris can result in false echoes, leading to inaccurate readings, or direct failure of the device as it physically impacts the hardware or cabling. Cooper et al. (2000) reported that debris damage led to the loss of the entire hardware system in field tests in Indiana. Lastly, sonar pulses are emitted as a discrete cone defined by the hardware itself. As the pulse reaches the scour hole, its diameter may be smaller or larger than the hole itself, depending upon the distance between the two objects. In this case, if the hole is small relative to the beam diameter at the bed, it is possible to have reflected waves returned by the unscoured channel bed. This presents a problem for the determination of scour with sonar devices.

Another scour monitoring technique that has received attention is time domain reflectometry (TDR), which uses electromagnetic waves to determine the location of water/sediment interface. The TDR system consists of rods buried into the riverbed, which act as waveguides for EM pulses. The EM pulses are reflected at various interfaces, such as the water/sediment interface or the air/water interface. TDR devices have been studied extensively in the lab and the investigations have included evaluating the device precision with various sediments, the impact of suspended sediments in the water as well as salinity effects [(Yankeilun and Zabilansky, 1999), (Yu and Yu, 2006), (Yu and Yu, 2011), (Yu and Zabilansky, 2006)]. The device has also been used to monitor the development of scour under ice at the Hwy 16 Bridge in Missouri, where the growth and refill of scour holes on the order of 0.15 m were measured [(Ettema and Zabilansky, 2004), (Zabilansky et al., 2002)]. While the method is more robust than sonar

to debris, its sensitivity to conditions within the channel remain a concern. Yu and Yu (2011) evaluated the performance of a TDR device in saline and turbid water conditions. In their laboratory tests, the device was tested in saline solutions up to 750 parts per million (PPM) and revealed that the measured depth values were within 5% of an independently measured depths of sediment. For these tests, the TDR device was encased in a plastic sleeve that reduced the dissipation of the EM pulse from the tube wave guides. Data was not reported for the device in its original, un-sleeved configuration. While promising, these results only represent the performance of the TDR system within a narrow range of saline conditions, which can vary from 50 PPM in the upper reaches of a watershed to 17,500 PPM in near coastal waters [(USGS, 2006a), (USGS, 2006b)]. In a similar manner, the temperature of the water in the river can affect the speed of the EM pulse, leading to inaccuracies in the measured lengths. For instance, temperatures can vary from 7 to 20 °C [(USGS, 2006a), (USGS, 2006b)], which can lead to errors in the assumed speed of EM waves in the channel. If the two factors are combined, the result can deviate from the true depth considerably.

Given the variability in the environmental conditions in natural channels that can have an effect on scour monitoring equipment, it is necessary therefore to understand the impact these conditions can have on a measured scour hole depth. To that end, an experimental campaign is undertaken to evaluate the performance of sonar and TDR instruments under simulated field conditions. In addition, a novel method, discussed in Fisher, et al. (2012a), is also evaluated to determine its sensitivity to these conditions.

The performance of the sonar, TDR, and the novel method are considered under the following environmental conditions, where appropriate:

- Saline conditions, from 0 to 35.5 PPT,
- Water temperatures, from 5 to 40 °C,
- Water with suspended sediments, for turbidities up to 900 NTU, including stratification effects,
- Scour hole size,
- Flow angle of incidence,
- Minimum channel velocity,
- Bed sediment type.

The objective of these experiments is to facilitate the deployment of these scour monitoring systems in the field, and to provide information on the relative strengths and weaknesses of the devices. This can aid in selecting the optimal device for the anticipated field conditions. In addition, the factors that should be considered during installation can be drawn from these results.

## **4.2 THEORY AND BACKGROUND**

### **4.2.1 Sonar**

As discussed in Chapter 2, the speed of sound in water,  $c$ , is the fundamental parameter that can affect sonar transducer results. Typically, the speed of sound is assumed to be constant; however it has been shown to vary with temperature, salinity and depth [(Kuwahara, 1939), (Leroy, 1969), (Urlick, 1975), (Mackenzie, 1981)]. For a

temperature change of 20 °C the error can be up to 4%, corresponding to nearly 0.15 m for an initial depth of 3.75 m (Fisher et al., 2012b). Changes in the speed of sound due to salinity also cannot be ignored. For an increase in salinity of 18 PPT, not uncommon for near-coastal waters, the percent error in the measured result can be as much as 1.4 to 1.6 % (Fisher et al., 2012b).

In addition to temperature and salinity effects, the suspended sediment concentration can affect the measured sonar results. The suspended sediment manifests itself as a density gradient across the channel depth, with a distinct peak occurring near the bed for highly stratified turbid flows. To account for this effect it is possible to use a model developed by Robins (1990), which accounts for the density gradient effect on the reflection coefficient (the ratio of the incident to reflected signals at an interface). Based upon this model it is possible to determine the reflection coefficient from the bed material and that from any turbidity stratification in the flow. As revealed in Fisher et al. (2012b), the reflection coefficient for the channel bed ranges from 0.2 to 0.3. For the stratified flows, however, it is necessary to have a suspended sediment concentration of 800 g/L before the reflection coefficient approaches 0.2. As typical channels have a suspended sediment concentration of 10 g/L (Gray et al, 2003), it is possible to conclude that the sonar pulse will not be significantly affected by the stratified flow, and the main reflection will occur at the channel bed.

#### 4.2.2 Time Domain Reflectometry

As with sonar, the TDR method is also affected by the channel salinity, temperature and suspended sediment concentration. Using Stogryn's (1971) model, it is

possible to account for the impact of salinity and temperature on the dielectric constant, which was discussed in Chapter 2 as a key parameter that governs the TDR results. Temperature alone is predicted to lead to an increase in the percent error of the bed measurements by as much as 5% (Fisher et al, 2012b). When the salinity effects are combined, this can increase to over 6%. Therefore, the impact of salinity and temperature on the TDR method must be considered. Yu and Yu (2011) developed a method which can be used to quantify the effect of the effect of suspended sediment on the dielectric constant of turbid waters. Using this model, it was determined that error introduced into the TDR bed measurements is limited to within a 1% relative error for typical channel sediment concentrations (Fisher et al, 2012b).

#### 4.2.3 Dynamic Turbulent Pressure Based Sensor

Given the variation in performance of TDR and sonar scour monitoring methods to suspended sediment, salinity and temperature, a novel method has been proposed that exploits the natural turbulence in the channel to measure the growth of a scour hole in a channel bed (Fisher et al., 2012a). The device consists of a series of sensors located along the length of a partially buried, vertical pipe that is installed immediately upstream of the bridge pier or abutment. Each sensor is equipped with a flexible disk that has been selected to respond to the dynamic pressure from the turbulent fluctuations in the flow, which gives rise to the sensor name, vibration-based turbulent pressure sensor (VTP). The vibrations of the VTPs are measured with an accelerometer in the time domain. The mean squared signal from each sensor, referred to as the energy content, is computed and is proportional to the vibrational energy of each VTP. The energy content of the array of



VTPs is then monitored. It was shown that the energy content of the VTPs in the flow are one to two orders of magnitude greater than the VTPs located in the sediment (Fisher et al., 2012a). This variation is then used to determine the water/sediment interface location, and thus monitor the formation of scour holes.

As the VTP method relies upon the turbulent pressure fluctuations to determine which sensors are located in the flow, it is essential to assess the performance of the method to the environmental properties in the flow that could impact the turbulence characteristics in natural channels. To that end, a disposition on the impact of suspended sediments, salinity and temperature on turbulence in open channels is required.

Since the VTP method relies upon the turbulent velocity fluctuations ( $u'$ ,  $v'$ , or  $w'$ ) in the channel flow, any impact to these turbulent characteristics could influence the performance of the novel method. The available literature on the influence of suspended sediment on turbulent flows suggests that the impact is not well understood. Itakura and Kishi (1980) evaluated the results from previously published turbulence measurements in suspended sediments and concluded that the von Karman constant decreases with increasing sediment concentration. Additionally, they concluded that the presence of the suspended particles reduced the magnitude of the turbulent velocity fluctuations. Coleman (1981), however, conducted several experiments and concluded that while the velocity profile can change shape in the presence of suspended sediments, the von Karman constant is independent of concentration. More recently, Nezu and Azuma (2004) concluded that there is a small decrease in the von Karman constant with increasing sediment load. In regards to the velocity fluctuations, Nezu and Azuma (2004)

concluded that in the outer region of the flow, the particles have little effect, while in the region near the wall, the turbulent fluctuations are enhanced by the presence of suspended sediment. In addition to the increase in near bed turbulence due to suspended sediment, the impact of the sediment particle on the VTP in the flow may further enhance the measured energy content. Thus in all likelihood, the presence of suspended sediment may improve the difference in the energy content between the VTPs buried in the river bed and the ones in the flow.

To evaluate the impact on the VTP due to changes in the channel salinity or temperature, it is necessary to consider the effect these two parameters may have on the turbulent quantities in the flow. For turbulent open channel flows, velocity fluctuations increase in magnitude with Reynolds number, until the point at which the flow becomes fully turbulent (also called rough turbulent flow). Henderson (1966) reported that for  $u_*k_s/\nu$  of greater 100, the flow in open channels is fully turbulent, where  $u_*$  is the shear velocity based on the bed shear stress,  $k_s$  is the surface roughness, and  $\nu$  is the kinematic viscosity of the fluid. For a straight, uniform channel, the  $k_s$  value is approximately 0.3 cm, for a depth of 0.4 m and velocity of 25 cm/s,  $u_*$  is 3.5 cm/s and the corresponding  $u_*k_s/\nu$  is greater than 100. These values represent a very shallow, low velocity natural channel. Thus, it is safe to assume that for natural channels of interest for scour monitoring, the flow will be fully turbulent irrespective of temperature and salinity changes. The salinity has a minor effect on the kinematic viscosity in rivers (the maximum salinity in near coastal areas is about 17PPT). The decrease in temperature

causes reduction in kinematic viscosity. However, in natural channels, the irregular bed and higher bed roughness will dominate and lead to an increase in the values of  $u_*k_s/\nu$ .

Lastly, in the ideal case the axis of the disk in the VTPs is aligned with the mean flow direction. It is possible for the mean flow angle relative to the VTP to shift as the channel overflows onto the flood plain. As such, it is necessary to consider the misalignment of the probe.

Given the potential impact of temperature and salinity on the TDR and sonar instruments, it is necessary to evaluate their performance under realistic channel conditions. All methods show a potential sensitivity to the presence of suspended sediment in the channel (i.e. turbidity), and require experimental investigations. Furthermore, due to the nature of an expanding sonar beam, it is also important to evaluate the performance of a sonar device subject to scour holes of varying size. Finally, VTP performance should be evaluated when the probe is not fully aligned with the main channel direction.

#### **4.3 MEASUREMENT SETUP**

To investigate the effects of environmental parameters on sonar, TDR, and VTP instruments, several experiments are conducted in the Clemson Hydraulics Laboratory (CHL). The experimental setup for the TDR and sonar devices is reviewed extensively in Fisher et al. (2012b). The focus in this section of Chapter 4 is to discuss the pertinent details of the setup for the novel scour monitoring method.

To evaluate the VTP performance, experiments are conducted to investigate the effect of suspended sediment and misalignment between the main flow direction and the

VTP axis. Additionally, the effect of bed material is investigated to determine the impact to the sensors located below the channel bed level. Lastly, the flow rate is varied in order to determine the minimum flow rate required for a distinct difference between the VTPs located in the bed and in the channel flow.

The VTP configuration consists of sensors with a 2 cm radius neoprene disk, instrumented with a PCB 325A24 accelerometer of 0.8 grams, with a sensitivity of 10 mV per  $m\ s^{-2}$ . The VTPs are installed along the length of an aluminum support pipe, spaced at intervals of 10 cm, as shown in Figure 4.1. The measured results were recorded with a Bruel and Kjaer Lan XI 3050A-060 data acquisition system, operating at a sampling frequency of 25.6 KHz. A convergence study reveals that a 4 minute measurement period is sufficient to yield results that are within 1% of the long time period value. For each measurement condition, three repeat measurements are taken.



Figure 4.1 - VTP setup as installed in CHL flume for channel effects study.

For the turbidity tests, the VTP is evaluated in the CHL flume, with flow depths of 62 cm, velocities from 7 to 12 cm/s, and turbidities from 0 to 900 NTU in 300 NTU increments. For the flow misalignment tests, the flow velocity is held constant at 27 cm/s while the alignment angle was increased in increments of 15° to 90°. For the minimum flow rate tests, the velocity ranges from 14 to 30 cm/s, with flow depths up to 0.34 m.

#### **4.4. Results and Discussion**

The following sections outline the experimental results for the various methods. The sonar results are shown in section 4.4.1, the TDR results are reviewed in section 4.4.2, and the VTP results are discussed in section 4.4.3.

##### 4.4.1 Sonar

The measured sonar results indicate that the errors in the bed depth ranged from 1.8 to 6.0 %, relative to the depth at 20 °C (Fisher et al., 2012b). This is consistent with the models available to account for the change in the speed of sound. As this effect is not minor, it is necessary to correct for temperature change by measuring this parameter along with the sonar results and adjusting for the effect on the speed of sound. Salinity effects also revealed that the impact is not minor, with a 3.8% increase in the relative error for 35.5 PPT (Fisher et al., 2012b). This can also be accounted for by measuring the channel conditions and correcting for changes in the speed of sound.

The turbidity effects, as discussed in Fisher et al. (2012b) are also measured and revealed that for still, turbid waters there is no impact due to suspended sediment, up to

the maximum turbidity tested of 525 NTU. For channel flows with a uniform turbidity, however, the relative error in the bed measurements increases from 1 to 3% for velocities less than 9 cm/s. The results also reveal that suspended sediment concentration was not a factor in the results. Above 9 cm/s, the standard deviation of the measured 30 second time histories was above the sonar device tolerance limit of 3 cm, indicating an inability to determine a stable bed level. This effect was also present in the stratified turbidity tests, which show a maximum increase in the relative error in the bed level of 17.5%. From these cumulative turbidity test results it can be concluded that sonar should not be used independently in highly turbid zones. Lastly, the sonar results for varying beam width to scour hole size reveal that the sonar device reports the minimum water depth encountered. This presents a problem when measuring scour holes of varying topography and size. This can be mitigated by placing the device closer to the bed.

#### 4.4.2 Time Domain Reflectometry

The impact of the channel conditions on the TDR method is also evaluated. The results, as discussed in Fisher et al. (2012b), reveal that temperature and salinity have an effect on the measured TDR signal. The temperature effects result in relative errors in the bed level of 1.4 to 5%, which is in line with predictions using Stogryn's (1971) model. This effect can be accounted for by measuring the channel temperature and correcting the dielectric constant accordingly. Salinity effects have a more significant effect on the measured TDR signal, to the point that the waveform becomes indistinct above certain concentrations. The results show that above a salinity of 500 PPM, the TDR signal features cannot be distinguished accurately. Therefore, TDR should be confined to

freshwater conditions. Lastly, the results showed that the suspended sediment concentration had no measureable effect on the TDR signal, which is in line with the predictions using the Yu and Yu (2011) method.

#### 4.4.3 VTP Based Method

As discussed in Section 4.2, the VTP based method has the potential to be affected by the turbidity in the flow, as well as any misalignment between the main flow direction and the VTP axis. Also, in order to fully evaluate the VTP method, it is necessary to consider the effect of different sediment types on the measured energy content in the bed. Lastly, as the minimum channel velocity needed to achieve a measurable difference between those VTPs located in the flow and those in the sediment should be determined. The tests used to evaluate the performance of the VTP device under these conditions are discussed in the following section.

The impact of dynamic turbidity on the VTP's turbulent energy content is shown in Figure 4.2 for turbidities ranging from 0 to 900 NTU and flow velocities from 7 to 12 cm/s. The results indicate that the registered energy content shows a slight increase with turbidity. The increase in the VTP energy content with flow velocity is expected since  $\sqrt{u'^2}$  increases with the mean flow velocity.

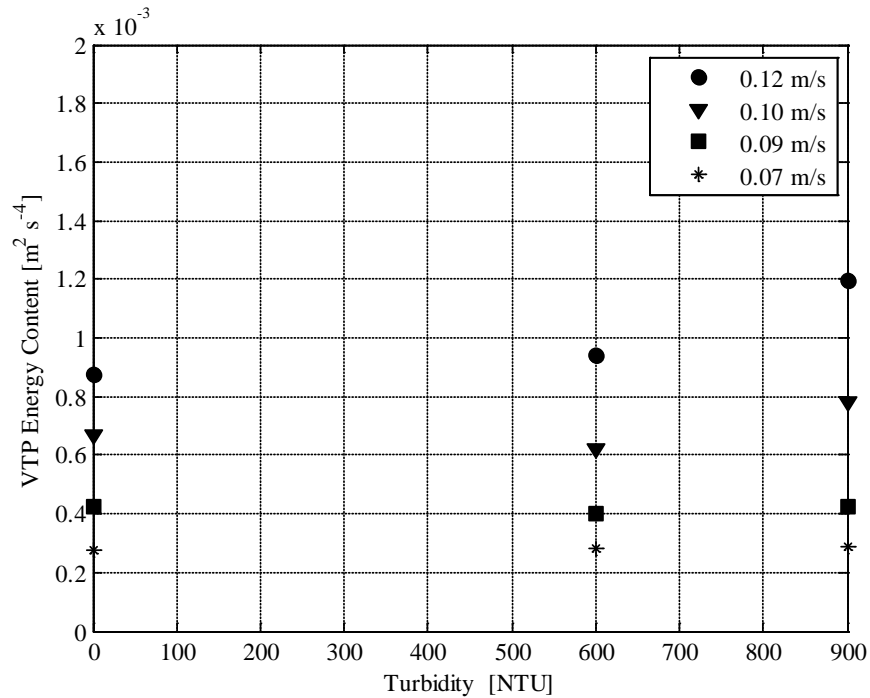


Figure 4.2 - VTP Energy content for various turbidity levels and channel flow velocities.

The results shown in Figure 4.2 indicate that the VTP's energy content response increases with the presence of turbidity in the flow, and thus the device can be deployed without the need to monitor the channel condition. The energy content of the VTP buried in the bed was not affected by turbidity and flow velocity.

During high flow events, it is possible that the main flow direction can shift from the nominal flow condition. Therefore, it is necessary to understand how a VTP performs as the flow direction relative to the probe changes. Figure 4.3 reveals the VTP energy content for three sensors located at different depths within the channel. VTP #6 is located in the sediment and therefore the response should not be a function of the flow angle. This is revealed in the results shown in Figure 4.3. VTP #5 is located within a scour hole, and the results reveal that the response for VTP #5 is insensitive to flow angle. This is



attributed to the fact that in the scour hole, the flow is separated. Thus the sensor in a scour hole is subject to velocity fluctuations from the separated flow instead of the turbulent free stream velocity fluctuations. The recorded energy content for VTP #5 is order of magnitude higher than the VTP in the bed (#6), indicating that the method can be used to determine the water/sediment interface. The energy content recorded by VTP #4 is sensitive to the flow angle, dropping from  $0.016 \text{ m}^2 \text{ s}^{-4}$  at  $15^\circ$  to  $0.0075 \text{ m}^2 \text{ s}^{-4}$  at  $90^\circ$ . This is expected as the magnitude of the turbulent fluctuations normal to the VTP surface diminishes with increasing misalignment. It is also important to note that the results are still order of magnitude higher than the VTP located below the bed. The ratio between VTP #4 and VTP #6 at  $90^\circ$  is approximately 75. This suggests that the method can still be used in highly misaligned flows. For the higher flow angles, the separated flow around the probe itself maintains the energy content at a level much higher than the energy content in the sediment.

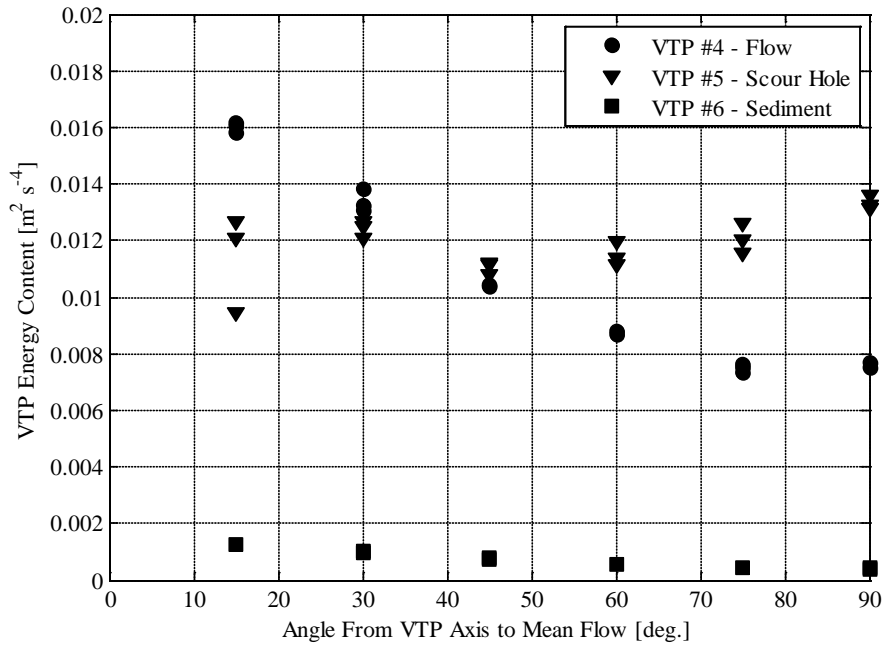


Figure 4.3 - VTP Energy content as a function of the flow misalignment.

Chapter 3 revealed that the minimum energy content in the flow should be at least one order of magnitude greater than in the sediment. To investigate the impact of velocity, the energy content of two VTPs are recorded for depth averaged channel velocities from 14.7 to 30 cm/s, as shown in Figure 4.4. The results reveal that the energy content of the VTP in the sediment decreases with decreasing velocity, to a minimum of  $4E-5 \text{ m}^2 \text{ s}^{-4}$ . For the VTP in the flow, the energy content decreases to  $0.002 \text{ m}^2 \text{ s}^{-4}$ . This value is low compared to the higher velocity energy content values, however, it is still greater than the sediment values by a factor of 50. Thus, the VTP method is still able to determine the water/sediment interface. Based upon these results, it can be concluded that the VTP method will function for a depth averaged channel velocity of at least 14.7 cm/s.

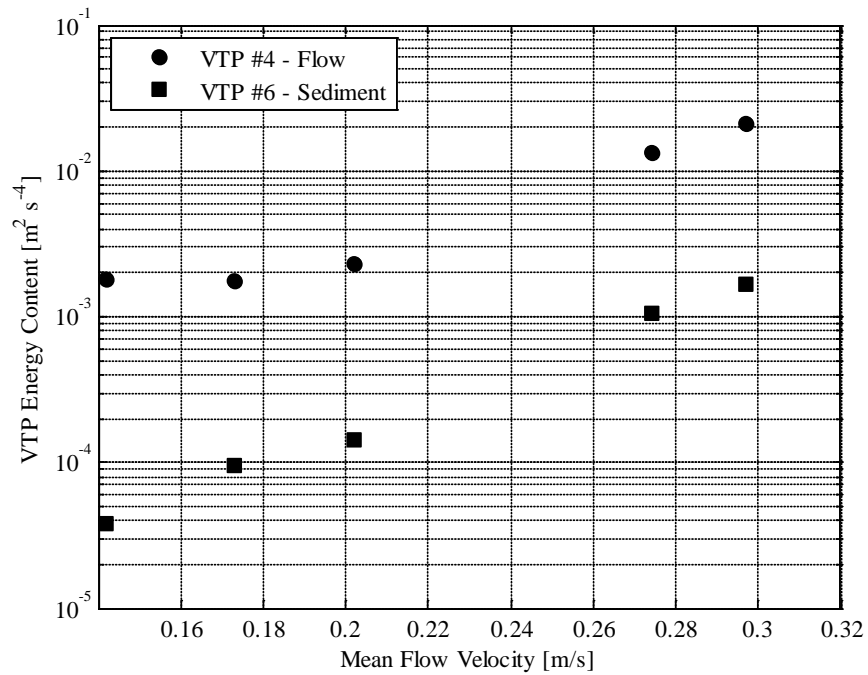


Figure 4.4 – Variation of VTP energy content with channel velocity.

Lastly, when considering the response of the VTP method, it is also important to investigate the impact of varying sediment types on the energy content in the sediment. The potential effect of varying sediment types was investigated by conducting three experiments in two different quartz sands and a clay sediment. The results of these experiments are shown in Figure 4.5. The results shown in Figure 4.5 indicate that the sediment has no measurable impact upon the measured energy content for the VTPs located in the channel bed. Therefore, the device can reliably be deployed without being significantly affected by the nature of the sediment type in the channel.

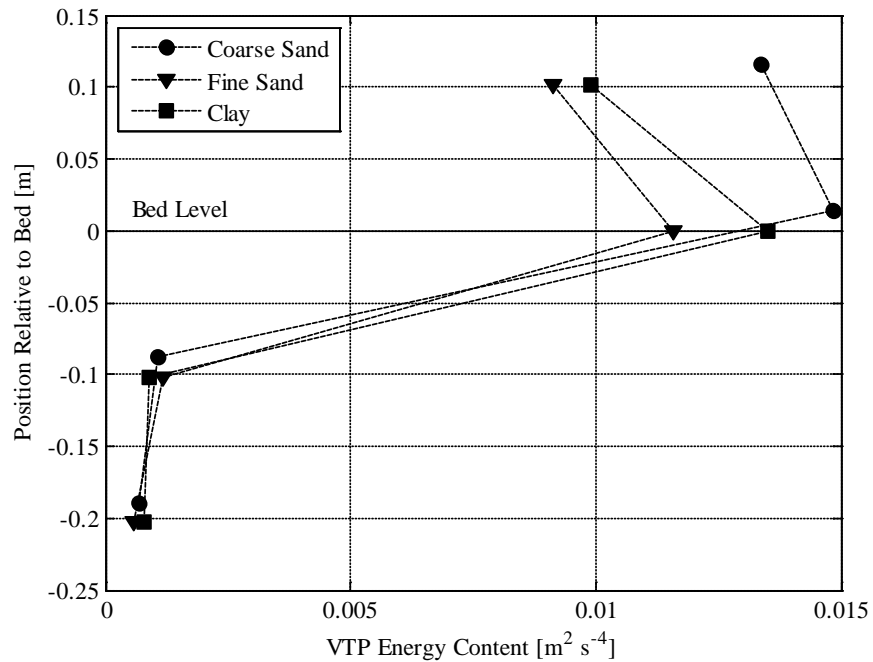


Figure 4.5 – Variation in VTP energy content for various bed sediment types.

#### 4.5 Conclusions

Given the fact that the changing environmental conditions in natural channels are inevitable, it is necessary to understand how these parameters can affect any scour monitoring system. A series of experiments were conducted on two common scour measurement devices, namely a sonar transducer and a time-domain reflectometry probe. In addition, the performance of a novel method which exploits the flow turbulence in the channel was also evaluated.

From the series of experiments conducted it can be concluded that for the sonar device, changes in the temperature can result in relative errors up to 6% in channel depth. This can be accounted for in the field by measuring the temperature and

accounting for the change in the speed of sound. Salinity can lead to relative errors of up to 3%, which is within the tolerance of the device tested.

The concentration of suspended particles does not affect the sonar results in still water. For dynamic turbidity, uniform as well as stratified, the relative error in bed level measurements can be significant. The results indicate that measuring the standard deviation of the recorded signal may be important to ascertain the viability of the measurements. Lastly, the beam width with respect to scour size and the height at which the sonar is located above the bed may significantly affect the accuracy of the scour depth measurements. It was determined that for variable bed topography, the sonar measures the shallowest depth.

The channel temperature can have a significant effect on the measured depth of a scour hole recorded with a TDR. The relative errors can be of the order of 5%. This effect, however, can be mitigated by monitoring the channel temperature in addition to the TDR waveform. Salinities greater than 500 PPM result in a loss of the distinct features needed in the TDR waveform that are required to determine the length of the water and sediment around the probe. It may be necessary to avoid the installation of TDR in brackish conditions. Turbidity in the channel flow had no effect on the TDR measurements and can be used for monitoring scour in highly turbid zones.

The performance of a VTP was evaluated under turbid flow conditions and varying flow angles. There was no significant change in the energy content recorded by the VTP based method for varying turbidities. Thus, it is possible to use the method in turbid zones. The energy content recorded by the VTP located in the flow decreased with

increasing misalignment between the probe and the main flow direction. At 90°, the energy content of the VTP in the flow is an order of magnitude greater than the VTP in the sediment. Thus, it can record the location of the water/sediment interface. In addition, it was determined that the VTP method is not affected by the bed sediment type and performs in coarse and fine sand beds as well as in clay beds. The study into the minimum flow rate revealed that for depth averaged channel velocities of 14.7 cm/s or greater, the device can determine those sensors in the channel flow.

Based upon the results presented for the various methods it is possible to evaluate potential scour monitoring sites and to select methods that are insensitive to the anticipated channel conditions, resulting in more robust field measurements.

#### **4.6 References**

- Arneson, L.A., Zevenbergen, L.W., Lagasse, P.F., Clopper, P.E., (2012). “Hydraulic Engineering Circular No.18: Evaluating Scour at Bridges, 5<sup>th</sup> Ed.”, U.S. Dept. of Transportation, Federal Highway Administration, Publication No. FHWA-HIF-12-003.
- Brice, J. C., and Blodgett, J. C. (1978). “Countermeasures for Hydraulic Problems at Bridges,” Vol. 1 & 2, FHWA/RD-78-162 & 163, Federal Highway Administration, U.S. Department of Transportation, Washington, D.C.
- Butch, G.K., (1996). “Evaluation of Selected Instruments for Monitoring Scour At Bridges in New York.”, North American Water and Environment Congress, ASCE.
- Coleman, N. L., (1981). “Velocity Profiles with Suspended Sediment”, Journal of Hydraulic Research, Vol. 19, No. 3., pp.: 211-229.
- Cooper, T., Chen, H. L., Lyn, D., Rao, A. R., Altschaeffel, A.G., (2000). “ A Field Study of Scour-Monitoring Devices for Indiana Streams: Final Report” FHWA/IN/JTRP-2000/13, October 2000.

- DeFalco, F., Mele, R., (2002). "The Monitoring of Bridges for Scour and Sediment", *NDT&E International*, Vol. 35, pp. 117-123.
- Ettema, R., Zabilansk, L., (2004). "Ice Influences on Channel Stability: Insights from Missouri's Fort Peck Reach", *Journal of Hydraulic Engineering*, Vol. 130, No. 4, A.S.C.E, pp. 279-292.
- Fisher, M., Atamturktur, S., Khan, A., (2012a). "A Novel Vibration-Based Monitoring Technique for Bridge Pier and Abutment Scour", *Journal of Structural Health Monitoring*.
- Fisher, M., Chowdhury, M. N., Khan, A., Atamturktur, S., (2012b). "The Effect of Channel Conditions of Scour Measurements", *Journal of Flow Measurements and Instrumentation*.
- Gray, J. R., Melis, T. S., Patiño, E., Larsen, M. C., Topping, D. J., Rasmussen, P. P., Figueroa-Alamo, C. (2003, October). US Geological Survey research on surrogate measurements for suspended sediment. In *Proceedings of the 1st Interagency Conference on Research in Watersheds* (pp. 95-100).
- Henderson, F. M., (1966), *Open Channel Flow*, Prentice Hall Inc., Upper Saddle River, NJ.
- Holnbeck, S. R., McCarthy, P. M., (2011). "Monitoring Hydraulic Conditions and Scour at I-90 Bridges on Blackfoot River Following Removal of Milltown Dam Near Bonner, Montana, 2009" in *Scour and Erosion: Proceedings of 5<sup>th</sup> International Conference on Scour and Erosion*. Ed: Burns, S.E., Bhatia, S.K., Avila, C. M. C., Hunt, B. E., November 7-10, 2010, San Francisco, CA., A.S.C.E.
- Hunt, B. E., (2005). "Scour Monitoring Programs for Bridge Health." *Transportation Research Record: Journal of the Transportation Research Board*, Washington D.C., pp.: 531-536.
- Hunt, D. (2009). "Monitoring scour critical bridges." *NCHRP Synthesis 396*, Transportation Research Board, Washington, DC
- Itakura, T., Kishi, T., (1980). "Open Channel Flow with Suspended Sediments", *Journal of the Hydraulics Division, Proceedings of the American Society of Civil Engineers*, Vol. 106, No. HY8, A.S.C.E., pp.: 1325-1343.
- Kuwahara, S., (1939), "Velocity of sound in sea water and calculations of the velocity for use in sonic soundings". *Hydrogeologic. Review.*, v. 16, p. 123-140.

- Lagasse, P. F., E. V. Richardson, J. D. Schall, and G. R. Price., (1997). *NCHRP Report 396: Instrumentation for Measuring Scour at Bridge Piers and Abutments*. TRB, National Research Council, Washington, D.C.
- Lagasse, P.F., Clopper, P.E., Pagán-Oriz, J.E., Zevenbergen, L.W., Arneson, L.A., Schall, J.D., Girard, L.G., (2009). Bridge scour and stream instability countermeasures: Experience, selection and design guidance. Hydraulic Engineering Circular No.23, 3rd Ed., Publication No. FHWA-NHI-09-111, U.S. Department of Transportation, Federal Highway Administration.
- Leroy, C.C., (1969). “Development of Simple Equations for Accurate and More Realistic Calculation of the Speed of Sound in Seawater”, *The Journal of the Acoustical Society of America*. Vol. 46, No. 1B.
- Lin, Y. B., Lai, J. S., Chang, K. C., Li, L. S., (2006). “Flood Scour Monitoring System Using Fiber Bragg Grating Sensors” *Smart Materials and Structures*, Vol. 15, pp. 1950-1959.
- Mackenzie, K.V., (1981). “Nine-term equation for sound speed in the oceans” *Journal of the Acoustical Society of America*, Vol.70, Issue 3, pp. 807-812.
- Mason, R. R., Sheppard, D. M., (1994). “Field Performance of an Acoustical Scour-Depth Monitoring System” in *Fundamentals and Advancements in Hydraulic Measurements and Experiments*, Ed: Pugh, C.A., Proceedings of the Symposium, Buffalo, N.Y., August 1-5, 1994. A.S.C.E.
- Mueller, D. S. (2000). “National bridge scour program-measuring scour of the streambed at highway bridges.” U.S. Geological Survey, Reston, Va.
- Murillo, J.A., (1987). “The Scourge of Scour”, *Civil Engineering*, July 1987, A.S.C.E., pp: 66-69.
- Nassif, H., Ertekin, A. O., Davis, J., (2002). “Evaluation of Bridge Scour Monitoring Methods: Final Report” Federal Highway Administration, Report FHWA-NJ-2003-09, March, 2002.
- Nezu, I., Azuma, R., (2004). “Turbulence Characteristics and Interaction between Particles and Fluid in Particle-Laden Open Channel Flows”, *Journal of Hydraulic Engineering*, Vol. 130, No. 10, A.S.C.E., pp.: 988-1001.
- N.T.S.B., (1987). “Collapse Of New York Thruway (I-90) Bridge, Schoharie Creek , Near Amsterdam, New York, April 5, 1987”, NTSB Number: HAR-88/02, NTIS Number: PB88-916202.



- N.T.S.B., (1989). "Collapse Of The Northbound U.S. Route 51 Bridge Spans Over The Hatchie River, Near Covington, Tennessee, April 1, 1989", NTSB Number: HAR-90/01, NTIS Number: PB90-916201.
- Rhodes, J., Trent, R., (1993). "Economics of Floods, Scour and Bridge Failures" in *Hydraulic Engineering '93: Proceedings of 1993 Conference*. Ed: Shen, H.W., Su, S. T., Wen, F., July 25-30, 1993, San Francisco, CA, A.S.C.E.
- Richardson, J.R., Price, J., (1993). "Emergent Techniques in Scour Monitoring Devices" in *Hydraulic Engineering*, Ed: Wen Shen, H., Su, S.T., Wen, F., Proceedings of the 1993 Conference, San Francisco, CA, July 25-30, 1993, A.S.C.E.
- Robins, A. J. (1990). "Reflection of Plane Acoustic Waves From a Layer of Varying Density." *Journal of the Acoustical Society of America*, Vol. 87, No 4, pp. 1546-1552.
- Stogryn, A., (1971). "Equations for Calculating the Dielectric Constant of Saline Water", *IEEE Transactions on Microwave Theory and Techniques*, August, 1971, pp. 733-736.
- Urick, R. J., (1975). *Principles of Underwater Sound*, McGraw-Hill Inc.
- USGS, (2006a), "Water Data Report 2006: 02172053 Cooper River at Mobay Near North Charleston, S.C.", U.S. Dept. of Interior, U.S. Geological Survey.
- USGS, (2006b), "Water Data Report 2006: 02156500 Broad River Near Carlisle, S.C.", U.S. Dept. of Interior, U.S. Geological Survey.
- Yankielun, N.E., Zabilansky, L. (1999). "Laboratory Investigation of Time Domain Reflectometry System for Monitoring Bridge Scour", *ASCE Journal of Hydraulic Engineering*, Vol. 125, No. 12 pp. 1279-1284.
- Yu, X., Yu, X., (2006). "Time Domain Reflectometry Tests of Multilayered Soils" *Proceedings of the TDR 2006*, Purdue University, West Lafayette, U.S.A., Sept. 2006.
- Yu, X., Yu, X., (2011). "Development and Evaluation of an Automatic Algorithm for a Time-Domain Reflectometry Bridge Scour Monitoring System" *Canadian Geotechnical Journal*, Vol. 48 pp. 26-35.
- Yu, X., Zabilansky, L. J., (2006). "Time Domain Reflectometry for Automatic Bridge Scour Monitoring", in *GeoShanghai 2006: Site and Geomaterial*

*Characterization, GSP 149.* Ed. Puppala, A. J., Fratta, D., Alshibli, K., and Pamukcu S., A.S.C.E.

Zabilansky, L., Ettema, R., Weubeen, J., Yankielun, N., (2002). “Survey of River Ice Influences on Channel Bathymetry Along the Fort Peck Reach of the Missouri River, Winter 1998–1999”, Technical Report ERDC/CRREL TR-02-14., US Army Corps of Engineers, Engineer Research and Development Center, September, 2002.

## CHAPTER FIVE

### OPTIMIZATION OF VTP FOR FIELD DEPLOYMENT

#### **5.1 Introduction**

To fully account for the interaction between a fluid and structure, a 3D flow model and an associated structural analysis model are necessary. To capture the full turbulent flow spectrum, the 3D fluid model must be capable of calculating the instantaneous velocity field. This is required to determine the dynamic response of a structure to both large and small scale turbulent eddies (low and high frequency incident forces). Only Large Eddy Simulation (LES) or Direct Numerical Simulation (DNS) methods are available to fully capture the velocity field (Breuer and Münsch, 2008). These models, however, require significant computational time and resources, even without considering the structural analysis component. Hence, these models are generally not applied to design optimization problems.

To solve the fluid-structure interaction of a dynamic structure and the turbulent flow, this study aims to develop a semi-empirical model integrating closed form solutions for the structural response and empirical relationships for the turbulent open channel flow. The applicability of this semi-empirical model is demonstrated by predicting the response of a flexible disk subject to turbulent open channel flows. The flexible disk studied herein is a part of a scour monitoring sensing system as discussed in Fisher et al. (2012). The device called vibration based turbulent pressure sensor (VTP), measures the

vibrational energy content of a flexible disk. The response of a VTP within the flow and in the sediment bed is used to locate the water sediment interface and thus monitor scour.

The objective in this manuscript is to consider the development of a simplified, semi-empirical model that predicts the response of a flexible plate to turbulent open channel flow and to validate the model predictions with appropriate experimental measurements. This is accomplished by considering empirical descriptions for the turbulent flow and analytical solutions to a single degree of freedom oscillator, which are discussed in Section 2. In Section 3, the model developed is verified, calibrated, and validated using experimental data sets obtained from modal tests and vibration measurements conducted in an open channel flume. Section 4 presents a case study application of the simplified model to optimize the VTP device through a parametric analysis. Results from tests on the field prototype are discussed in Section 5 while pertinent conclusions from this work and avenues for further research are discussed in Section 6.

## **5.2 Modeling Approach**

The nature of the flows studied in fluid dynamics can be divided into two groups, laminar and turbulent. All natural channels flow under turbulent conditions. The instantaneous turbulent velocity at any given point may be divided into two components; a time-averaged velocity component also called the mean velocity and a fluctuating part. Turbulent flow is characterized by the presence of flow instabilities that are responsible for velocity fluctuations. The root mean squares (RMS) of these fluctuations vary in

magnitude from 5% of the mean flow for turbulent open channels to as much as 10 to 30% in aerodynamic boundary layers (Panton 2005).

Fluctuations are present in all of the velocity components and pressure of a flow, which can be described through Reynolds' decomposition into the mean component,  $U$ ,  $V$ , and  $W$  in the three cardinal directions in Figure 5.1 ( $x$  is along the flow direction,  $y$  is normal to the bed, and  $z$  is across the channel width), and the fluctuation components,  $u'$ ,  $v'$ , and  $w'$ . Thus, when describing the instantaneous flow velocities,  $\tilde{U}$ ,  $\tilde{V}$ , and  $\tilde{W}$  at any point, it is necessary to include both components as given by Equation (5.1), see Figure 5.2.

$$\begin{aligned}\tilde{U} &= U + u' \\ \tilde{V} &= V + v' \\ \tilde{W} &= W + w'\end{aligned}\tag{5.1}$$

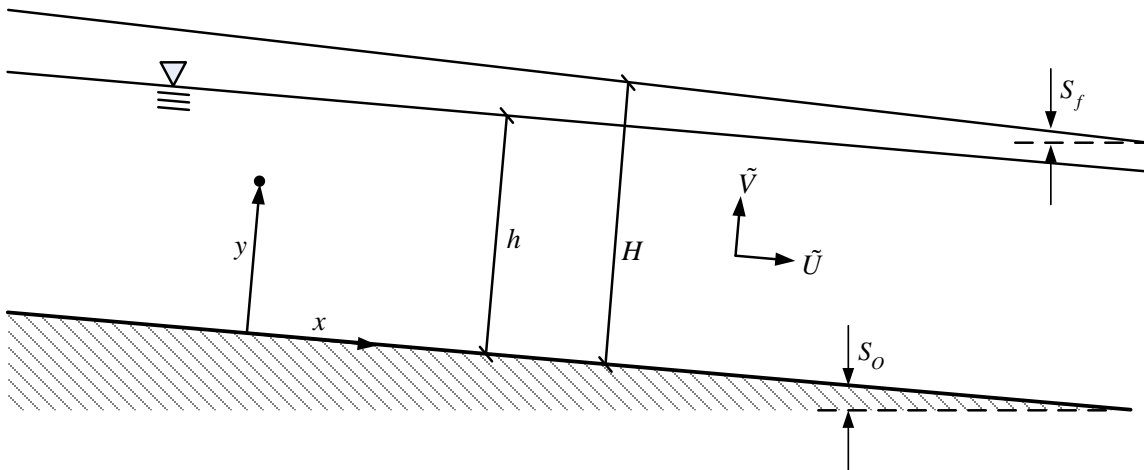


Figure 5.1 - Channel parameters relevant to the Navier-Stokes equations.

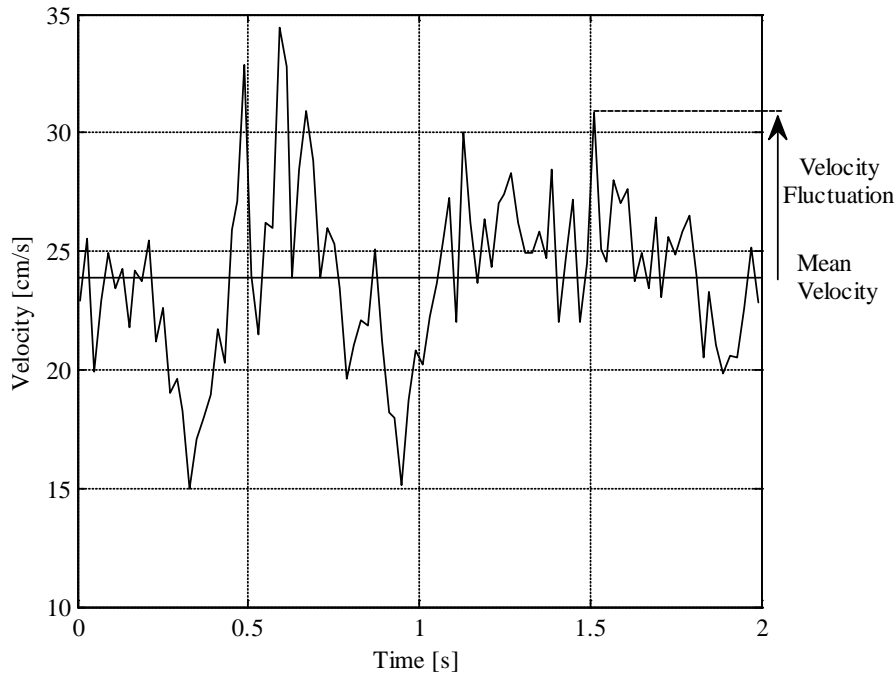


Figure 5.2 - Sample turbulent velocity time history.

A similar expression can be developed for the pressure in the flow,  $\tilde{P}$ , which can be decomposed into its mean pressure,  $P$ , and the fluctuating component,  $p'$ . Based upon these definitions, it is necessary then that the average values of  $\tilde{U}$ ,  $\tilde{V}$ , and  $\tilde{W}$  yield  $U$ ,  $V$ , and  $W$ ; thus the long term average of  $u'$ ,  $v'$ , and  $w'$  are zero.

Turbulent flows are also characterized by eddy motions. Eddies are instabilities in the flow that are spatially and temporally correlated and are responsible for the velocity and pressure fluctuations. These eddies vary in size, with smaller eddies contained within larger eddies, up to the largest eddy in the flow. These eddies vary in scale from the molecular level where the smallest eddies are dissipated due to viscous forces as heat, to the large eddies which depend upon the size of the main channel (Panton 2005). The distribution of eddy sizes in the flow leads to the energy cascade from the larger eddies

responsible for the production of turbulence to the small scale, low energy eddies responsible for the viscous dissipation of turbulence. The turbulent flow features discussed above will be utilized in developing a model to predict the response of a VTP under turbulent flow conditions.

### 5.2.1 Model for Prediction of RMS Values of Fluctuating Turbulent Velocity

Wall bounded turbulent flows can be divided into two regions, the inner region (IR) close to the wall, and the outer region (OR) near the free surface (Nezu and Nakagawa, 1993). For all wall bounded flows, the inner region is further decomposed into the viscous sub-layer (VSL), where viscous forces dominate, a buffer layer, and the log-law layer (LLL). Adjacent to the LLL is the outer region, which for open channel flows is affected by the presence of the free surface. The OR is broken down into the free surface region (FSR) and the equilibrium region (ER), which lies between the inner layer and the FSR. For smooth beds, the thickness of the VSL is defined as  $\delta_v = 5\nu/U_*$ , where  $\nu$  is the kinematic velocity of the fluid and  $U_*$  is the friction velocity, which is typically small, of the order of 0.5 mm (Nezu, 2005). Throughout the inner region ( $y/h < 0.2$ ), turbulence is generated by low speed streaks, which are ejected from the near wall region and subsequently burst (Davidson, 2004, Nakagawa et al., 1975). For rough boundary layers, as  $k_s$  (equivalent sand roughness) increases, the large eddies are interrupted by the roughness elements, leading to an increasingly isotropic turbulence (Nezu and Nakagawa, 1993). Immediately outside the IR lies the ER, ( $0.2 < y/h < 0.6$ ), where neither the free surface or wall effects dominate (Nezu and Nakagawa, 1993). In this

region, the rates of turbulent production and dissipation are approximately equal. The remaining OR, ( $0.6 < y/h < 1.0$ ), corresponds to the FSR, where the viscous dissipation exceeds any production of turbulence and is roughly equivalent to the rate at which turbulent is transported from the IR (Nakagawa et al, 1975).

In the VSL, Prandtl's mixing length model leads to Equation (5.2) (Nezu, 2005, Nezu and Rodi, 1986), where  $U^+ = U/U_*$  and  $y^+ = y\nu/U_*$ . In the log-law-layer, the mean flow can be described by Equation (5.3). Based upon experimental evaluation,  $\kappa$  and  $A$  for open channel flows have been found to be 0.41 and 5.29 for smooth beds, respectively (Nezu and Rodi, 1986). Equations (5.2) and (5.3) are valid for  $y/h < 0.2$ , additional models are required outside this region.

$$U^+ = y^+ \quad (5.2)$$

$$U^+ = \frac{1}{\kappa} \ln y^+ + A \quad (5.3)$$

Coles (1956) proposed that the deviation from the log-law in boundary layers outside of  $y/h > 0.2$  could be accounted for with a wake function,  $\Psi$ . The resulting modification to Equation (5.3) are shown in Equation (5.4). The wake function parameter  $\Pi$  is equal to 0.55 for zero-pressure gradient boundary layers (Nezu, 2005).

$$\left. \begin{aligned} u^+ &= \frac{1}{\kappa} y^+ + A + \Psi \\ \Psi &= \frac{2\Pi}{\kappa} \sin^2 \left( \frac{\pi y}{2h} \right) \end{aligned} \right\} \quad (5.4)$$



Thus, from Equations (5.2), (5.3), and (5.4), it is possible to describe  $U^+$  throughout the depth of open channel flows. Also, as  $U_* = \sqrt{ghS_o}$  for uniform flow, it is also possible to describe  $U$ . Aside from the mean flow distribution in the channel, it is also necessary to describe the nature of the turbulent velocity fluctuations throughout the flow. Nezu (1977) showed that the turbulence intensity terms (RMS values), outside the VSL are independent of the Reynolds number,  $Re$ , and Froude number,  $Fr$ , and can be described by Equations (5.5), (5.6), and (5.7), with the empirically determined constants  $D_U = 2.3$ ,  $D_V = 1.27$ ,  $D_W = 1.63$ , and  $C_K = 1$  (Nezu, 2005).

$$\frac{\sqrt{u'^2}}{U_*} = D_U \exp\left(-C_K \frac{y}{h}\right) \quad (5.5)$$

$$\frac{\sqrt{v'^2}}{U_*} = D_V \exp\left(-C_K \frac{y}{h}\right) \quad (5.6)$$

$$\frac{\sqrt{w'^2}}{U_*} = D_W \exp\left(-C_K \frac{y}{h}\right) \quad (5.7)$$

Equation (5.8) is valid for the RMS value of  $u'$  in the VSL, which can be incorporated in Equation (5.5) to describe the velocity fluctuations throughout the depth of the flow, as shown in Equation (5.9) (Nezu, 2005), where  $Re_* = hU_*/\nu$ ,  $B$  has a value of 10, and  $\Gamma = 1 - \exp(-y^+/B)$ .

$$\frac{\sqrt{u'^2}}{U_*} = 0.3y^+ \quad (5.8)$$

$$\frac{\sqrt{u'^2}}{U_*} = D_U \exp\left(-\frac{y^+}{\text{Re}_*}\right) \Gamma + 0.3y^+ (1-\Gamma) \quad (5.9)$$

### 5.2.2 Spectral Model for Turbulence

Velocity fluctuations lead to the driving force behind the operation of the VTP method, therefore it is necessary to determine the spectral content of these velocity fluctuations. Experiments have shown that the power spectral density of  $u'$ ,  $\Phi_{uu}$ , are self-similar when appropriately normalized, even under different flow conditions. An appropriate model is developed to describe  $\Phi_{uu}$ , which can be leveraged in modeling the response of a structure to turbulent flow.

The power spectral density can be related to the spatial correlation function,  $R_x(r)$ , as shown in Equation (5.10), for two velocity measurements  $u'(x)$  and  $u'(x+r)$  separated by a distance  $r$ . Note that  $R_x(r)$  can be measured experimentally. This correlation function has been shown to be an even function (Meechan, 1958), thus the power spectral density can be determined from the Fourier Cosine Transformation, as shown in Equation (5.11).

$$R_x(r) = \frac{u'(x)u'(x+r)}{\overline{u'^2}} \quad (5.10)$$

$$\Phi_{uu} = \frac{2}{\pi} \int_0^{\infty} R_x(r) \cos(kr) dr \quad (5.11)$$

The power spectral density  $\Phi_{uu}$  is independent of flow conditions and turbulent flow structure when normalized by the mean eddy macroscale,  $L_x$ . Several models for

$\Phi_{uu}$  have been proposed to predict power spectral density for the production, inertial, and viscous subranges of turbulent flows. The two models considered in this analysis are the von Karman and Heisenberg models. These models are typically described in wave number space,  $k$ . However, under Taylors Hypothesis of frozen turbulence, it is possible to convert the parametric equations to frequency space,  $f$ , where  $k = 2\pi f / \bar{U}$ , where  $\bar{U}$  is the depth-averaged mean flow velocity.

The von Karman spectra, shown in Equation (5.12) (von Karman, 1948) is a function of  $L_x$  and the characteristic wavenumber/frequency,  $k_o$ .

$$\Phi_{uu} = \frac{2}{\pi} L_x \overline{u'^2} \left( 1 + \left( \frac{k}{k_o} \right)^2 \right)^{-5/6} \quad (5.12)$$

The mean eddy macroscale can be determined from the measured correlation function, and corresponds to  $L_x = \pi/2 \Phi_{uu}(0)$  (Nezu and Nakagawa, 1993). The distribution of  $L_x$  has been determined experimentally and can be described by the relationship shown in Equation (5.13). The coefficient  $B_1$  varies from 1.1 for an  $Re_*$  of 600 to 1.0 for an  $Re_*$  of 1600, where  $Re_* = U_* h / \nu$

$$\left. \begin{aligned} \frac{L_x}{h} &= B_1 \left( \frac{y}{h} \right)^{1/2} \quad \text{for } \frac{y}{h} < 0.6 \\ \frac{L_x}{h} &= 0.77 B_1 \quad \text{for } \frac{y}{h} > 0.6 \end{aligned} \right\} \quad (5.13)$$

The characteristic wave number can be determined from mean eddy macroscale as shown in Equation (5.14), where the parameter C is the Kolmogoroff Constant with a value of 0.5 and  $K$  is given by Equation (5.15).

$$k_o = \left( K \left( \frac{2}{\pi C} \right)^{-1.5} \right)^{-0.4} L_x^{-1} \quad (5.14)$$

$$K = 0.691 + 3.98 (Re_L)^{-0.5} \quad (5.15)$$

The Reynolds number,  $Re_L$ , in Equation (5.15) is based upon the RMS value of  $u'$  for the velocity scale and  $L_x$  for the length scale. The von Karman model corresponds to the productive and inertial subranges of the turbulent energy spectral space,  $0 \leq k \leq \lambda^{-1}$ , where  $\lambda$  is the Taylor microscale of turbulence. Roughly, the von Karman model covers the open channel flow from the VSL to the ER. In the VSL, turbulence is produced and transported into the equilibrium region while in the ER the rate of production equals the rate of dissipation (Nakagawa et al., 1975).

Another model is required to overlap the von Karman model from the inertial subrange to the viscous subrange, where the production is zero and the viscous dissipation equals the rate of transport. This is achieved with the Heisenberg model, shown in Equation (5.16). The new terms introduced in Equation (5.16) include the dissipation rate for turbulent energy,  $\varepsilon$ , the constant  $\gamma'$ , and the Kolmogorov microscale of turbulence,  $\eta$ .

$$\overline{u'^2} \Phi_{uu}(k) = C \varepsilon^{2/3} k^{-5/3} \left( 1 + \gamma' (k\eta)^4 \right)^{-4/3} \quad (5.16)$$

The dissipation rate can be determined from Equation (5.17). The  $u'$  terms are typically not measured to the resolution required to construct an accurate representation of Equation (5.17). Therefore, it is common to exploit the isotropic turbulent assumption, leading to the right hand side of Equation (5.17) (Nezu and Nakagawa, 1993). This

assumption is an appropriate simplification, since turbulent fluctuations in all three directions are of the same order for open channels.

$$\varepsilon = 15\nu \left( \frac{\partial u'}{\partial x} \right)^2 = \frac{15\nu \overline{u'^2}}{\lambda^2} \quad (5.17)$$

The Taylor and Kolmogorov microscales  $\lambda$  and  $\eta$  are defined as shown in Equations (5.18) and (5.19), respectively. These microscales are practically solved via the fits employed in Equations (5.20) and (5.21). Lastly, the constant  $\gamma'$  is taken as 100, as it gives the optimal fit with measured and published results from Kironoto and Craff (1994) and Nakagawa and Nezu (1993).

$$\lambda = \sqrt{\frac{15\nu \overline{u'^2}}{\varepsilon}} \quad (5.18)$$

$$\eta = \left( \frac{\nu^3}{\varepsilon} \right)^{1/2} \quad (5.19)$$

$$\frac{L_x}{\lambda} = \left( \frac{K}{15} \right)^{1/2} Re_L^{1/2} \quad (5.20)$$

$$\frac{L_x}{\eta} = K^{1/4} Re_L^{3/4} \quad (5.21)$$

The aforementioned model describes the RMS values of the turbulent flow quantities with depth, along with the spectral representation of the turbulent quantities. The next step is to calculate dynamic pressure due to these velocity fluctuations.

### 5.2.3 Dynamic Pressure

In Equation (5.5), the RMS value of  $u'$  is defined, which can be coupled with Equations (5.12) and (5.16) to arrive at the spectral representation of the turbulent

fluctuations in the open channel flow. These turbulent fluctuations lead to a time varying dynamic pressure, which excites the VTP. This spectrum is a function of the position across the channel depth. Given the variation of  $\sqrt{u'^2}$ , the dynamic turbulent pressure impinging on the VTP disk can be determined by integrating the pressure distribution across the disk diameter, Figure 5.3.

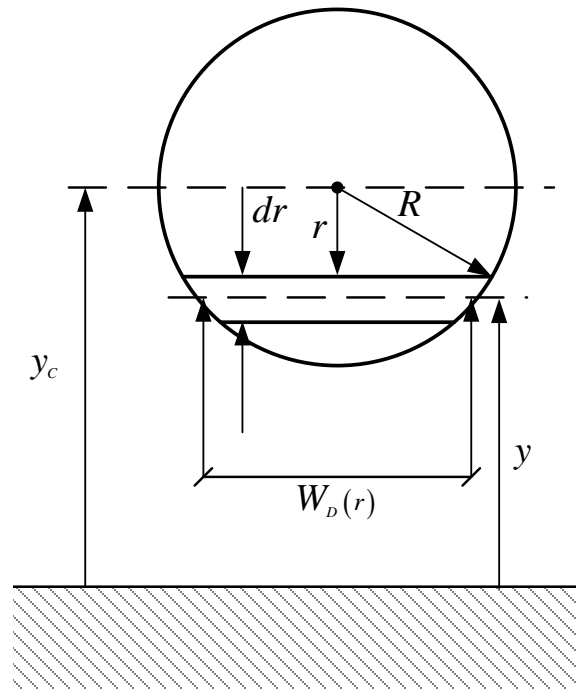


Figure 5.3 - Area integration of dynamic turbulent pressure distribution across VTP disk.

At a point in the flow, the dynamic turbulent pressure spectrum is computed as shown in Equation (5.22). By integrating Equation (5.22) across the VTP, the average pressure quantity,  $\bar{\Phi}_{pp}$ , can be computed as shown in Equation (5.23), where  $r$  extends from the center of the VTP to the radius of the disk,  $R$  (see Figure 5.3). It is not

convenient to integrate  $\Phi_{pp}(r)$ , however it is possible to replace this term with a function of  $y$ , as  $y_C = y - r$ . Additionally, the integrand in Equation (5.23) can be replaced with the product of the differential radius  $dr$  and the element width,  $W_D(r) = 2\sqrt{R^2 - r^2}$ . The resulting expression is shown in Equation (5.24).

$$\Phi_{pp} = \left( \frac{1}{2} \rho u^2 \right)^2 \Phi_{uu} \quad (5.22)$$

$$\bar{\Phi}_{pp} = \frac{1}{A_{VTP}} \int_{-R}^R \Phi_{pp}(r) dA \quad (5.23)$$

$$\bar{\Phi}_{pp} = \frac{1}{A_{VTP}} \int_{-R}^R \Phi_{pp}(r) W_D dr \quad (5.24)$$

#### 5.2.4 Structural response

Having established the variation of the dynamic turbulent pressure across the channel depth, it is necessary to relate the dynamic pressure to the response of the VTP. Following the method outlined in Blevins (1990), it can be shown that the response of a plate, for each mode, is described by Equation (5.25), where  $\omega_i$  is the undamped natural frequency of mode  $i$  in radians/second,  $\zeta_i$  is the modal damping factor,  $J_i$  is the joint acceptance,  $p_i(t)$  is the turbulent dynamic pressure, and  $x_i$  is the displacement for mode  $i$ .

$$\frac{1}{\omega_i^2} \ddot{x}_i + \frac{2\zeta_i}{\omega_i} \dot{x}_i + x_i = J_i p_i(t) \quad (5.25)$$

In the case where the joint acceptance is unity, the mode shape and the pressure distribution are spatially correlated for a given mode (Blevins, 1990), and  $J$  is equal to 1.

This results in the governing equation for a single degree of freedom oscillator. The steady state frequency response function of an oscillator,  $|H(\omega)_i|^2$ , to a random, stationary, ergodic, and Gaussian pressure spectrum can be computed from Equation (5.25) as shown in Equation (5.26) (Blevins, 1990). As turbulence in open channels can be categorized as random, stationary, Gaussian, and ergodic (Blevins, 1990; Nezu and Nakagawa, 1993; Galanti and Tsinober, 2004), the dynamic turbulent pressure determined by these velocity fluctuations can be categorized in the same manner.

$$|H(\omega)_i|^2 = \frac{1}{\left(1 - (\omega/\omega_i)^2\right)^2 + (2\zeta_i \omega/\omega_i)^2} \quad (5.26)$$

The response function shown in Equation (5.26) represents the transfer function from the input force to the displacement response of the structure. The power spectral density of the displacement of the VTP can be computed from the product of Equations (5.24) and (5.26). As the joint acceptance is not always unity, Blevins (1977) suggests a correction method that requires the inclusion of the joint acceptance. Also, as the input force is derived from the dynamic pressure, the characteristic modal pressure,  $\tilde{P}_{iC}$ , is included to arrive at a displacement response spectrum. The characteristic modal pressure at the center of the VTP is shown in Equation (5.27) (Blevins, 1977). The parameters in Equation (5.27) are the density of the VTP disk,  $\rho_D$ , the disk thickness  $t$ , and the displacement of the VTP center  $x_{iC}$ .

$$\tilde{P}_{iC} = \rho_D t (\omega_i)^2 |x_{iC}| \quad (5.27)$$



Equation (5.27) is then used to compute the displacement for mode  $i$  in physical units,  $\Phi_{xxi}$ , as shown in Equation (5.28). Further, due to the Central Limit Theorem for random, independent processes, the mean squared sum of these processes is equal to the sum of the mean square of the individual processes. Thus, given that the turbulence in open channels is stationary and random, the overall displacement response spectrum of the VTP can be computed from the sum of the individual responses of each mode  $i$ , shown in Equation (5.29).

$$\begin{aligned}\Phi_{xxi} &= \frac{\bar{\Phi}_{PP}}{\left(1 - (\omega/\omega_i)^2\right)^2 + (2\zeta_i \omega/\omega_i)^2} \frac{J_i^2 x_{iC}^2}{P_{iC}^2} \\ &= \frac{\bar{\Phi}_{PP}}{\left(1 - (\omega/\omega_i)^2\right)^2 + (2\zeta_i \omega/\omega_i)^2} \frac{J_i^2}{\left(\rho_D t(\omega_i)^2\right)^2}\end{aligned}\tag{5.28}$$

$$\Phi_{xx} = \sum_i \Phi_{xxi}\tag{5.29}$$

Lastly, for random processes, the mean squared displacement response  $\overline{x^2}$  can be related to the power spectral density, as shown in Equation (5.30) (Blevins, 1990).

Velocity and acceleration response spectra and mean squared response values can be derived from Equations (5.29) and (5.30).

$$\overline{x^2} = \int_{f_1}^{f_2} \Phi_{xx} df\tag{5.30}$$

To solve Equation (5.28) it is necessary to include the natural frequencies and the modal damping factors. The natural frequency for a circular disk fixed at all boundaries (an appropriate approximation of the VTP device), can be calculated from Equation

(5.31), where  $E_D$  is the modulus of elasticity for the disk,  $\rho_D$  is the density of the disk,  $\nu_D$  is Poisson's ratio for the disk, and  $\lambda^2$  varies from 10.22 to 21.26 for the first two modes (Blevins, 1979). An additional mode, which accounts for the mass of the accelerometer located at the center of the VTP is also required. The natural frequency for this mode can be calculated from Equation (5.31), where  $\lambda^2$  equals 5.34, as discussed in Roberson (1951).

$$\omega_i = \frac{\lambda^2}{r^2} \left( \frac{E_D t}{12 \rho_D t (1 - \nu_D^2)} \right)^{1/2} \quad (5.31)$$

Another component of Equation (5.28) is the modal damping factor. Due to the presence of the fluid around the VTP disk, this damping will consist of the damping from the disk material itself,  $\zeta_s$ , taken as 0.05 (Berger et al., 2003), and the fluid damping  $\zeta_f$ . For moving channel fluid, the fluid damping can be estimated from Equation (5.32) with an appropriate substitution of the drag coefficient,  $C_D$ , taken as 1.28 for a plate in cross flow, and  $\tilde{m}$  as the mass per unit length of the disk (Blevins, 1990).

$$\zeta_f = 2 \frac{U}{\omega_i D} \frac{\rho R^2}{\tilde{m} t} C_D \quad (5.32)$$

Finally, it is necessary to consider the assumption regarding the joint acceptance. The joint acceptance can be computed from the mode shape,  $\tilde{x}_i(r, \theta)$  and the pressure distribution,  $\tilde{P}_i(r, \theta)$ , (normalized by  $m(\omega_i)^2$  for each mode) as shown in Equation (5.33). The parameters in Equation (5.33) are the mass per unit area  $m$  and angle  $\theta$ , which varies from 0 to  $2\pi$ .

$$J_i = \frac{\int_A \tilde{P}_i(r, \theta) \tilde{x}_i(r, \theta) dr d\theta}{\omega_i^2 \int_A m \tilde{x}_i^2(r, \theta) dr d\theta} \quad (5.33)$$

For the first mode of the VTP disk, the mode shape and dynamic turbulent pressure distribution are shown in Figure 5.4. For the first three modes the joint acceptance values are 1.11, 1.06, and 1.83 respectively. The natural frequency of the subsequent modes, as will be shown in Section 3, are greater than 500 Hz, typically outside the range of the VTP response spectra and subsequently have a negligible impact on the mean squared response value. The joint acceptance values listed above are incorporated into the analytical model, Equation (5.28).

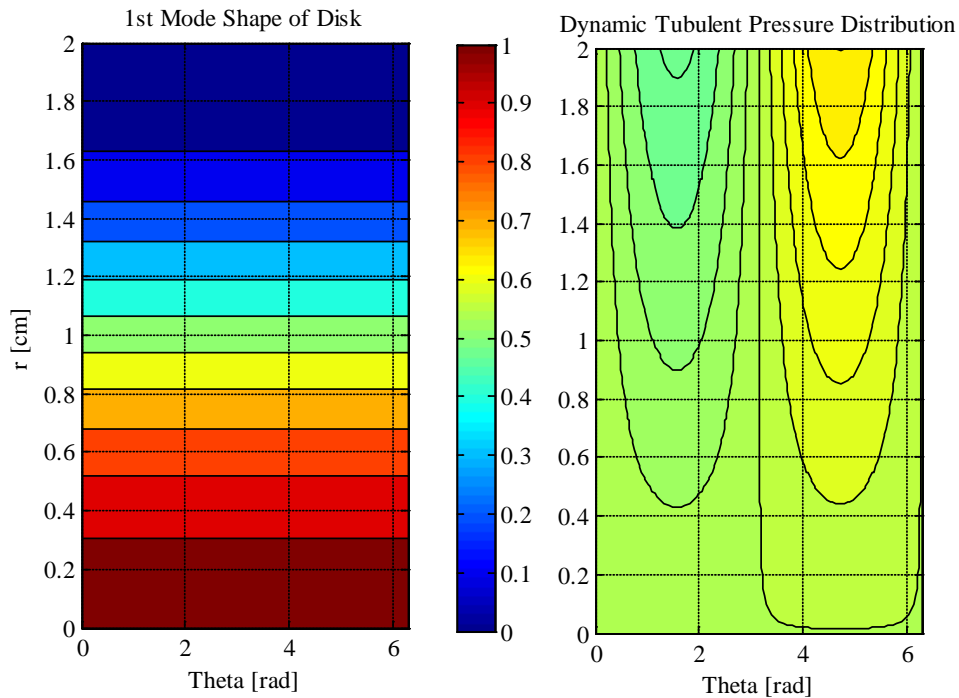


Figure 5.4 - Components of the Joint Acceptance for the 1st Plate Mode.

### **5.3 Model Verification, Calibration, and Validation**

A numerical model is prone to errors that originate from the mathematics and the physics of the problem. The errors and uncertainties introduced while solving the mathematical equations include round-off, discretization, and truncation errors. These errors are accounted for under the broad topic of model verification. The second source of error in a model arise from uncertainties introduced from an imperfect model definition of underlying physical principles as well as the imprecise values for the associated parameters of the chosen model (Atamturktur et al., 2012). Models and their associated parameters can be conditioned based on the experimental data to reduce the uncertainties and infer biases in model predictions. It is important to note that validation of a model requires a data set independent from those that are used in the calibration step (Trucano et al., 2002).

The following sections assess the predictive capabilities of the developed semi-empirical model and will be used for optimization of the field prototype. The verification activities involve investigation of the impact of the dynamic pressure integration across the VTP. This is then followed by a calibration of the model performance to an experimental data set in order to account for the variability inherent in the model input parameters. Finally, the model is validated by comparing the predictions against an independent data set.

#### **5.3.1 Model Verification**

It has been well documented (Nezu and Rodi, 1986) that the variation of  $u'$  across the channel depth is non-linear, with the peak occurring near the bed. Given that the

VTPs are designed to typically operate at  $y/h < 0.3$ , it is necessary to consider the variation in the turbulent velocity fluctuations across the depth of the VTP surface (generally having a diameter from 4 to 6 cm). In Equation (5.24) this is accounted for by integrating the pressure distribution, which is dependent on  $u'$ , across the disk surface. To investigate the effect of the numerical integration step width,  $dr$ , for each element, the pressure is integrated with decreasing step width, as shown in Figure 5.5. The results reveal that after 10 element strips, the result for both  $y/h$  of 0.15 and 0.35 are within 1% of the 20 element result. From this result, it can be concluded that 15 elements are sufficient to capture the pressure variation across the VTP.

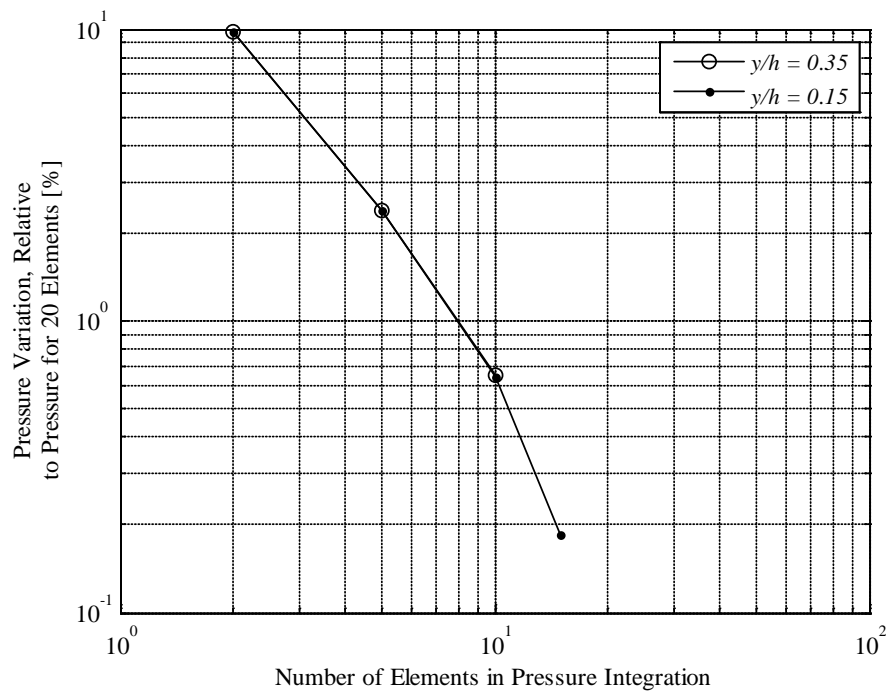


Figure 5.5 - Variation in VTP turbulent pressure, as a function of number of elements.

### 5.3.2 Model Calibration

**Structural dynamic model:** The parameter values used in the development of the model, reviewed in Section 2, are best estimates obtained from literature review. Therefore, it is necessary to condition the parameter values against the actual measured response of the structure. The parameters considered in this calibration include the disk material properties,  $E_D$ ,  $\zeta_D$ , and  $\rho_D$ , as well as the turbulent flow characteristics,  $U_*$ ,  $\zeta_F$ , and  $\sqrt{u'^2}$ . The calibration of the disk parameters is accomplished by conducting an experimental modal analysis on the VTP disk and calibrating the natural frequencies to the measured natural frequencies. The calibration of the turbulent flow quantities is accomplished via experiments conducted in the Clemson Hydraulics Laboratory (CHL) flume.

To calibrate the natural frequency predictions for the various modes in the VTP, model predictions are compared with the measured natural frequencies for a 3.2 mm thick, 2.54 cm radius, Neoprene rubber VTP. The measured values are obtained by rigidly fixing the VTP and attaching a shaker to the disk surface. The force transmitted to the plate is measured with a Bruel and Kjaer 8200+2646 force transducer, with a sensitivity of  $-4$  mV/N. The acceleration response of the VTP is recorded with a Kistler 8732A500 accelerometer, with a sensitivity of 9.64 mV/g. The neoprene test is conducted with a span of 800 Hz and 6400 lines, leading to a frequency resolution of 125 mHz. The shaker ranges bi-directionally for 1 to 1000 Hz at a rate of 125 Hz/s.

The comparisons between the calculated and measured natural frequencies are shown in Table 1 for the first six modes. For the higher modes, the prediction results are

within 10% of the measured frequencies. The first mode is calculated including the presence of the accelerometer as a point mass. Model calibration can be completed to minimize the disagreements between the measured and calculated natural frequencies considering all six modes. However, the disagreement observed for the first mode is believed to be due to the stringer connecting the shaker to the VTP sensor. Also, the third observed mode is believed to be a spurious mode resulting from the interaction between the stringer and the VTP, which is not included in the model. Therefore, the first and the third modes are excluded from the calibration activities.

Table 1 - Model and measured natural frequencies for modes in neoprene.

Mode Shape	Neoprene 30A			Calibrated Results	
	Model	Meas.	% Error	Model	% Error
1 <sup>1</sup> .	80.17	70.3	14		
2	248	292	-15	260	-11
3 <sup>2</sup> .	NA	366	NA	NA	NA
4	515	534	-3.6	540	1.1
5	845	773	9.3	886	15
6	963	903	6.6		

<sup>1</sup>. Affected by stringer mass & stiffness. <sup>2</sup>. Stringer/plate coupled mode.

The natural frequencies presented in Table 1 are dependent upon the model parameters  $E_D$ ,  $\rho_D$ ,  $t$ , and  $R$ . The geometric parameters  $t$  and  $R$  are design parameters, which can be controlled during the manufacturing of the prototype, and thus are known with high certainty. Furthermore, the density parameter can be measured with relative ease and high accuracy. Therefore, the only remaining parameter that is poorly-known is the Young's Modulus of the plate, which nominally is 8.3 MPa. An optimal fit is achieved considering modes 2, 4 and 5 with a 10% increase in the modulus of the disk

while all other remain at their nominal values. The results of this analysis are also shown in Table 1. As indicated, the fit of modes 2 and 4 improve with the calibration in the model parameters. This represents an optimal fit since the contribution of each mode to the overall response is not equal. Mode 2 contributes 100 times more to the overall measured acceleration response than mode five. Thus a 4% reduction in the percent error for mode 2 is significant.

**Turbulence Model:** To calibrate the turbulence characteristics developed in the semi-empirical model, channel velocity is measured in the CHL flume with a Sontek acoustic doppler velocimeter (ADV), A701F, at 50 Hz. The sample time of five minutes is found to adequately capture all eddy scales. The flume bed consists of quartz sand with a median grain size of 1.5 mm. The velocity measurements are made throughout the depth, from  $y/h$  of 0.10 to 0.60. Pertinent flow parameters for each of the three runs are shown in Table 2.

Table 2 - Flow parameters for CHL flume tests.

Run	$h$ [cm]	$U$ [cm/s]	$U_*$ [cm/s]	$Re_*$ [N.A.]
1	29.3	35.7	2.2	6360
2	26.4	31.1	1.4	3710
3	32.7	27.4	1.6	4560

It is also necessary to determine the value for  $U_*$ , an input for the turbulent channel flow model. This can be accomplished from the measured results in two ways. Equation (5.3) can be fit, using the least squares method, to the measured values of  $U$  within the LLL. The coefficient of this fit is equal to the quotient of  $U_*$  and  $\kappa$ . Since the



von Karman constant is known, this coefficient can be solved for the friction velocity. A second approach considers the contribution of the velocity gradient and the turbulent shear stress to the bed shear stress. The offset of a linear fit through the product  $-\rho u'v'$  as a function of  $y$  is equal to the bed shear stress,  $\tau_o$ , which can be related to the friction velocity, as in Equation (5.34). These two methods yield similar results for runs 1-3. The friction velocity values shown in Table 2 are based on the first method. The fit through these data points are shown in Figure 5.6 and 5.7.

$$U_* = \sqrt{\frac{\tau_o}{\rho}} \quad (5.34)$$

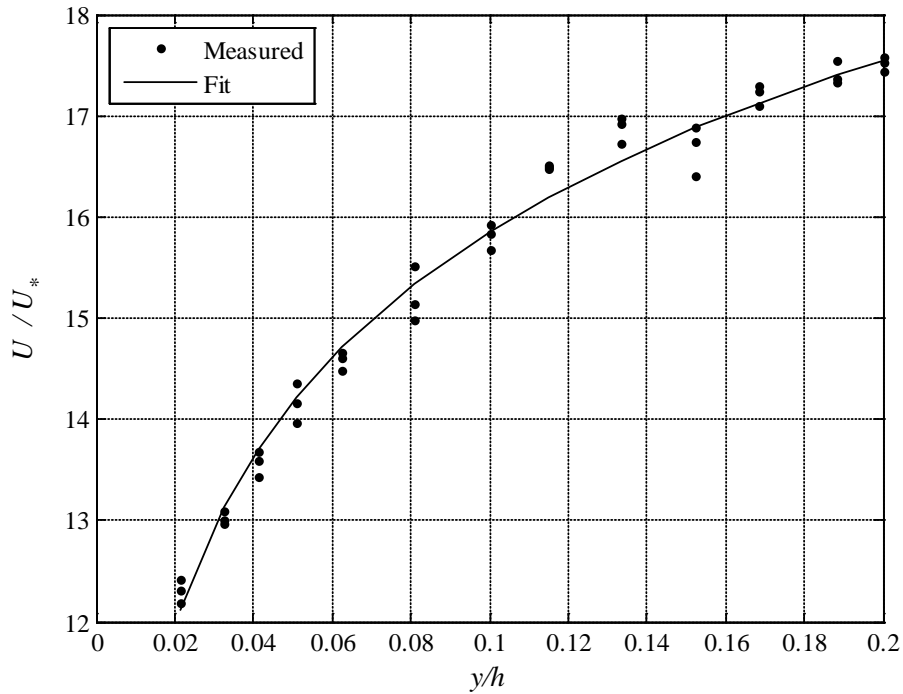


Figure 5.6 - Distribution of  $U/U_*$  as a function of depth in the channel, for run 1.

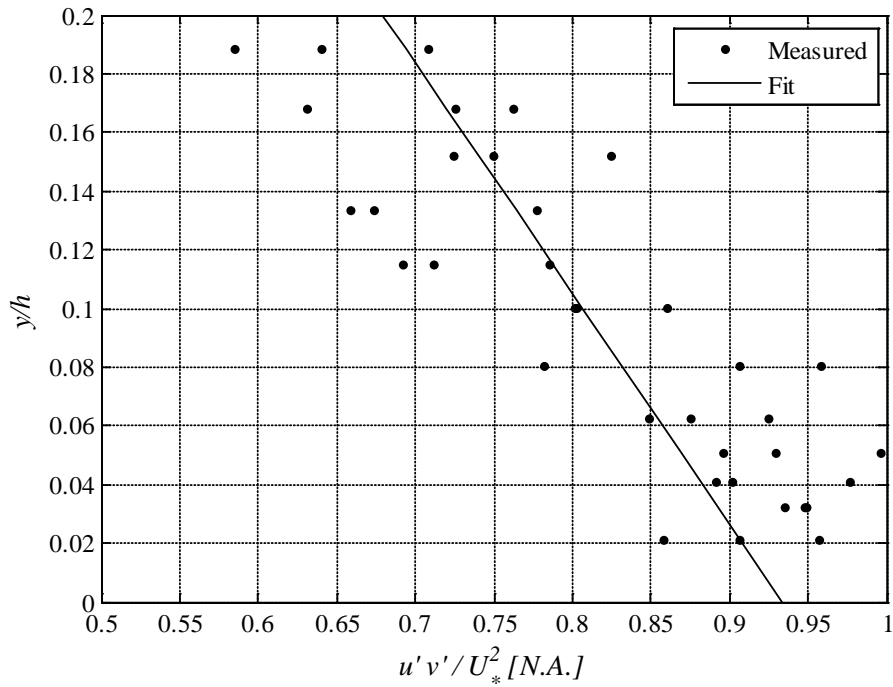


Figure 5.7 - Distribution of  $u'v'$ , as a function of depth in the channel, for run 1.

With  $U_*$  determined, it is then possible to compute the analytical model response for the turbulent fluctuations as a function of depth. The velocity fluctuations are computed using Equation (5.5) and compared with the measured results, as shown in Figure 5.8. The coefficient of determination between the measured values and the model is 0.73 for run 1, 0.87 for run 2, and 0.82 for run 3, indicating an acceptable representation of the measured data by the turbulence model.

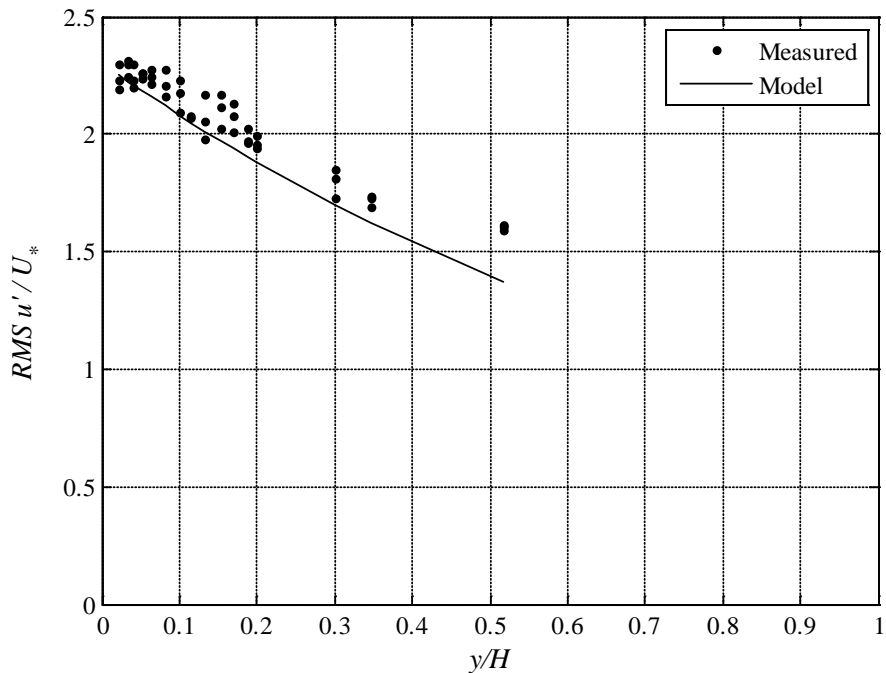


Figure 5.8 - Measured and model root mean square of  $u'$  ratio with friction velocity, as a function of depth in the channel (Run 1).

In addition to the turbulent velocity fluctuations, the semi-empirical model must accurately represent the velocity spectra. Several spectra are available in the published literature, two of which are shown in Figures 5.9 and 5.10. Figure 5.9 shows the comparison of the model predictions against the data published by Kironoto and Graf (1994). As shown in the figure, the model fit falls within the published data set. The coefficient of determination is 0.89. Similarly, the comparison of the model results with the data published in Nakagawa and Nezu (1993) are shown in Figure 5.10, where the coefficient of determination is 0.97. The results shown in Figure 5.10 indicate that the model captures the same trend as the measured data.

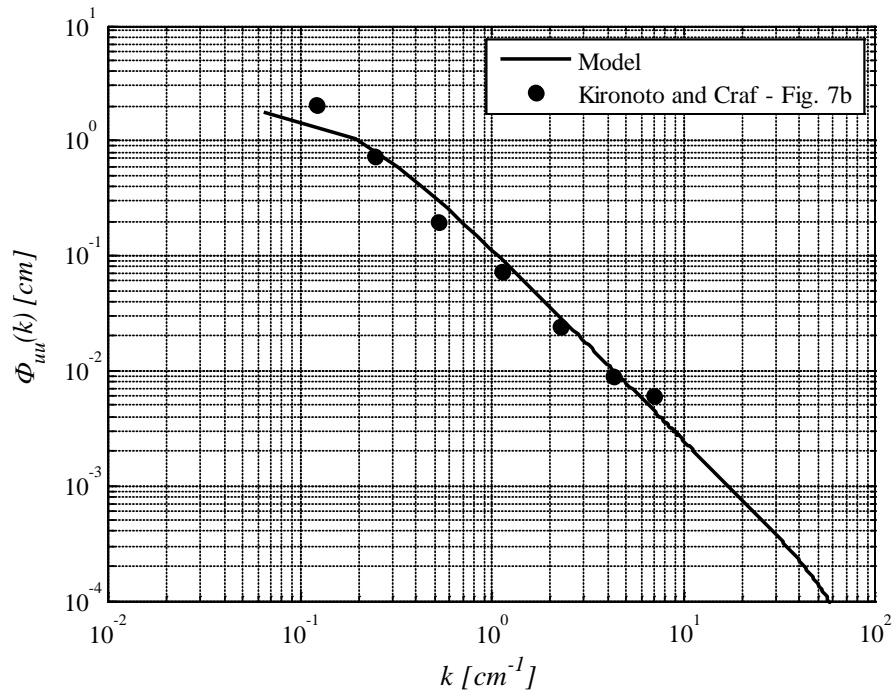


Figure 5.9 – Comparison of model turbulent velocity fluctuation spectra with published results from Figure 7b of Kironoto and Craff (1994).

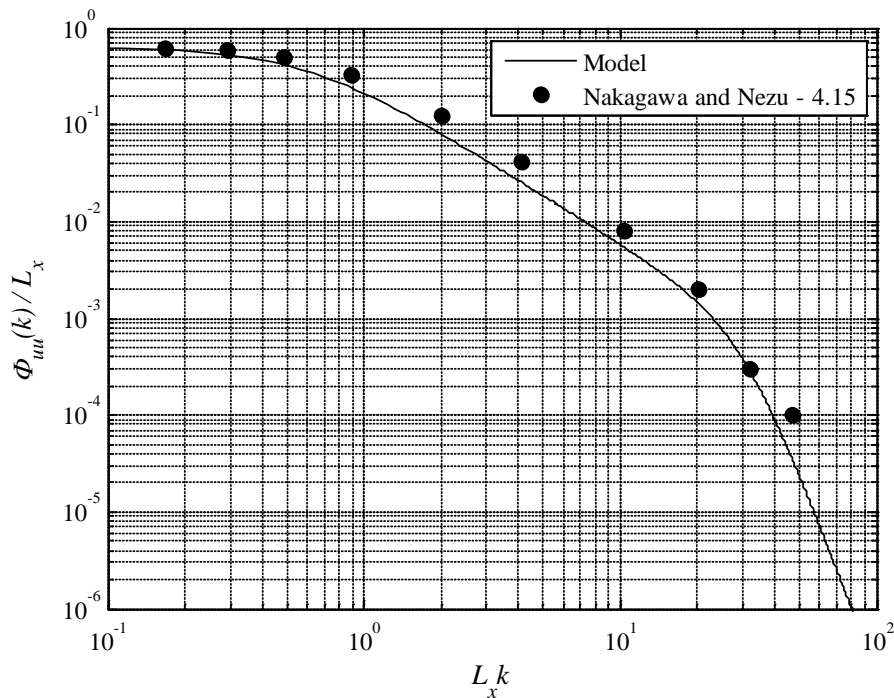


Figure 5.10 - Comparison of model turbulent velocity fluctuation spectra with published results from Figure 4.15 of Nakagawa and Nezu (1993).

Turbulent spectra can also be constructed from the measured ADV data for runs 1-3. The power spectral density of the turbulent velocity fluctuations for run 1, for  $y/h$  of 0.1, 0.2, and 0.3 are shown in Figures 5.11 through 5.13, respectively. The figures indicate that the model captures the shape and magnitude of the measured turbulent spectra, with coefficient of determination of 0.87, 0.79, and 0.92 respectively. For the higher frequencies, the model results under predict the measured spectra. This deviation is expected due to the nature of the ADV measurements. It is possible to correct the measured data as discussed in Hurther and Lemmin (2001). However, this requires a sonar device with a fourth probe to correct for the noise in the measured signal. The Sontek ADV device used in this study is not equipped with this additional probe, so this correction is not possible.

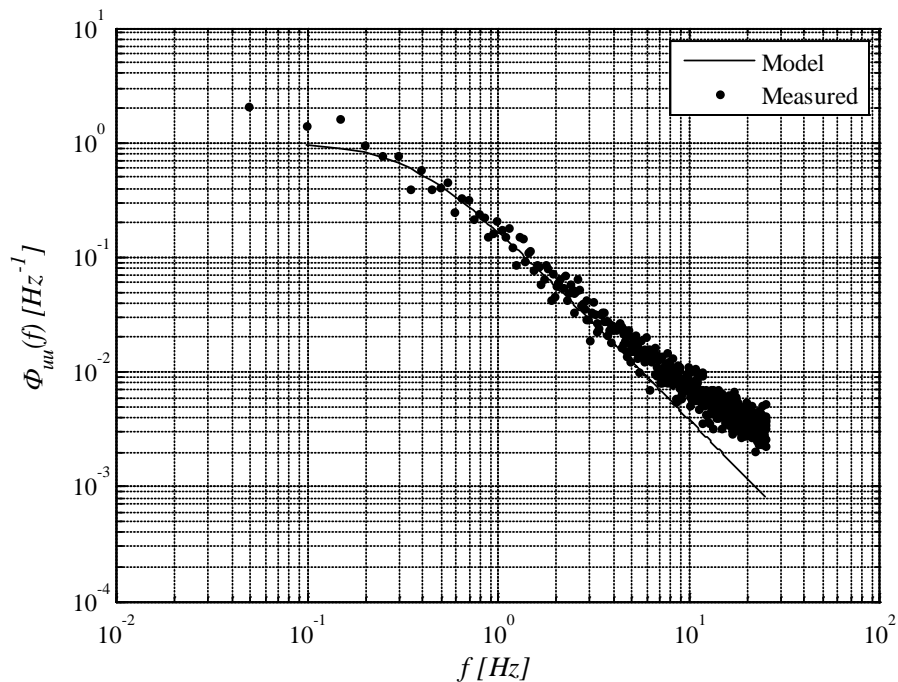


Figure 5.11 - Power spectral density of  $u'$  at a  $y/h$  of 0.1, from run 1.

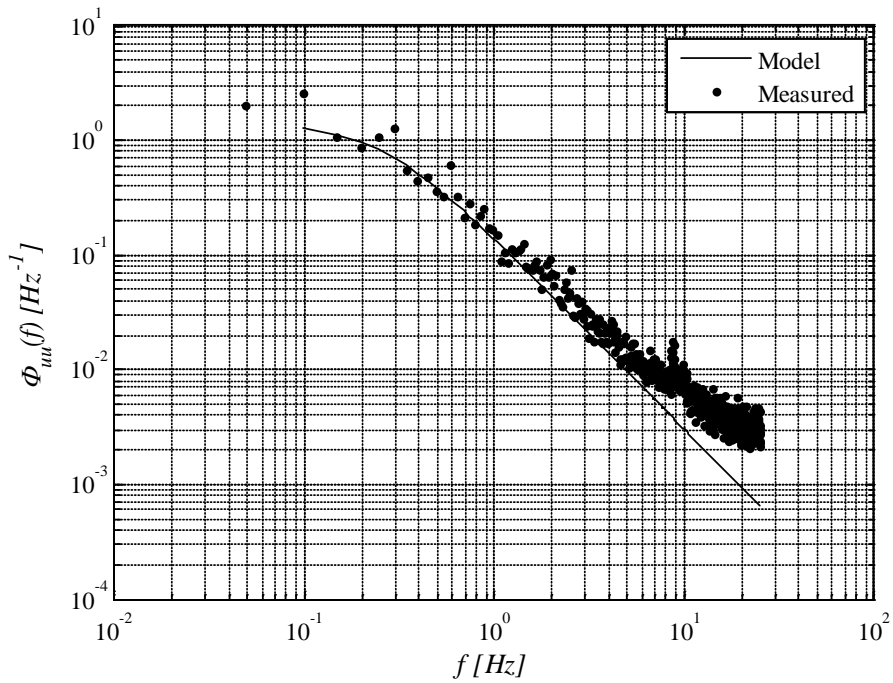


Figure 5.12 - Power spectral density of  $u'$  at a  $y/h$  of 0.2, from run 1.

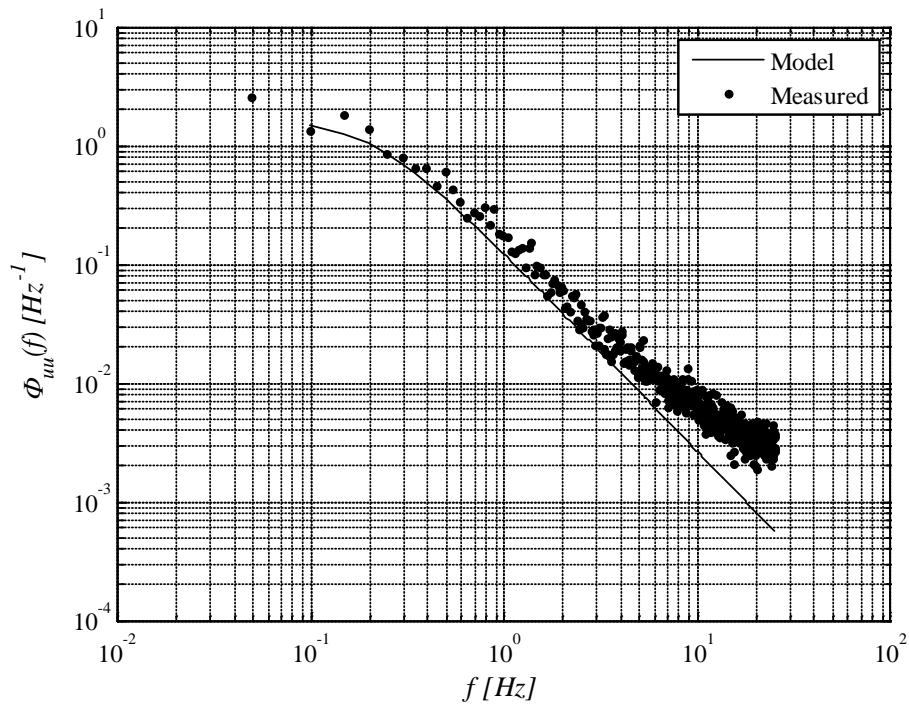


Figure 5.13 - Power spectral density of  $u'$  at a  $y/h$  of 0.3, from run 1.

Figures 9 through 13 reveal that the power spectral density of the  $u'$  velocity fluctuations as presented in the turbulence model are in agreement with both published spectra and those measured in the CHL flume. In addition, the magnitudes of the velocity fluctuations, shown in Figure 5.8, correspond to the measured values obtained with the ADV measurements. Thus, it can be concluded that the semi-empirical model component for the turbulent open channel flow does not require calibration in order to predict the magnitude and spectra of  $u'$ .

The objective of the overall semi-empirical model is to predict the mean squared acceleration response of the VTP. These results will also have to be calibrated in order to use the model for prediction and optimization of the VTP for field deployment. Data sets corresponding to the conditions for Run 1 are recorded experimentally, as discussed in Fisher et al. (2012), and are used to calibrate the model result. The measured VTP energy content response is recorded at  $y/h$  of 0.16 and 0.51. The mean energy content from this data set for the lower VTP is  $0.0220 \text{ m}^2 \text{ s}^{-4}$  with a standard deviation of  $0.0015 \text{ m}^2 \text{ s}^{-4}$ . The model predictions for this VTP's mean energy content is  $0.14 \text{ m}^2 \text{ s}^{-4}$ . For the upper VTP, the mean energy content is  $0.0150 \text{ m}^2 \text{ s}^{-4}$  with a standard deviation of  $0.0011 \text{ m}^2 \text{ s}^{-4}$ . The model predictions for this VTP's mean energy content is  $0.0063 \text{ m}^2 \text{ s}^{-4}$ . Based upon these results, it is necessary to calibrate the model. The objective of the calibration is to configure the results such that the model predictions are within 10 times the standard deviation of the measured energy contents for the various positions within the channel. This will result in a calibrated model that can predict the VTP energy response within the appropriate order of magnitude but does not overly constrain the response. Since the

model is being used to determine the geometry of the prototype, this will ensure that the predicted results are sufficiently accurate to capture the difference between VTPs located in the sediment and in the flow.

The remaining parameters under consideration for calibration include the combined structural and fluid damping, the friction velocity, the mean flow velocity and a factor introduced in Equation (5.22) that accounts for variations in the proportionality of the turbulent velocity fluctuations to the dynamic pressure. These parameters are varied by up to 20%. The largest variation in the model response occurs for the friction velocity, resulting in a variation in the mean energy content of up to 80%. Given this variability in the model results,  $U_*$  is chosen for calibration. Based upon the measured variation in the model response as a function of position within the channel flow, the friction velocity is calibrated by a linear function of position, with a slope of 0.833 and an intercept of 0.668. The resulting model predictions are 0.0367 and 0.0150  $\text{m}^2 \text{s}^{-4}$  for  $y/h$  for 0.16 and 0.51 respectively, a significant improvement in the model results.

The obtained model is conditioned based on the measured data during calibration and thus, it is necessary to validate the model by comparing the predictions against an independent data set.

### 5.3.3 Model Validation

The data set used for validating the analytical model consists of the measurements taken during Run 3, an independent data set not used for calibration. The measured VTP responses are recorded at positions in the channel of  $y/h$  for 0.35 and 0.66. The measured energy content response for each VTP is 0.013 and 0.0079  $\text{m}^2 \text{s}^{-4}$  for the lower



and upper VTPs respectively. Using the calibrated model, the predictions are 0.0158 and 0.0075  $\text{m}^2 \text{s}^{-4}$  for these two positions, which are within the desired model tolerance.

In addition to computing the mean squared energy content response for the VTPs, it is also possible to compare the measured acceleration power spectral density with the model predictions. For the two VTP positions, the measured and model acceleration power spectra are shown in Figures 14 and 15, respectively. In addition to the synthesized modal response of the VTP, the first three modes of the VTP are also shown in order to highlight their contribution to the overall response. As shown in Figures 14 and 15, the results indicate that the first mode is responsible for the majority of the low frequency response. The model response for the first mode also indicates that the model mode is underdamped relative to the measured response. This suggests that further refinements in the model are possible. However, given that the objective of the model development is to optimize a field deployable scour monitoring device, the current model precision is acceptable.

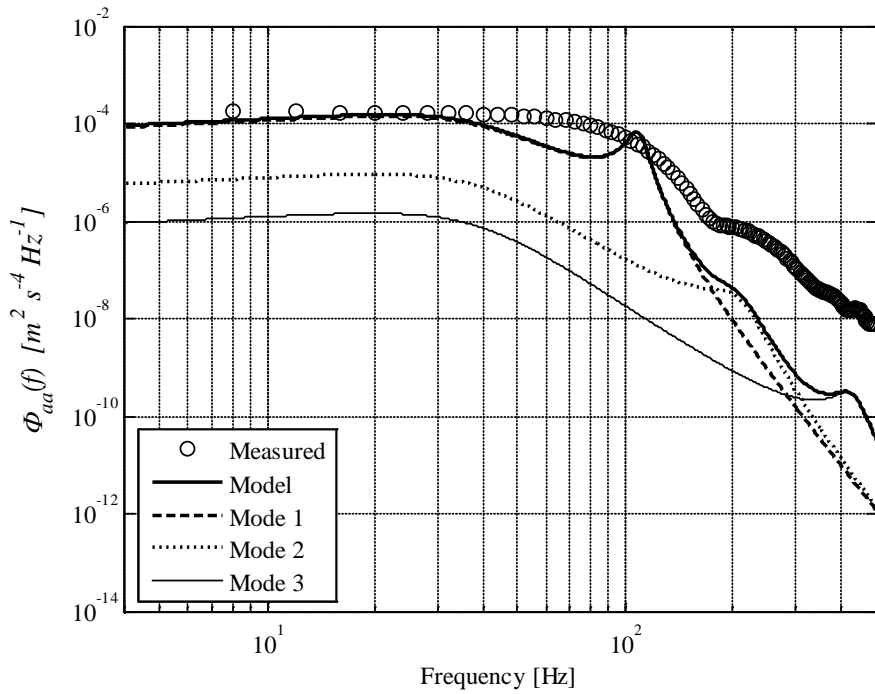


Figure 5.14 - Measured and model acceleration response spectra for run 3 conditions,  $y/h$  of 0.35. VTP plate is 1.6 mm thick, 2 cm radius neoprene.

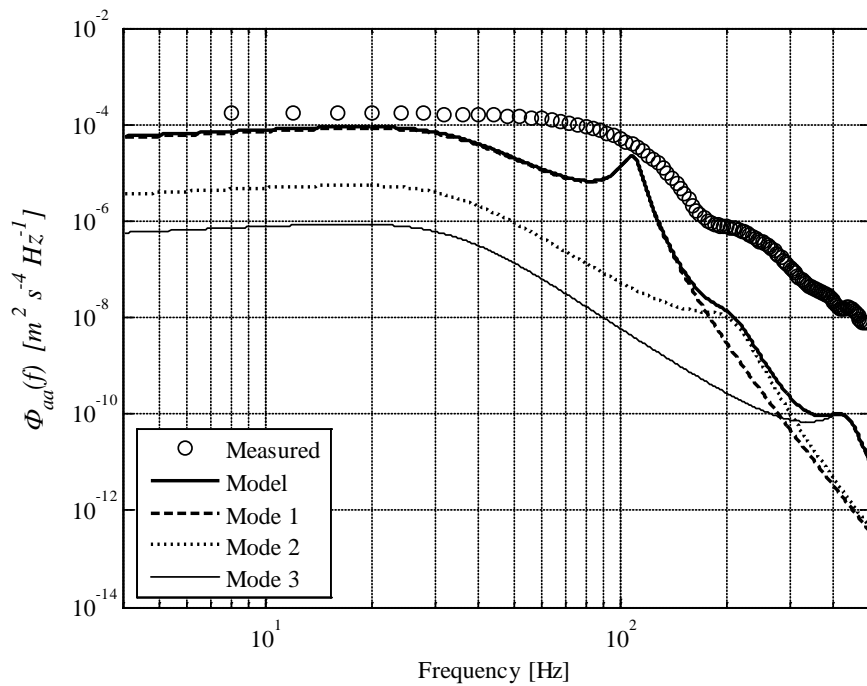


Figure 5.15 - Measured and model acceleration response spectra for run 3 conditions,  $y/h$  of 0.66. VTP plate is 1.6 mm thick, 2 cm radius neoprene.

## 5.4 VTP Optimization for Field Deployment

Having verified, calibrated, and validated the model, it is appropriate to use the model to predict the VTP energy content as the geometry of the device changes. In Fisher et al. (2012) it has already been shown that nonmetallic disks for the VTP are preferred over metallic disks, due to the lower stiffness, and higher acceleration response for a given turbulent dynamic pressure. Additionally, it has already been shown that circular VTPs are preferred over square geometries. Therefore, the optimization for field deployment considers only the radius and thickness of the disk as design parameters.

From the measured results of the VTP energy content presented in Fisher et al. (2012), it was determined that the maximum response from the VTPs located in the sediment was  $0.009 \text{ m}^2 \text{ s}^{-4}$ . In order to ensure the response of the VTP located in the flow are at least one order of magnitude greater than the VTPs in the sediment, a threshold energy content value is set to  $0.01 \text{ m}^2 \text{ s}^{-4}$ . This ensures that the VTP device can be used for scour monitoring. Additional constraints imposed on the optimization process included that the resolution of the device is at equal to that of a magnetic sliding collar, which can resolve the bed depth to 0.15 m (Legasse et al., 1997). Also, the material selected should be able to withstand the conditions that are likely to occur in the field. Given the performance of the neoprene in the experimental results conducted previously, the decision is made to select this material for the field deployment.

Based upon the conditions discussed previously, several predictions are made with the analytical model for VTP thicknesses of 1.6 to 3.2 mm and radii from 1.5 to 3.5 cm. A minimum spacing of 6.2 cm between adjacent VTPs is required for the additional

hardware necessary to mount the sensors. It is possible to consider the VTP response versus the resolution of the VTPs, as shown in Figure 5.16. The optimal VTP will respond above the required threshold and with a minimum spacing (leading to an improved resolution).

The results reveal that the optimal VTP for a thickness of 1.6 mm has a resolution of 10.2 cm, and corresponds to a VTP radius of 2 cm. For the 3.2 mm thick neoprene, the minimum resolution is determined to be greater than 13 cm (3.5 cm VTP radius). From these results, it is determined that the 1.6 mm, 2.0 cm radius is preferred over the thicker and larger VTP due to the improved resolution achievable with the smaller device. As expected, the model indicates that the energy content to be higher for the thinner VTPs for the same dimension. Therefore, it is anticipated that the minimum flow rate that can be resolved with the smaller, thinner VTP will exceed that of the larger, thicker VTP.

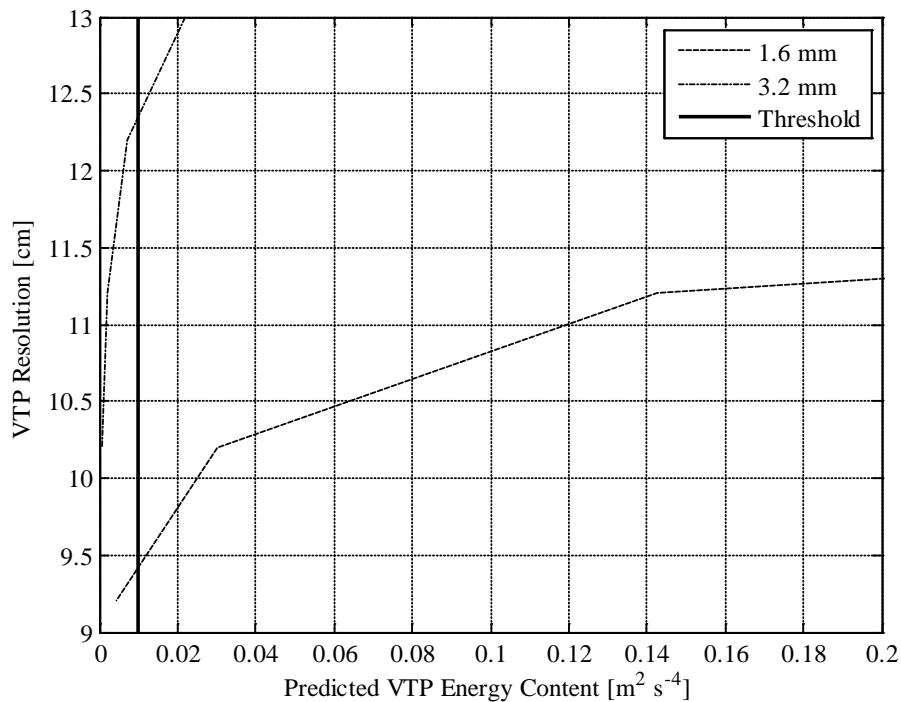


Figure 5.16 - Optimization of VTP size and thickness for field deployment.

## 5.5 Field Prototype Performance

Based upon the results presented in Section 4 of this work, the optimal VTP configuration is determined to have a disk radius of 2 cm and a thickness of 1.6 mm. A field prototype is constructed with 8 VTPs distributed along a 1 m length of the support pipe. The VTPs are spaced 10.2 cm apart and housed within removable units which are designed to aid maintenance in the field and to ensure that damage to one device does not allow water to penetrate into the undamaged VTPs. A schematic of the device is shown in Figure 5.17. The fully assembled prototype is shown in Figure 5.18. The accelerometers installed in the field prototype are PCB model 352A24, with a sensitivity of  $10 \text{ mV/m s}^{-2}$ . The accelerometers are connected to the bulkhead shown in Figure 5.17, in order to provide a water tight seal through which the accelerometer signal is routed. On the interior of the support pipe, the signal is carried by a wiring harness to the top flange of the pipe, where it passes through a water tight bulkhead and into a wet-mateable fitting for connection to the data lines and the data collection units.

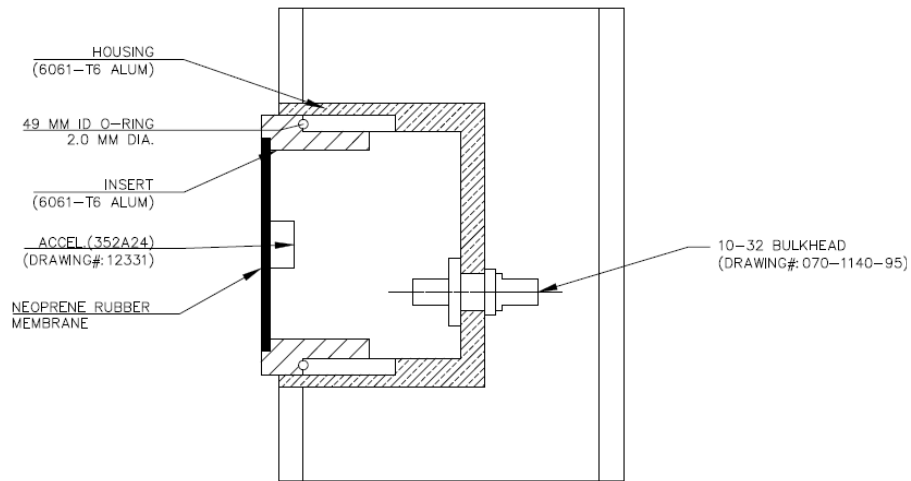


Figure 5.17 - Schematic of Field VTP Configuration.



Figure 5.18 - Field prototype.

### 5.5.1 Measured Energy Content Profile

The fully assembled field prototype is tested in the CHL flume to ensure the performance of the device. Tests are conducted in the channel flow with velocities from 14 to 30 cm/s. The results from these tests are shown in Figure 5.19.

The results indicate that the VTP located in the channel flow and closest to the bed surface responds with an energy content that is at least one order of magnitude greater than the VTPs in the sediment. Therefore, it is possible to conclude that the objective of the model development and optimization process has produced a device that will meet the required field performance metrics. Additionally, the results in Figure 5.19 indicate that for the velocity in the range of 14.2 to 20.2 cm/s, the energy content of the VTP near the bed varied from 0.0031 to 0.0046  $\text{m}^2 \text{s}^{-4}$ . These values are lower than the design threshold in the optimization due to lower mean channel flow velocities used in these tests. However, the difference between the VTP located in the flow and the sediment for these three cases ranged from a factor of 20 to 31. Thus, even for the low velocity cases, the field prototype will still indicate the water/sediment interface and therefore can monitor any scour hole development.

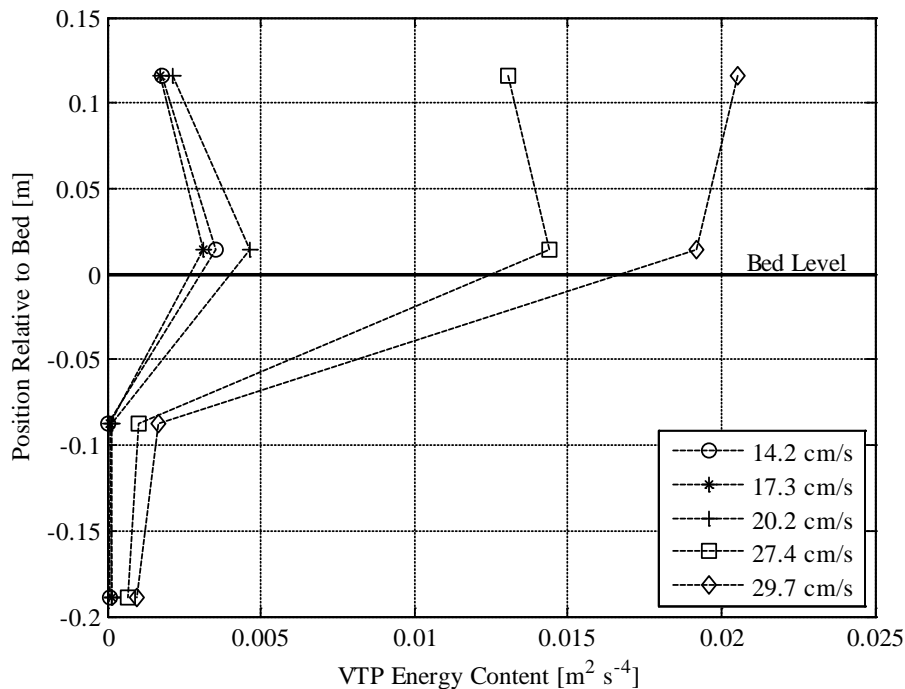


Figure 5.19 - Performance of field prototype in CHL flume.

### 5.5.2 Measured and Predicted Sensitivity to Flow Misalignment

The field prototype is also tested against varying flow misalignment between the main flow and the VTP axis. The results from these tests are compared against the semi-empirical model, which is shown in Figure 5.20. The model and measured results reveal that as the misalignment increases, the response from the VTP decreases. The model response approaches the measured results for smaller angles of misalignment. As the misalignment increases, the model results begin to deviate from the measured results. This is expected, as the flow around the probe will begin to separate at the upstream edge of the VTP with increasing misalignment. This effect is not accounted for in the analytical model. Despite this, the model is able to capture the measured decay in energy content with increasing misalignment. This serves to confirm that the semi-empirical model is capturing the governing physics that dictate the VTP energy content response.



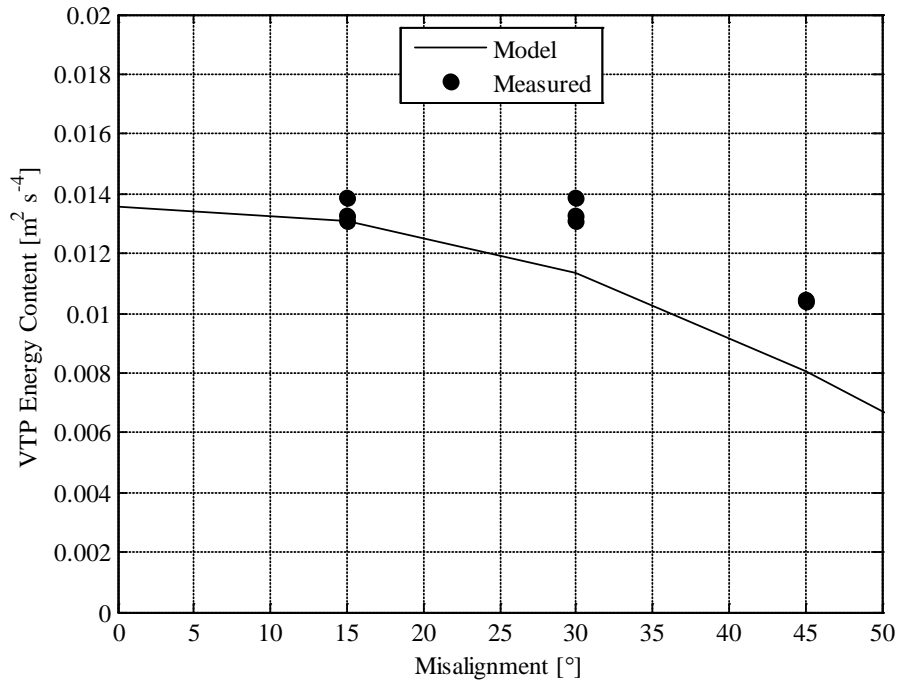


Figure 5.20 - Measured and analytical model response as a function of flow misalignment.

## 5.6 Conclusions

A semi-empirical model that can predict the energy content response of a flexible plate to turbulent open channel flow is developed. This model includes an empirical relationship between channel conditions and turbulent velocity fluctuations. The turbulent flow model is coupled to a dynamic structural response model which translates variations in the dynamic turbulent pressure impinging on the VTP into a prediction of the mean acceleration response.

A mesh refinement study is completed to determine the number of elements across the VTP surface required during integration of surface pressure. The study shows that result converge to within 1% of its final value for an element number greater than 10. Furthermore, the first three natural frequencies are calibrated with a 10% increase in the

modulus for the neoprene disk. The turbulent model calibration is investigated and reveals that the measured and predicted values are within the expected measurement error and is not adjusted. The final calibration showed that the model is sensitive to the friction velocity, which is then calibrated against a measured data set.

The calibrated model is then validated against an independently measured data set and reveals that the predicted values are within the desired tolerance of  $0.015 \text{ m}^2 \text{ s}^{-4}$ . The predicted responses from the calibrated model range from 3 to 22% of the measured energy content responses for the independent data set. This represents a significant improvement in the model over the uncalibrated model.

After calibrating the model, a VTP is optimized for field deployment by considering variations in the VTP size and thickness. Optimal thickness is determined to be 1.6 mm while the ideal size is determined to be 2.0 cm. The resulting device is sensitive to the turbulent velocity fluctuations while also being sufficiently robust for field deployment.

Based upon the optimized results, a field prototype is developed and tested in the laboratory. These tests indicate that the energy content variation across the channel depth is sufficient to allow for a determination of the water/sediment level. The model also captures the decay in energy with increasing flow misalignment.

## **5.7 References**

Atamturktur, S. Hemez, F. M., Laman, J. A., (2012). “Uncertainty Quantification in model Verification and Validation as Applied to Large Scale Historic Masonry Monuments”, *Engineering Structures*, Vol. 43, pp.: 221-234.

- Berger, E.H., Royster, L.H., Royster, J. D., Driscoll, D.P., Layne, M., (2003) “The Noise Manual”, 5<sup>th</sup> Ed., American Industrial Hygiene Association, Fairfax, Va,
- Blevins, R. D., (1977). “An Approximate Method for Sonic Fatigue Analysis of Plates and Shells”, *Journal of Sound and Vibration*, Vol, 129, No. 1, pp. 51-71.
- Blevins, R.D., (1979). *Formulas for Natural Frequency and Mode Shape*. Van Nostrand Reinhold Co., New York.
- Blevins, R.D., (1990). *Flow Induced Vibration*. Van Nostrand Reinhold Co., New York.
- Bruer, M., Münch, M., (2008). “Fluid–Structure Interaction Using LES – A Partitioned Coupled Predictor–Corrector Scheme.” *Proceedings in Applied Mathematics and Mechanics*, Vol. 8, No. 1, pp.: 10515 – 10516.
- Coles, D., (1956) "The Law of the Wake in the Turbulent Boundary Layer," *Journal of Fluid Mechanics*, Vol. 1, pp.: 191-226.
- Davidson, P. A., (2004) *Turbulence, an Introduction for Scientists and Engineers*. Oxford University Press Inc., New York.
- Galanti, B., Tsinober, A., (2004) “Is turbulence ergodic?”, *Physics Letters A* 330, pp.: 173–180.
- Hurther, D., Lemmin, U., (2001). “A Correction Method for Turbulence Measurements with a 3D Acoustic Doppler Velocity Profiler”, *Journal of Atmospheric and Oceanic Technology*, Vol. 18, pp.: 446- 458.
- Kironoto, B. A., Craff, W. H., (1994). “Turbulence characteristics in rough uniform open-channel flow”, *Proceedings of the ICE - Water Maritime and Energy*, Vol. 106, No. 4, pp.: 333 –344.
- Lagasse, P.F., Richardson, E.V., Schall, J.D., Price, G.R., (1997). Instrumentation for measuring scour at bridge piers and abutments. NCHRP Report 396, TRB, National Research Council, Washington, D.C., 1997.
- Meecham, W. C., (1958). “Relationship between Time Symmetry and Reflection Symmetry of Turbulent Fluids”, *The Physics of Fluids*, Vol. 1, No. 5, pp.: 408-410.
- Nakagawa, H., Nezu, I., Ueda, H., (1975). “Turbulence of Open Channel Flow Over Smooth and Rough Beds”, *Proceedings of the Journal of Society of Civil Engineers*, No. 241, September.

- Nezu, I., Nakagawa, H., (1993). *Turbulence in Open-Channel Flows*. IAHR, AIRH Monograph, A.A. Balkema Publishers, Rotterdam, Netherlands.
- Nezu, I., Rodi, W., (1986) “Open-Channel Flow Measurements with a Laser Doppler Anemometer”, American Society of Civil Engineers, Journal of Hydraulic Eng., Vol. 112, No. 5, pp.: 335 – 355.
- Nezu, I., (1977) Turbulent Structure in Open-Channel Flows. Ph.D. Thesis presented to Kyoto University, Kyoto, Japan.
- Nezu, I. (2005). ”Open-Channel Flow Turbulence and Its Research Prospect in the 21st Century”, American Society of Civil Engineers, Journal of Hydraulic. Eng., Vol. 131, No. 4 pp.: 229–246.
- Panton, R., L., (2005). *Incompressible Flow, 3<sup>rd</sup> Edition*. John Wiley and Sons, Inc., Hoboken, New Jersey.
- Roberson, R. E., (1951). “Vibration of a Clamped Circular Plate Carrying Concentrated Mass”, West Coast Conference of the Applied Mechanics Division, The American Society of Mechanical Engineers, Stanford, CA, June 22-23., pp.: 349 – 352.
- Trucano, T.G.; Pilch, M; Oberkampf, W. L., (2002).” General concepts for experimental validation of ASCI code applications.” Sandia National Labs, Report No. SAND2002-0341.
- Von Karman, T. (1948). “Progress in the Statistical Theory of Turbulence.” Proceedings of the National Academies in Science, Vol. 34, pp. 530-539.

## CHAPTER SIX

### CONCLUSIONS

#### **6.1 Summary of Research**

Scour remains the leading cause of bridge failure in the United States and is responsible for hundreds of millions of dollars in damage to the nation's transportation infrastructure. It has also been directly linked to the loss of lives resulting from the collapse of bridges during peak flow events. Given the threat to these critical components of any transportation system, the research presented in this work has outlined the state of the art and has made key contributions to overcoming deficiencies in the existing methods that advance the field of scour monitoring.

In order to deploy any system for the purpose of monitoring scour hole formation around a bridge pier or abutment it is necessary to evaluate the underlying physics that govern the operation of the proposed device. It is also necessary to further consider the potential impact of various environmental channel conditions on the proposed scour measurement method. In Chapter Two, the existing techniques are reviewed, including both point scour measurement devices and distributed scour monitoring methods. The available techniques reviewed include devices such as magnetic sliding collars, which rely upon the movement of key parts to indicate the presence of scour, to advanced 3D sonar systems that are capable of recording the bed topography around a bridge pier. As highlighted in Chapter 2, however, each device has certain strengths and weaknesses,

which should be considered when deploying any system in the field. To facilitate the development of robust scour monitoring systems, the failure modes and effects analysis is proposed as a means of designing scour monitoring systems that are more resilient to changes in the common environmental factors that exist in natural channels, such as temperature, salinity, and suspended sediment.

A novel method is developed in response to several of the common weaknesses in existing scour monitoring methods. The novel method employs sensors that are selected to be sensitive to the natural turbulence in open channel flows. It is hypothesized that these sensors, denoted as vibration-based turbulent pressure sensors (VTP), will vibrate at significantly higher amplitudes when in the flow as compared to in the sediment. Therefore, it is surmised that monitoring the mean squared acceleration response, which is denoted as the energy content in this work, across the depth of a bridge pier or abutment, can be used to determine the bed level. This method is tested experimentally in Chapter 3 and proved that the distribution of energy content can be used to monitor scour hole formation.

Having established the existing best in class measurement techniques in Chapter 2 and given the results of the VTP method in Chapter 3, the performance of sonar, time domain reflectometry, and the novel method are evaluated against common environmental factors found in natural channels. These tests, discussed in Chapter 4, reveal key findings about the impact of temperature, salinity, and suspended sediment on these three devices. In particular, the tests revealed the strength of the VTP method against channel turbidity, flow angle misalignment, and bed sediment type.

Having evaluated the governing hypothesis of the VTP method in Chapter 3, it is also necessary to consider the optimization of the device for field deployment. The development, verification, calibration, and validation of an analytical model that describes the governing physics behind the VTP method are discussed in Chapter 5. The results yield an optimal VTP configuration for field deployment, which is then tested and indicate the required performance of the device for monitoring the formation of scour holes around bridge piers and abutments.

## **6.2 Advancements to the State of the Art**

Through the research program outlined in Section 6.1, several key results that advance the state of scour monitoring have been identified. These key findings are reviewed in the following section.

In Chapter Two the available scour monitoring systems were reviewed and indicated that sonar fathometers and time domain reflectometry devices are the best in class techniques for monitoring bridge pier and abutment scour. In addition, the physical principles behind the operation of these two devices are evaluated and revealed a potential sensitivity to channel turbidity, salinity, and temperature.

The key findings that relate to the operational principle behind the VTP method, as discussed in Chapter Three, include:

- The fact that the energy content distribution across the pier/abutment depth varies, from a minimum in the bed, to a maximum immediately adjacent to the bed in the channel flow. The variation in the flow is consistent with the nature of turbulent open channel flow.

- The energy content of the VTP sensors in the sediment are one to two orders of magnitude below the level experienced in the turbulent channel flow.
- The point of maximum slope in the energy content can be used as a feature to determine the location of the water/sediment interface.
- Due to increases in the magnitude of the turbulent velocity fluctuations in a scour hole, the measured energy content increases for VTPs surrounded by a scour hole.

With the performance of the VTP method established and the best in class existing techniques identified, it is necessary to evaluate the performance of these devices against commonly encountered channel conditions. The tests performed for each device indicated that:

- The sonar method is sensitive to channel salinity and temperature, which can be corrected for by measuring these two parameters in addition to the sonar reading.
- Turbidity can influence the sonar device, up to the point at which it no longer can determine a stable bed reading. This is indicated by an increase in the standard deviation of the device above the sonar fathometer tolerance limit.
- The size of the scour hole within the sonar beam can influence the measured depth as the sonar device appears to record the minimum water depth within the beam width.
- The TDR method is sensitive to salinity above 500 PPM, at which point the waveform becomes indistinct.
- Temperature effects can influence the TDR readings, but can be accounted for by measuring the channel temperature and applying an appropriate correction.
- Suspended sediment concentration has no measured effect on the TDR method.



- Suspended sediment in the channel has only a minor impact to the VTP method, with the measured energy content increasing slightly for an increase channel turbidity.
- The flow alignment between the VTP probe and the main channel flow can influence the results. However, at 90°, the energy content in the flow is still one order of magnitude greater than that of the VTP in the sediment.
- The sediment type has little impact on the measured energy content in the channel bed.
- The minimum channel velocity tested revealed that for low depth averaged channel velocity, the response from the VTP in the flow was an order of magnitude greater than the VTP in the sediment, indicating adequate performance even in low flow conditions.

After establishing the performance of the VTP method in Chapter 3, it is then necessary to optimize the VTP configuration for deployment in the field. An analytical model was constructed to guide the optimization and revealed that after appropriate verification and calibration, the resulting model predicted the performance of the VTP device to within 20% of an independently measured data set. The optimal VTP configuration was determined to have a radius of 2.0 cm, made from 1.6 mm thick neoprene rubber. This field prototype was then evaluated in the CHL flume and indicated that the measured energy content in the flow was an order of magnitude greater than for the same VTPs located in the sediment.

### **6.3 Limitations of the Work and Avenues for Further Study**

In Chapter Two the current state of the art was reviewed and highlighted many of the existing, proven techniques for monitoring scour. Given the threat to bridges around the globe, many researchers are conducting studies with new and novel methods for monitoring scour and the state of the art is evolving rapidly. The current best practices include using sonar and TDR for monitoring the formation of scour holes. These two methods are sensitive to temperature, salinity and suspended sediment (not TDR). However, due to the constant introduction of new and novel methods, scour monitoring techniques will continue to evolve that advance the state of the art, but at the same time expose these devices to new and unanticipated channel conditions that can influence performance.

In regards to the novel VTP method, the experiments conducted in this research program revealed that the device is not sensitive to the common channel conditions that affect the performance of sonar and TDR. It is possible, however, that other unanticipated conditions can occur which can influence the performance of the VTP method. These parameters will be uncovered as the device is monitored in the field. Therefore, long term measurements with the VTP method are required in order to evaluate the device. After this, the VTP device can be deployed independently in the field.

Additionally, in developing the analytical model to predict the performance of the VTP to turbulent open channel flow, it was necessary to calibrate both the structural and turbulent flow parameters. These calibrations were based on particular data sets corresponding to neoprene VTPs. As indicated in Chapter 3, non-metallic disks have a

superior performance over metallic disks. Therefore, the analytical model in its present form should be restricted to neoprene disks. It is entirely possible, however, to perform a similar calibration and validation process as outlined in this report to include additional materials, should they be required based upon long term VTP field performance tests.

In addition to the limitations and opportunities for further research outlined above, it is also possible to consider the performance of the VTP device for flow misalignments greater than  $90^\circ$ . In this case, the VTP structure will be excited by the separated flow around the support pipe. The magnitude of these fluctuations have the potential to be on the order of the turbulent velocity fluctuations and could yield acceptable performance of the VTP device. The advantage presented by this case is that the device will be less sensitive to potential impacts from debris located in the channel. Damage to the VTP itself is less likely in this configuration. It remains, however, to be seen if the separated flow velocity fluctuations are sufficiently large so as to excite the device.

In closing, the research conducted in this project has developed a novel method which has been experimentally shown to provide reliable information about the location of the water/sediment interface on a bridge pier or abutment. This method was developed in response to key deficiencies in the current state of scour monitoring equipment, including sensitivities to common environmental conditions in natural channels. The novel method was shown to be insensitive to suspended sediment, flow misalignment, and other common channel parameters that can influence the VTP device. It was also optimized for field deployment, and performed adequately under laboratory simulated field conditions.

## APPENDIX

### SEMI-EMPIRICAL MODEL MATLAB CODE

#### **Turbulent Model:**

```
function [u_prime_sq_bar,Lx,Re_L,S_f,F_f,kw,fw,P_f_sq_mskg]=...
turbulence_model(parameters)
y_h = parameters.y_h;
U = parameters.U;
h = parameters.h;
temp = parameters.temp;
rho_fluid = parameters.rho_fluid;
U_star = parameters.U_star;

% Interpolate for nu_fluid based on Temp;
t1 =10; nu1 = 1.307E-6 * 100^2;
t2 =20; nu2 = 1.004E-6 * 100^2;

nu_fluid = (temp - t1) * (nu2 - nu1) / (t2 - t1) + nu1;

% Location of VTP:
y = y_h * h;

% Universal Function for u_prime
Du = 2.3;
B = 10;
C = 0.3;
Re_star = U_star * h / nu_fluid;
y_plus = y * U_star / nu_fluid;
gamma_y_plus = 1 - exp(-y_plus/B);
u_prime_U_star = Du * exp(-y_plus/Re_star)*gamma_y_plus + ...
    C*y_plus*(1-gamma_y_plus);
u_prime = u_prime_U_star * U_star;
u_prime_sq_bar = u_prime * u_prime;

% Determine Lx
% - first interpolate B1 for Re_star
R2 = 1600; B12 = 1.0;
R1 = 600; B11 = 1.1;
if Re_star > 1600
    B1 = 1.0;
```

```

elseif Re_star < 600
    B1 = 1.1;
else
    B1 = (Re_star - R1) * (B12 - B11) / (R2 - R1) + B11;
end
count = 0;
diff_Lx = 1000;
Lx_corr = 1;
while diff_Lx > .1

    if y/h < 0.6
        Lx_h = B1*(y/h)^.5;
        Lx = Lx_h * h;
    elseif y/h >= 0.6
        Lx_h = 0.77*B1;
        Lx = Lx_h * h;
    end
    Lx = Lx * Lx_corr;

    % ko = (1/Lx)*.75;

    % Determine Lamda
    Re_L = u_prime * Lx / nu_fluid;
    K = 0.691+3.98/sqrt(Re_L);
    Lx_lamda = (K/15)^.5 * Re_L^.5;
    lamda = Lx / Lx_lamda;

    % Determine Eta
    Lx_eta = K^.25*Re_L^.75;
    eta = Lx / Lx_eta;

    % Determine Epsilon
    epsilon = 15 * nu_fluid * u_prime_sq_bar / lamda^2;

    % Determine ko
    ko = (K / (2/(pi*C))^1.5)^(2/5) / Lx;

    check_Lx = (K^(2/3)* u_prime_sq_bar / epsilon^(2/3))^(3/2);
    diff_Lx = abs(Lx - check_Lx);
    Lx_corr = Lx / check_Lx;
    count = count +1;
    if count > 10
        break
    end
end

```

```

end

%% Setup Spectra
% Setup k and f
k1 = 0.01:0.02:lamda^-1; % m
k2 = lamda^-1:0.02:eta^-1*10; % m
kw = [k1,k2];
f1 = k1 * U / 2 / pi; % Hz
f2 = k2 * U / 2 / pi; % Hz
fw=[f1,f2];
fo = ko * U / 2 / pi; % Hz

% Determine gamma_prime
gamma_p = 1E2; % 1E2;

% Von Karman's Formula
S_f1 = 2 / pi * Lx * u_prime_sq_bar * (1 + (k1/ko).^2).^(-5/6);
%F_f1 = 4 * Lx / U * u_prime_sq_bar * (1 + (f1/fo).^2).^(-5/6); % s (Hz^-1)
F_f1 = 4 * Lx / U * (1 + (f1/fo).^2).^(-5/6); % s (Hz^-1)

% Heisenberg's Formula
S_f2 = C * epsilon^(2/3).*(k2).^(-5/3) .* (1+gamma_p*(k2*eta).^4).^(-4/3);
%F_f2 = 2*pi/U * (C * fudge_factor) * epsilon^(2/3).*(2*pi*f2./U).^(-5/3) .*
(1+gamma_p*((2*pi*f2./U)*eta).^4).^(-4/3);
F_f2 = 2*pi/U / u_prime_sq_bar * C * epsilon^(2/3).*(2*pi*f2./U).^(-5/3) .*
(1+gamma_p*((2*pi*f2./U)*eta).^4).^(-4/3);

S_f = [S_f1,S_f2];
F_f = [F_f1,F_f2];

% Convert Frequency Spectrum to Standard m, kg, units
rho_fluid = rho_fluid / 100^3; % [kg/m^3]

% Setup Force and Pressure
P_f_sq_mskg = (0.5 * rho_fluid * u_prime_sq_bar/100^2)^2 * F_f;

end

VTP Response Model:
function [U_f,V_f,A_f]=...
    vtp_model(parameters, P_f_sq_mskg,fw)
%% 1D Simple Model for Plate Response
% Setup Workspace

```

```

r = parameters.r;
thick = parameters.thick;
zeta_set = parameters.zeta;
material = parameters.material;
accel_mass = parameters.accel_mass;

%% Setup Disk Properties
if material == 'neop '
    load('neop.mat');
end

% Convert to Standard m, kg, units
r = r / 100; % [m]
thick = thick / 100; % [m]
A = pi * r^2; % [m^2]

%% Calculate Plate Response
% Calculate FRF for Clamped Circular VTP
lamda_sq_c = [10.22,21.26,34.88,51.04; 39.77, 60.82, 84.58, 111.0;...
    89.10, 120.1, 153.8, 190.3; 158.2, 199.1, 242.7, 289.2;];
f_n = lamda_sq_c ./ (2*pi*(r)^2) .* ( (E*thick^3) / (12 * rho * thick * (1 - nu^2)) )^0.5;
sorted_f = sort([f_n(1,:),f_n(2,:),f_n(3,:),f_n(4,:)]);

for count = 1:3;%length(sorted_f)
    if length(zeta_set)>1
        if count <= length(zeta_set)-1
            zeta = zeta_set(count);
        else
            zeta = 0.05;
        end
    else
        zeta = zeta_set;
    end
    FRF_temp = 1 ./ ( (1-(fw./sorted_f(count)).^2).^2 + (2*zeta*fw./sorted_f(count)).^2);
    FRF_modifier = 1.06^2 / (rho * thick * (2 * pi * sorted_f(count))^2)^2;
    if count == 2
        FRF_modifier = 1.83^2 / (rho * thick * (2 * pi * sorted_f(count))^2)^2;
    end
    FRF_temp = FRF_temp .* FRF_modifier;

    H_f_bleve(count+1,:) = FRF_temp;
    clear FRF_temp FRF_modifier
end

```

```

% Calculate FRF for Clamped Circular VTP with Mass
lamda_sq_table = [0,0.05,0.1,0.2,0.4,0.6,1.0,1.4; 10.2,9.0,8.1,6.9,5.4,4.75,3.8,3.3;]';
lamda_sq_c1 = interp1(lamda_sq_table(:,1),lamda_sq_table(:,2),accel_mass /
(rho*thick*pi*(r)^2));
f_n3 = lamda_sq_c1 / (2*pi*(r)^2) * ( (E*thick^3) / (12 * rho * thick * (1 - nu^2)) )^.5;
FRF_modifier = 1.11^2 / (rho * thick * (2 * pi * f_n3)^2)^2;
H_f_blev3 = 1 ./ ( (1-(fw/f_n3).^2).^2 + (2*zeta_set(4)*fw/f_n3).^2);
H_f_blev3 = H_f_blev3 .* FRF_modifier;

% Calculate Combined FRF
H_f_blev(1,:) = H_f_blev3;%H_f_blev + H_f_blev3;

H_f_blev(end+1,:) = sum(H_f_blev,1);

% Calculate Response Spectra
for i = 1:size(H_f_blev,1)
    U_f_mskg_sq(i,:) = H_f_blev(i,:) .* (P_f_sq_mskg); % ./ (rho * thick *
(2*pi*f_n3).^2).^2;

    U_f_mskg(i,:) = U_f_mskg_sq(i,:);%.^5;

% Convert Frequency Spectrum to Standard cm, kg, units
U_f(i,:) = U_f_mskg(i,:) * 100^4;
V_f(i,:) = U_f(i,:) .* (fw.*(2*pi));
A_f(i,:) = U_f(i,:) .* (fw.*(2*pi)).^2;

end

end

```